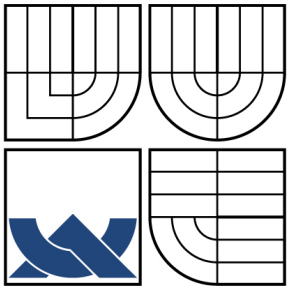

VYSOKÉ UČENÍ TECHNICKÉ V BRNĚ

BRNO UNIVERSITY OF TECHNOLOGY

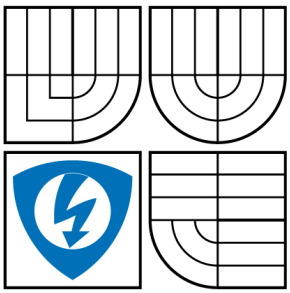

FAKULTA ELEKTROTECHNIKY A KOMUNIKAČNÍCH TECHNOLOGIÍ

ÚSTAV ELEKTROTECHNOLOGIE

FACULTY OF ELECTRICAL ENGINEERING AND COMMUNICATION

DEPARTMENT OF ELECTRICAL AND ELECTRONIC TECHNOLOGY

GEL POLYMER ELECTROLYTES FOR ELECTROCHROMIC DEVICES

GELOVÉ POLYMERNÍ ELEKTROLYTY PRO ELEKTROCHROMNÍ PRVKY

DOKTORSKÁ PRÁCE

DOCTORAL THESIS

AUTOR PRÁCE — Ing. ONDŘEJ KREJZA

AUTHOR

VEDOUCÍ PRÁCE — prof. Ing. JIŘÍ VONDRÁK, DrSc.

SUPERVISOR

BRNO 2009

LICENČNÍ SMLOUVA
POSKYTOVANÁ K VÝKONU PRÁVA UŽÍT ŠKOLNÍ DÍLO

uzavřená mezi smluvními stranami:

1. Pan/paní

Jméno a příjmení: Ing. Ondřej Krejza

Bytem: Tomečkova 4, 638 00 Brno

Narozen/a (datum a místo): 8. 4. 1980, Hradec Králové

(dále jen „autor“)

a

2. Vysoké učení technické v Brně

Fakulta elektrotechniky a komunikačních technologií

se sídlem Údolní 244/53, 602 00, Brno

jejímž jménem jedná na základě písemného pověření děkanem fakulty:

.....

(dále jen „nabyvatel“)

Čl. 1
Specifikace školního díla

1. Předmětem této smlouvy je vysokoškolská kvalifikační práce (VŠKP):
   - ☒ disertační práce
   - ☐ diplomová práce
   - ☐ bakalářská práce
   - ☐ jiná práce, jejíž druh je specifikován jako .....

   (dále jen VŠKP nebo dílo)

Název VŠKP:	Gel polymer electrolytes for electrochromic devices
Vedoucí/ školitel VŠKP:	Prof. Ing. Jiří Vondrák, DrSc.
Ústav:	Ústav elektrotechnologie
Datum obhajoby VŠKP:	

VŠKP odevzdal autor nabyvateli v*:

- ☒ tištěné formě – počet exemplářů 1
- ☒ elektronické formě – počet exemplářů 1

2. Autor prohlašuje, že vytvořil samostatnou vlastní tvůrčí činností dílo shora popsané a specifikované. Autor dále prohlašuje, že při zpracovávání díla se sám nedostal do rozporu s autorským zákonem a předpisy souvisejícími a že je dílo dílem původním.
3. Dílo je chráněno jako dílo dle autorského zákona v platném znění.
4. Autor potvrzuje, že listinná a elektronická verze díla je identická.

Článek 2
Udělení licenčního oprávnění

1. Autor touto smlouvou poskytuje nabyvateli oprávnění (licenci) k výkonu práva uvedené dílo nevýdělečně užít, archivovat a zpřístupnit ke studijním, výukovým a výzkumným účelům včetně pořizovaní výpisů, opisů a rozmnoženin.
2. Licence je poskytována celosvětově, pro celou dobu trvání autorských a majetkových práv k dílu.
3. Autor souhlasí se zveřejněním díla v databázi přístupné v mezinárodní síti
   - ☐ ihned po uzavření této smlouvy
   - ☐ 1 rok po uzavření této smlouvy
   - ☒ 3 roky po uzavření této smlouvy
   - ☐ 5 let po uzavření této smlouvy
   - ☐ 10 let po uzavření této smlouvy

   (z důvodu utajení v něm obsažených informací)
4. Nevýdělečné zveřejňování díla nabyvatelem v souladu s ustanovením § 47b zákona č. 111/ 1998 Sb., v platném znění, nevyžaduje licenci a nabyvatel je k němu povinen a oprávněn ze zákona.

Článek 3
Závěrečná ustanovení

1. Smlouva je sepsána ve třech vyhotoveních s platností originálu, přičemž po jednom vyhotovení obdrží autor a nabyvatel, další vyhotovení je vloženo do VŠKP.
2. Vztahy mezi smluvními stranami vzniklé a neupravené touto smlouvou se řídí autorským zákonem, občanským zákoníkem, vysokoškolským zákonem, zákonem o archivnictví, v platném znění a popř. dalšími právními předpisy.
3. Licenční smlouva byla uzavřena na základě svobodné a pravé vůle smluvních stran, s plným porozuměním jejímu textu i důsledkům, nikoliv v tísni a za nápadně nevýhodných podmínek.
4. Licenční smlouva nabývá platnosti a účinnosti dnem jejího podpisu oběma smluvními stranami.

V Brně dne: …….

…….. ……

Nabyvatel Autor

Vysoké učení technické v Brně Fakulta elektrotechniky a komunikačních technologií
Ústav elektrotechnologie

POPISNÝ SOUBOR ZÁVĚREČNÉ PRÁCE

Autor: Ing. Ondřej Krejza

Název závěrečné práce: Gelové polymerní elektrolyty pro elektrochromní prvky

Název závěrečné práce ENG: Gel Polymer Electrolytes for Electrochromic Devices

Anotace závěrečné práce: Předkládaná práce se zabývá výzkumem nových materiálů a metod přípravy gelových polymerních elektrolytů (GPE) na bázi methakrylátů, které lze zejména vzhledem k jejich mechanickým vlastnostem s výhodou využít při konstrukci elektrochromních (EC) prvků.

Anotace závěrečné práce ENG: This work deals with the research on the methacrylate based gel polymer electrolytes (GPEs) primarily but not solely designed for use in electrochromic (EC) devices, but also in other Li-ion applications. An EC device comprises an active solar control film whose transmittance in the visible and near IR part of the spectrum can be reversibly modulated by a low DC voltage. The poly(methyl methacrylate) PMMA based redox electrolyte with I3-/I- pair was introduced. The method of in-situ thermal polymerization of the gel was used to prepare a hybrid FTO|WO3|redox GPE|Pt|FTO cell in a vacuum bag. The relationship between the electrolyte composition and the parameters such as change of transmittance, response time and stability was discussed based on results from coupled optoelectrochemical measurements. The hybrid EC cell showed moderate optical modulation (ca 30 % of dT at 634 nm), slow initial state recovery and relatively low coloration efficiency (10.5 cm2/C). On the other hand the switching speeds (< 20s) were observed. The new poly(ethyl methacrylate) PEMA and poly(2-ethoxyethyl methacrylate) PEOEMA based polymer gel electrolytes with entrapped solutions of LiClO4 in propylene carbonate (PC) were prepared by direct, UV initiated polymerization. The electrolytes exhibit good ionic

POPISNÝ SOUBOR ZÁVĚREČNÉ PRÁCE

conductivity (up to 1.9 mS/cm at 20 °C) as well as electrochemical stability up to 5.1 V vs. Li/Li+ on gold electrode. The electrolytes were successfully tested as ionic conductors in the electrochromic device FTO/WO3/Li-electrolyte/V2O5/FTO. The transmittance change was found to be ca 53 % of dT at 634 nm. Further the GPEs based on PMMA-PC- LiClO4 or NaClO4 electrolytes were prepared using either the commercial product Superacryl or directly by the heat or UV induced polymerization of a monomer. The nanostructured aluminum oxide added to the latter mentioned systems in various ratios was found to enhance their ionic conductivity.

Klíčová slova: Gelový polymerní elektrolyt, Specifická vodivost, Methakrylát, Elektrochromní prvek, Propylenkarbonát, Oxid hlinitý, Nanočástice, Redoxní elektrolyt, Lithium

Klíčová slova ENG: Gel-polymer electrolyte, Ionic conductivity, Methacrylate, Electrochromic device, Propylene carbonate, Aluminium oxide, Nanoparticles, Redox electrolyte, Lithium

Typ závěrečné práce: dizertační práce

Datový formát elektronické verze: pdf

Jazyk závěrečné práce: angličtina

Přidělovaný titul: Ph.D.

Vedoucí závěrečné práce: prof. Ing. Jiří Vondrák, DrSc.

Škola: Vysoké učení technické v Brně

Fakulta: Fakulta elektrotechniky a komunikačních technologií

Ústav / ateliér: Ústav elektrotechnologie

Studijní program: Elektrotechnika, elektronika, komunikační a řídicí technika

Studijní obor: Mikroelektronika a technologie

Bibliographic citation

KREJZA, O. *Gel polymer electrolytes for electrochromic devices.* Brno: Brno University of Technology, Faculty of Electrical Engineering and Communications, 2009. 117 s. Tutor Prof. Ing. Jiří Vondrák, DrSc.

Statutory declaration

I hereby declare that the thesis has been written by myself without any external unauthorized help. Any parts, words or ideas, of the thesis, however limited, and including tables, charts, pictures etc., which are quoted from or based on other sources have been acknowledged as such without exception.

Brno, 12th February 2009

…….

Ing. Ondřej Krejza

Acknowledgements

I would like to thank to my tutor Prof. Ing. Jiří Vondrák, DrSc. for his guidance and eligible suggestions on this project.

Also I would like to thank to Doc. Ing. Marie Sedlaříková, CSc. for her professional and endless personal support thorough my doctorate studies.

Special thank goes to RNDr. Jakub Reiter, PhD. for his supervision and flawless cooperation.

Many thanks to researchers from the Institute of Inorganic Chemistry in Prague, namely to Ing. Jana Velická for her contribution to the conductivity data and Ing. Kamil Lang, CSc. for his help with coupled UV-VIS measurements.

Many thanks also to the members of Chemical Institute in Slovenia. Sincere thank to Dr. Angela Šurca Vuk for her supervision during the stay and valuable inputs on the HEC issue.

I would like to thank to the scientific staff from Advanced Coating Division at BTC for running peel tests and thermal analysis for me. My very sincere thank goes to Dr. Nadine Vandevelde for her leadership during my time in Belgium.

I give special thanks to my office-mates Peter, Michal, Jirka, Petr and Víťa for making pleasant my stay at the department and for number of valuable discussions.

Finally I would like to sincerely thank to Veronika and both my families for their patience endless encouragement and also financial support during all my studies.

Contents

Symbols and abbreviations

a	Electrolyte's degree of dissociation
A	Electrode area
ACN	Acetonitrile
AcOH	Acetic acid
AIBN	2,2'-azobis(isobutyronitrile)
BEE	Benzoine ethylether
BP	Boiling point
c	Analyte concentration
C	Ideal capacitance
C_b	Electrolyte capacitance
C_d	Double-layer capacitance
C_e	Electrode capacitance
CE	Coloration efficiency
CE	Counter electrode
CLSM	Confocal laser scanning microscopy
CPE	Constant phase element
CV	Cyclic voltammetry
DEC	Diethyl carbonate
DMC	Dimethyl carbonate
DC	Direct current
DMA	Dynamic mechanical analysis
DSC	Differential scanning calorimetry
DME	Dropping mercury electrode
D_{of}, D_{or}, D_o	(Forward, reverse) Apparent diffusion coefficient
E	Electrode *(*Electrochemical) potential (IUPAC)
E	Young´s modulus
E'	Storage modulus
E''	Loss modulus
E_A	Apparent activation energy
EC	Ethylene carbonate
EC, ECD	Electrochromic (device)
EDMA	Ethylene dimethacrylate
E_{el}	Born's electrostatic salvation energy

An interference of the two nomenclatures – IUPAC (a systematic method of naming organic chemical compounds as recommended by the International Union of Pure and Applied Chemistry) and SI (the international system of units) is denoted by brackets.

EIS	Electrochemical impedance spectroscopy
EMA	Ethyl methacrylate
EOEMA	2-ethoxyethyl methacrylate
E_p	Peak potential
$E_{p/2}$	Half-peak potential
E_{pa}, E_{pf}	Anodic/forward peak potential
E_{pc}, E_{pr}	Cathodic/reverse peak potential
EtOH	Ethanol
F	Faraday constant
F_{avg}	Average peel force
Fc/Fc^+	$Fe(\eta^5\text{-}C_5H_5)_2/[Fe(\eta^5\text{-}C_5H_5)_2]^+$; ferrocene/ferrocenium redox system
F_{max}	Maximal peel force
FRA	Frequency Response Analyzer (AUTOLAB software)
FT-IR	Fourier transform infrared spectroscopy
FTO	Fluoride doped tin oxide; SnO_2:F
GC	Glassy carbon
GPE	Gel polymer electrolyte
GPES	General Purpose Electrochemical System (AUTOLAB software)
HEC, HECD	Hybrid electrochromic (device)
HEMA	2-hydroxyethyl methacrylate
HexadiMA	1.6-hexanediol dimethacrylate (hexamethylene dimethacrylate)
HRTEM	High-resolution transmission electron microscopy
i_c	Double layer current
i_{cc}	Charge transfer current
ICS-PPG	3-isocyanatopropyltriethoxy silane - poly(propyleneglycol)-bis-(2-amino-propyl)ether
i_f	Faradaic current
IP	Initial potential
IR	Infra red spectrum
i_p	Peak current
i_{pf}	Forward peak current
i_{pr}	Reverse peak current
I	Electrical current
ITO	Tin doped indium oxide; In_2O_3:Sn
j	Current density
K'	Apparent dissociation constant
l	Electrode distance
LE	Liquid electrolyte
LSV	Linear sweep voltammetry
MeOH	Methanol

An interference of the two nomenclatures – IUPAC (a systematic method of naming organic chemical compounds as recommended by the International Union of Pure and Applied Chemistry) and SI (the international system of units) is denoted by brackets.

MMA	Methyl methacrylate; Methyl 2-methylprop-2-eonate (IUPAC)
MMA/SA	PMMA based GPE prepared from Superacryl® precursor
MMA/AIBN	PMMA based GPE prepared by direct, thermally initiated polymerization of MMA
MMA/BEE	PMMA based GPE prepared by direct, UV initiated polymerization of MMA
MP	Melting point
n	Number of transferred electrons
N_A	Avogadro's number
NMR	Magnetic resonance spectroscopy
OD	Optical density
OM	Optical microscope
PANI	Polyaniline
PB-PW	Iron (III) hexacyanoferrate (II); Prussian Blue-Prussian White redox system
PC	Propylene carbonate
PE	Polymer electrolyte
PEDOT	Poly(3,4-ethylenedioxythiophene)
PEMA	Poly(ethyl methacrylate)
PEN	Poly(ethylene nephthalate)
PEO	Poly(ethylene oxide)
PEOEMA	Poly(2-ethoxyethyl methacrylate)
PET	Poly(ethylene terephthalate)
PMMA	Poly(methyl methacrylate)
PP	Poly(propylene)
PTFE	Poly(tetrafluoroethylene)
PVdF	Poly(vinylidene difluoride)
Q	Charge capacity
Q_b	Bulk capacity (CPE)
QCM	Quartz crystal microbalance
Q_e	Electrode surface (CPE)
R	Ideal gas constant
r^2	Correlation factor
R_b	Electrolyte resistance
R_{ct}	Charge transfer resistance
R_Ω	Solution resistance
RE	Reference electrode
r_i	Proportional ionic radius
RT	Room temperature (25 °C)
SA	Superacryl®, commercial polymerization precursor
SCE	Saturated calomel electrode
SEI	Solid electrolyte interface

An interference of the two nomenclatures – IUPAC (a systematic method of naming organic chemical compounds as recommended by the International Union of Pure and Applied Chemistry) and SI (the international system of units) is denoted by brackets.

SEM	Scanning electron microscopy
TGA, DTGA	(Derivative) thermogravimetric analysis
TA	Thermal analysis
t, ζ	Temperature
t_i; t_+, t_-	Transference numbers
τ	Transmittance
$tan\ \delta$	Damping behaviour
TCO	Transparent conducting oxide
T	Absolute temperature
T_g	Glass transition temperature
T_0	Ideal glass transition temperature
T_i, T_f	Decomposition temperature limits
TMS	Sulfolane, tetramethylene sulfone; $C_4H_8O_2S$
v	Sweep rate
V^+	Single charged vacancy
V^0	Neutral vacancy
V^{2+}	Doubly charged vacancy
V_O	Open circuit voltage
VTF	Vogel-Tamman-Fulcher equation
WE	Working electrode
WLF	Williams, Landel and Ferry equation
x	Cross-sectional area
z	Charge of the ions
Z, Z^*_{total}	Complex impedance
Z'	Real part of complex impedance
Z''	Imaginary part of complex impedance
Z_f	Faradaic impedance
Z_W	Warburg's impedance
ε_S	Dielectric constant of the solvent
Λ	Molar conductivity
λ	Wavelenght
λ_i; λ_+, λ_-	Proportional molar conductivity
η	Viscosity (IUPAC)
μ_i	Proportional ionic mobility
σ	Specific conductivity of solid and gel polymer electrolytes
σ_0	Specific conductivity at the absolute temperature
κ	Specific conductivity of liquid electrolytes
ω	Angular frequency

An interference of the two nomenclatures – IUPAC (a systematic method of naming organic chemical compounds as recommended by the International Union of Pure and Applied Chemistry) and SI (the international system of units) is denoted by brackets.

1 Introduction

Nowadays when the global warming has become a copiously discussed issue, the need of energy efficient solutions increasingly attracts attention of private and governmental sectors. The use of eco-efficiency criterions can be considered as an indicator of energy efficient products. On a broader prospective, the eco-efficiency is regarded as a method to reach results for both the environmental and the economic performance of a product (or process) that can be used as decision making for investments, product improvement, product selection or public policy. The eco-efficiency is usually measured by operational performance indicators based on material and energy balances.[1] The reduction of cooling and heating energy consumption in the building construction sector for instance is of an economic and environmental concern. One of the approaches that comply with the eco-efficient criterion is implementation of electrochromic advanced glazing. The most prospective and challenging of these are so called "smart windows". It is an active solar control device whose transmittance in the visible and near IR part of the spectrum can be reversibly modulated by a low DC voltage. The electrochromic device can provide improved indoor comfort by being able to prevent glare and thermal discomfort and simultaneously large energy savings through a lowered cost for air cooling.[1,2] According to building simulations reported by Syrrakou et al. the electrochromic device implemented in cooling dominated areas can reduce the building energy requirements by 52%.[1]

There has been a lot of effort in recent years to bring the large scale electrochromic windows to the market. Only a few types of smart windows, having active layers sputtered on top of glass pane, are commercially available at the time.[3] For majority of applications, the all solid-state electrochromic device including ion conducting electrolyte ensures higher reliability and safety compared to those encompassing liquid electrolyte. The major drawback is their high purchase cost, induced by expensive manufacturing process, which prevents the technology expansion. One of the approaches towards cost reduction is use of flexible electrochromic device. Such lightweight solar control film could be easily mounted (retrofitted) on the top of a standard window pane with no need of replacement, the result would be a product price reduction, or simply shaped into virtually infinite forms. Moreover the batch production could be overcome by continuous processing flow with the use of low cost deposition techniques.[4] Recently the small scale flexible dimming foil laminated over a motorcycle visor was introduced.[2]

Despite numerous technology limitations at the time, we believe that the gel polymer electrolytes are the most convenient choice for the future flexible electrochromic applications. Our present work deals with development of acrylic based Li-ion conducting gel polymer electrolytes and their implementation in standard battery-type and hybrid electrochromic devices.

[1] SYRRAKOU, E., et al., *Science of the Total Environment*, 359 (2006) 267-282.

[2] NIKLASSON, G.A., GRANQVIST, C.G., *Journal of Material Chemistry*, 17 (2007) 127-156.

[3] *Sage Electrochromics*. Available from WWW: <www.sage-ec.com>.

[4] WIDJAJA, E.J., et al., *Solar Mat. and Solar Cells*., 92. (2007) 97-100.

2 Literature survey

Section 2.1 introduces the basic concepts of electrochromism and classifies electrochromic devices according to their active layer configuration as a standard "battery type" and hybrid electrochromic cells. Section 2.2 primarily focuses on gel polymer electrolyte as an ion conductor for electrochromic devices. The similar features and differences in between electrochromic devices and rechargeable thin film batteries are reviewed in section 2.3. Finally, section 2.4 introduces some key aspects and principles of the ion conduction mechanism in liquid, solid and gel polymer electrolytes.

2.1 *Electrochromism*

An electrochromic (EC) material is able to change its optical properties when a voltage is applied across it. The optical properties should be reversible; it means that the original state should be recoverable if the polarity of the voltage is changed. The materials colouring upon insertion are called cathodic and materials that colour upon extraction are called anodic. Cathodic colouration can be found in oxides of Ti, Nb, Mo, Ta, and W, with tungsten oxide being by far the most extensively studied one. Anodic colouration can be found in oxides of Cr, Mn, Fe, Co, Ni, Rh and Ir. Vanadium oxide is exceptional by the fact that the pentoxide (with V^{5+}) exhibits anodic and cathodic electrochromism within different wavelength ranges, while the dioxide (with V^{4+}) has anodic electrochromism. Not all the metal oxide phases of these materials possess electrochromic properties and in many cases a mixed oxide is used to enhance a particular property of the thin film.

These properties make electrochromic materials of considerable interest for devices where the optical modulation of transmittance, reflectance, absorbance, and emittance is desired. They can be applied as elements for information displays, light shutters, smart windows, variable-reflectance and variable-emittance thermal radiators. In the presence the largest and the most studied are so called "smart windows" for uses in building and automotive industry.

The electrochromic devices (ECDs) can be subdivided into two types according to their construction; (a) all-solid-state (multilayer solid thin films), and (b) laminated (solid thin films laminated together with a viscous polymer electrolyte). These constructions can be rigid if glass is used as substrate or flexible if a polymer foil is used instead [1-4].

According to operational mode we speak about three major electrochromic device configurations; (a) battery-like, (b) solution phase, and (c) hybrid structures. The latter two types are the so-called self erasing devices, commonly used in commercial electrochromic mirrors. They do not have open circuit memory, requiring continuous current injection to maintain the device in a coloured state, the properties unfavourable for use in switchable glazing for building and automotive industry [5].

The electrochromic devices discussed in this work come under the groups (a) and (c). Their brief structure overview and principle of operation is described in the two following chapters.

2.1.1 Standard "battery type" electrochromic devices (ECDs)

Figure 2.1 shows a battery type electrochromic device construction. The device consists of layers backed by a substrate that in many cases is a glass plate. The solid glass plate construction can be substituted by flexible foil (i.e. poly(ethylene terephthalate); PET or poly(ethylene nephthalate); PEN). The glass has a transparent and electrically conducting film (TCO) and a film of electrochromic oxide. This oxide has a mixed conduction for ions and electrons, and if ions are introduced from an adjacent electrolyte or via an adjacent ion conductor there is a corresponding charge-balancing counterflow of electrons from the transparent electron conductor. These electrons will remain in the electrochromic film, as long as the ions reside there, evoking the persistent change of the optical properties. Basically, when a voltage is applied between the TCO, as indicated in Fig. 2.1, a distributed electrical field is set up and ions are moved uniformly into (intercalated) and out (deintercalated) of the electrochromic film(s). The charge-balancing counterflow of electrons through the external circuit and ion storage film then leads to a variation of the electron density in the electrochromic material(s) and thereby a modulation of their optical properties. The ion storage film deposited on another transparent conducting oxide might or might not have electrochromic properties (the electrochromic devices with two electrochromic layers are a so-called complementary ECDs). The ion conductor can be a thin film or a bulk-like material. For practical devices a solid inorganic or organic (polymeric) material is preferred [1,6].

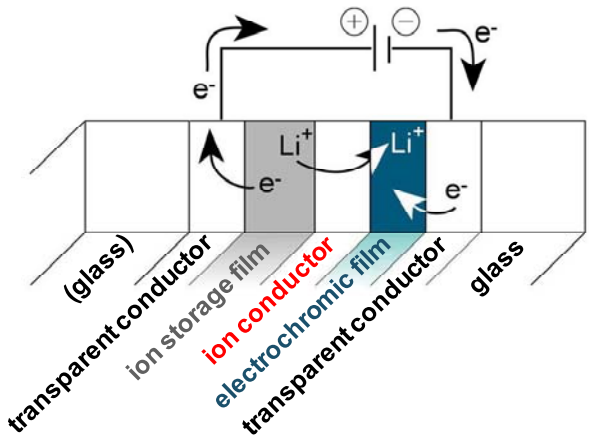

Fig 2.1 Structure of an electrochromic device. Arrows indicate the transport of Li^+ ions compensated by electron flow from adjacent TCOs; figure adopted from ref [7].

The device from Figure 2.1 is appropriate for transmittance modulation; however incorporation of a diffuse scatterer or a mirror behind the electrochromic film would convert the device into a reflectance modulator. The voltage applied between the outer films should be of the order of few volts only. Higher voltages would lead to a rapid deterioration of the device [1,6].

The essential requirements and materials used as the components of ECD from Fig. 2.1 can be summarized as follows:

The *transparent electrical conductors* should have a low sheet resistance (preferably below 30 Ω/□). They are made of oxide films such as In_2O_3, SnO_2, ZnO or doped versions based on In_2O_3:Sn referred to as ITO, SnO_2:F known as FTO and ZnO:Ga_2O_3 [2-6, 8-16].

Among the *cathodic electrochromic films* (darken upon intercalation), the tungsten oxide is the most common choice. It is a material based on corner-sharing WO_6 octahedra. Where each tungsten ion is surrounded by six oxygen ions forming an octahedron; each oxygen ion is bound to two tungsten ions in a linear configuration according to $W^{6+} - O^{2-} - W^{6+}$. Whereas in the single WO_3 crystal they are perfectly ordered, in the amorphous state (characteristic for electrochromic films) they are subject to bond angle and bond length variations. Tungsten oxide has a propensity to form sub-stoichiometric structures, manifested in the crystalline state as the Magnéli phases, with some edge-sharing octahedra. The spaces in between the octahedra are large enough to build the framework for accommodation of intercalated ions. In amorphous structures, the most common defect is the oxygen vacancy, which can be neutral (V^0), singly (V^+) or doubly charged (V^{2+}). It is expected that V^{2+} is the most common type of vacancy in tungsten oxide. The two electrons can be transferred to one or two adjacent tungsten ions, though it is energetically more advantageous to form V^{2+} along with two W^{5+} ions. Also an oxygen over-stoichiometry is possible in tungsten oxide; this excess of oxygen can be accommodated if there are hydroxyl bonds between adjacent oxygen atoms, schematically illustrated by $W^{6+} - (O - O)^{2-} - W^{6+}$. The extra oxygen atoms can be viewed as oxygen interstitials (neutral, singly or doubly charged entrapped electrons); being present simultaneously to vacancies in tungsten oxides. Persistent change in optical properties of electrochromic materials is induced by intercalation of small ions, typically being H^+, Li^+ or Na^+ and takes place highly schematically as follows;

$$WO_3 + xM^+ + xe^- \leftrightarrow M_xWO_3 \tag{2.1}$$

with M = H, Li, Na, etc. In reality, the oxide is substoichiometric, hydroxylated and hydrated, and ion intercalation may occur in conjunction with associated electrolyte molecules (i.e. H_2O, PC, etc) [1, 3, 4, 6]. Among others the electrochromic devices comprising conducting polymers with electrochromic properties such as poly(3,4-ethylenedioxythiophene) (PEDOT) [8-10] and multielectrochromic polyaniline (PANI) [8,11] were reported to have long cycle life, high contrast ratios and low operation voltages. Recently the new N-ethyl substituted poly(3,4-ethylenedioxypyrrole) multicolor electrochromic polymer was introduced by Kraft et. al [12].

Based on their optical properties the *anodic electrochromic films* can be subdivided into two major categories. Among the first ones, non-complementary (do not darken upon deintercalation), the most widely studied is vanadium oxide (V_2O_5) [1,13], furthermore iridium oxide (IrO_2) [1] and magnesium fluoride (MgF_2) [14] are used. The second group includes complementary ion storage films (darken upon deintercalation) such as nickel oxide (NiO) [1-4,15], PEDOT [8] and Prussian Blue-Prussian White redox system (iron (III) hexacyanoferrate (II), PB-PW) for non-aqueous environs [5,10,16]. The PB-PW is a polyelectrochromic conducting polymer with four corresponding redox states. The ECDs comprising PEDOT and PB-PW layers were known to suffer from poor cycling and at-rest stabilities. Though there have been cells with good electrochemical stability, electrode-electrolyte compatibility and long cycle life recently reported by Ho et. al [10].

Apparently there are many requirements on the electrochromic films. The optical modulation should be large enough for a practically realizable change in the electron density (high *coloration efficiency;* CE). The conductivity for electrons and ions must be sufficient, so that the optical modulation is not excessively slow. These requirements apply to both; anodic and cathodic electrochromic films. Thin electrochromic films can be produced by a variety of physical, chemical and electrochemical methods [1-6, 8-12, 14-20].

2.1.2 Hybrid electrochromic devices (HECDs)

Typical hybrid electrochromic device consists of a solid electrochromic film in contact with an electrolyte containing molecular redox chromophore (i.e. viologen dye attached to a nanostructured TiO_2 [17] or Prussian blue [18] films). When compared to a battery type ECDs, the HEC cells feature colouring/bleaching times in the range of seconds or less because the electrochemically active species are dissolved in a solution or deposited in polymeric form on the TCO electrode. Another difference is that they do not have an open circuit memory. Since a continuous passage of current is needed to retain the coloured state, they are more suitable for use in rear-view EC mirrors for cars and large segment of static displays than for smart windows.

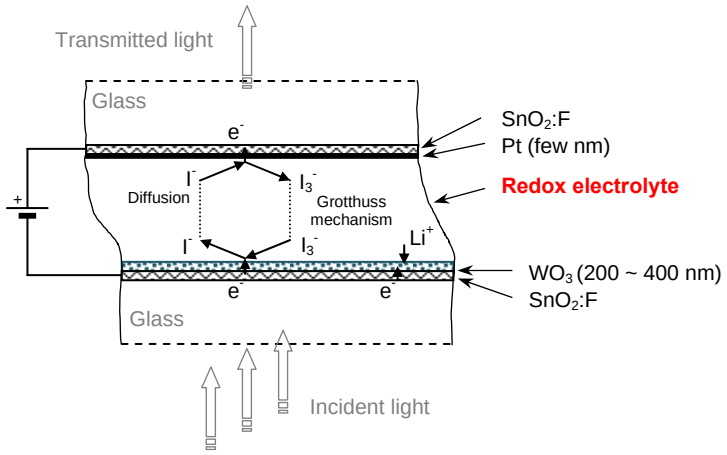

Fig. 2.2 Schematic representation of an HEC cell; figure adopted from ref. [20].

Figure 2.2 shows the cross-section of HEC cell having the ion storage electrode with intercalation properties replaced by a thin layer of platinum acting catalytically to facilitate the redox reaction. In the work of Orel et al. the standard chromophore-host model is being substituted by redox electrolyte based on triiodide/iodide redox pair. Characteristic feature of I_3^-/I^- electrolyte is the ability to perform following redox reaction

$$I_3^- + 2e^- \leftrightarrow 3I^- \tag{2.2}$$

ensuring the electrical contact between the two halves of the HEC device, at the same time providing I_3^- (formed at the Pt electrode during colouring) and I^- ions (formed at the WO_3 side during bleaching) which are needed for reversible Li^+ intercalation. The redox pair is formed due to a presence of iodine (I_2), and cations needed for the compensation of the charge (when the WO_3 film is cathodically coloured) are introduced in a form of LiI salt [19-20]. According to Byker the redox material can participate in electron transfer with the electrode in at least three ways; (a) by mass transport to the electrode, (b) via redox hopping (similar to von Grotthuss mechanism as shown in ref. [15]), and finally (c) via mediated electron transfer utilizing a redox material [21].

2.2 *Gel polymer electrolytes for electrochromic devices*

Electrochromic devices incorporate a material that serves to shuttle ions between an electrochromic film and ion storage film (also called counter electrode). One sometimes speaks of a "rocking chair" operation. For the five-layer design in Fig. 2.1 the ion conductor or electrolyte takes the middle position.

With respect to the specific application the electrolyte should comply with following requirements; (a) sufficient ion conductivity (between 10^{-4} and 10^{-7} $S.cm^{-1}$), (b) very low electron conductivity (preferably below 10^{-12} $S.cm^{-1}$), (c) high electrochemical and mechanical stability, (d) good optical properties (persistency against long-term UV irradiation, transparency/translucency). By its nature the electrolyte can be liquid, solid (inorganic) or polymer (organic). Among others the gel polymer electrolytes (GPEs) are of great interest for ECDs allowing convenient designs incorporating resilient and adhesive layers. In contrast with the liquid electrolytes, there are no obvious problems with liquid and fluid-mechanics-induced distortions, and in contrast with the solid electrolytes the complexities (stoichiometry and crystallinity control) during preparation of the thin layers from multielement materials can be avoided. On the other hand one has to pay attention to the drawbacks of GPEs; lower conductivity and propensity to degrade upon UV irradiation and extensive heating [1].

The gel polymer electrolytes continue to attract attention since their introduction by M. Armand [22]. So far various systems have been extensively investigated and among ECDs applied in high-energy lithium-ion batteries [23], electric double-layer supercapacitors [24], fuel cells [25], and chemical sensors [26]. In principle the gel polymer electrolyte can be classified as the two-phase system composed of ionically conducting medium entrapped in host polymer matrix. The most important ionic conductors are proton (H^+) and lithium (Li^+) based electrolytes. The first one are known for their high conductivity with the H^+ donors originating from e.g. sulphuric (H_2SO_4) or phosphoric (H_3PO_4) acid [1-3]. In the second group mobile Li^+ species are provided by dissolution of lithium perchlorates ($LiClO_4$) [1, 10, 14, 16, 21], triflates ($LiCF_3SO_3$) [21, 27-30], fluorophosphates ($LiPF_6$) or fluoroborates ($LiBF_4$) [1,21] in aprotic solvents. Furthermore the sodium, potassium or ammonium based electrolytes [5, 27] are known. Among others acetonitrile (ACN) [9, 10], propylene (PC) [10, 14, 29, 30] and ethylene carbonates (EC) [30] are the most common choices of aprotic solvents. Moreover the results on electrochromic applications encompassing γ-butyrolactone [bohnke], diethyl (DEC) or dimethyl (DMC) [1] carbonates were also reported. In order to overcome some of the particular drawbacks of afore mentioned systems their mutual conjugations, known as binary or ternary solvents, were employed (EC+PC, DMC+PC+EC, etc) [16, 30]. The polymer matrix ensures desired mechanical properties resulting in self-standing gel polymer electrolyte. Similarly to binary solvent systems we distinguish in between binary and single polymer matrixes. The first one often being a combination of cross-linked poly(propylene) (PP), poly(vinylidene difluoride) (PVdF), poly(tetrafluoroethylene) (PTFE) [31] enhancing the mechanical and adhesive strength, and so called conducting polymer, such as poly(ethylene oxide) (PEO), polyaniline (PANI), poly(methyl methacrylate) (PMMA) [10, 14, 21, 30], etc used to ensure good electrochemical properties. The second group comprises afore mentioned conducting polymers with enhanced mechanical properties, e.g. by the presence of crosslinkers (e.g. EDMA) [14, 21]. Furthermore, poly(2-hydroxyethyl methacrylate) [16] or methacrylate copolymers with poly(ethylene glycol), poly(propylene glycol) [9, 27-29] or other polymers like polyepoxides [28, 32] were also suggested for application in ECDs. Besides the electrochromic devices working on an intercalation

principle, also hybrid electrochromic devices based on redox systems such as iodide-iodine [19, 20] or viologene [18] were reported. The ionic liquids were also employed in electrochromic devices by Lu [33] and Marcilla [34]. Concerning gel polymer electrolyte fabrication there are two main approaches; first one being time consuming-casting the solution of a monomer and a co-solvent (e.g. EtOH, MeOH), which evaporates afterwards, onto a PTFE or ITO/FTO substrate. Resulting membrane can be either soaked by electrolyte or can have an electrolyte (plasticizer) dispersed in the initial composition. The second one is direct monomer polymerization of the monomer-initiator-electrolyte mixture (excluding EtOH solvents). The polymerization can be initiated by heat (AIBN, Dibenzoyl peroxide), electron beam or UV (BEE, Irgacure 184®) irradiation and can take place *in-situ* or *ex-situ* of ECD [14-16, 28-31].

2.3 *Similarities between battery-type ECDs and thin film batteries*

Looking at the cross-section of an electrochromic device from Fig. 2.1 one realizes that a battery-type ECD is in fact a rechargeable thin film battery (rocking chair) with transparent electrodes. The similar features and differences of electrochromics and rechargeable thin film batteries are reviewed in following table.

Table 2.1 Comparison of essential operating features and requirements for electrochromic devices and rechargeable Li-ion batteries [5].

Characteristic, requirements	ECDs	Rechargeable thin film batteries
Energy and charge density	Low, the essential characteristic is the colouration efficiency, CE > 150 cm^2/A is desired	High energy and charge density are required > 100 Wh/(kg)
Open circuit voltage (V_O)	As low as possible, V_O < 1 V, a high V_O leads to decrease of a cycling life time	V_O should be high ~ 2 – 3 V for the single cell, 4 V can be achieved
Optical properties	High contrast ratio also in the near IR, different colour tinting	Without importance
Porosity	Very disadvantageous, leads to scattering and clouding	Advantage for the intercalation properties, leads to increasing energy and power density
Speed of charge and discharge	Should be high, high diffusion coefficient and migration rate lead to increase of switching rate	Should be high, leads to
Cycle life	Cycle number > 10^5 cycles	Should be high but often < 1000 cycles
Electronic conductivity	Should be high in both cases, depends on the degree of intercalation therefore changes during the switches	
Polymer or gel electrolyte	No electronic and high ionic conductivity (10^{-3} – 10^{-4} $S.cm^{-1}$), transparent and with a good adhesion on a glass, flexible substrate	No electronic and high ionic conductivity, so far as possible > 10^{-3} $S.cm^{-1}$, stringent nonaqeous
Discharge depth	A deep discharge is necessary to achieve a high transmittance in the bleached state	Deep discharge must be avoided, leads often to decrease of the life time, irreversible changes of the structure of the host substances
Collector electrodes	Must be transparent, for smart windows FTO is preferred, problem: high sheet resistance (~18 Ω/□), for structured devices (displays) ITO is used	Use of graphite or special carbon electrodes which exhibit a good electronic conductivity

According to Heckner and Kraft the similar features of electrochromic and rechargeable thin film batteries concern the material properties (intercalation capability), structure of the layers, kinetics and mechanism of switching (charge/discharge cycles), energy and power density, extended open circuit memory and other electrochemical parameters, e.g. a high exchange current density. High electron transfer rates between collector electrodes and active layers, a good electron and ion conductivity within the active layers and high ion conductivity of the polymer electrolyte present much analogous features too. Essential differences concern the charge density in relation to the efficiency, the open circuit voltage V_O, the requirements in regard to porosity, the cycling life time, the discharge depth and the electrical and optical properties of collector electrodes and active layers [5].

2.4 *Ionic conductivity and conduction mechanism*

The conductivity of conducting materials with all different charge carriers can be represented by the following equation:

$$\sigma = \sum_i z_i n_i \mu_i \tag{2.3}$$

where σ (κ for liquid electrolytes) is specific ionic conductivity ($S.m^{-1}$), i.e. the charge transport across a unit cross sectional area per second per unit electric field applied. μ_i represents the ionic mobility; n_i and z_i are the number of each kind of carrier and its charges, respectively. The overall ionic conductivity is the total sum of the contribution from different charge carriers [1, 35, 37].

2.4.1 Liquid electrolytes (LEs)

The liquid electrolytes comprise a solute in a solvent. The salvation of the solute can be described in terms of Born's equation of electrostatic energy of salvation E_{el}

$$E_{el} = (N_A z^2 e^2 / 2r_i) \cdot (1 - \varepsilon_S^{-1}) \tag{2.4}$$

where z is the charge of the ions, r_i is the radius, N_A is Avogadro's number, and ε_S is the dielectric constant of the solvent [1, 35, 37].

For dilute electrolyte solutions, the conductivity κ is proportional to the concentrations of the constituent ions as follows:

$$\kappa = \sum |z_i| F \mu_i c_i = \sum \lambda_i c_i \tag{2.5}$$

here μ_i is the electric mobility of ion i and the proportionality constant $\lambda_i (= |z_i| F \mu_i)$ is the ionic conductivity or the molar conductivity of ion i.

If a strong electrolyte, consisting of v_+ pieces of cation B^{z+} and v_- pieces of anion B^{z-}, is dissolved to prepare a solution of concentration c ($mol.m^{-3}$), the following relation exist:

$$v_+ z_+ = -v_- z_- = v_- |z_-|, \; c = \frac{c_+}{v_+} = \frac{c_-}{v_-} \tag{2.5.1}$$

where c_+ and c_- are the concentrations of B^{z+} and B^{z-}, respectively. By substituting these relations in eq. (2.5), we obtain

$$\kappa = (u_+ + u_-) z_+ v_+ F c = (u_+ + u_-) |z_-| v_- F c = (v_+ \lambda_+ + v_- \lambda_-) c \tag{2.5.2}$$

The value Λ, given by eq. (2.5.2), is the molar conductivity of an electrolyte:

$$\Lambda = \frac{\kappa}{c} = (u_+ + u_-)z_+v_+F = (u_+ + u_-)|z_-|v_-F = v_+\lambda_+ + v_-\lambda_- \quad (2.6)$$

If the conductivity κ and the electrolyte concentration c are expressed in the respective SI units, the unit for the molar conductivity Λ is $S.m^2.mol^{-1}$. However, κ, c and Λ are often expressed as $S.cm^{-3}$, $mol.dm^{-3}$ and $S.cm^2.mol^{-1}$ respectively; in this case eq. (2.6) is replaced by:

$$\Lambda = \frac{1000\cdot\kappa}{c} \quad (2.7)$$

If Λ, λ_+ and λ_- at an infinite dilution are expressed by Λ^∞, λ_+^∞ and λ_-^∞, respectively,

$$\Lambda^\infty = v_+\lambda_+^\infty + v_-\lambda_-^\infty \quad (2.7.1)$$

Due to the influence of ion-ion interactions the values of Λ, λ_+ and λ_- decrease with increasing electrolyte concentration. Kohlrausch found the following experimental relation for dilute solutions of strong electrolytes:

$$\Lambda = \Lambda^\infty - kc^{1/2} \quad (2.7.2)$$

where k is a constant. A similar relation has been obtained theoretically. According to Debye-Hückel-Onsager limiting law:

$$\Lambda = \Lambda^\infty - (A\Lambda^\infty + B)c^{1/2} \quad (2.8)$$

where A and B are parameters that depend on ionic charges, viscosity and relative permittivity of solvent, and temperature. If we plot the value of Λ against $c^{1/2}$, we receive the approximate value of Λ^∞. In order to get the values of λ_+^∞ and λ_-^∞, we use transference numbers. The transference numbers is the fraction of the current carried by a given ion. The transference number of ion i, t_i is expressed by:

$$t_i = \frac{|z_i|\mu_i c_i}{\sum|z_i|\mu_i c_i} = \frac{\lambda_i c_i}{\sum\lambda_i c_i} \quad (2.9)$$

For a 1:1 electrolyte we receive

$$t_+ = \frac{u_+}{u_+ + u_-} = \frac{\lambda_+}{\lambda_+ + \lambda_-}, \quad t_- = 1 - t_+ \quad (2.9.1)$$

For the solution of a weak electrolyte, the $\Lambda - c^{1/2}$ relation is quite different from that for the solution of a strong electrolyte. If a weak electrolyte consists of v_+ of cation B^{z+} and v_- of anion B^{z-}, the following relations exist:

$$\kappa = a(v_+\lambda_+ + v_-\lambda_-)c, \quad \Lambda = a(v_+\lambda_+ + v_-\lambda_-) \quad (2.10)$$

where a is the degree of dissociation of the electrolyte. If a is small enough, the dissociated ions are dilute and behave ideally. In this case:

$$a \approx \Lambda/\Lambda^\infty \quad (2.10.1)$$

For a 1:1 electrolyte, the apparent dissociation constant K' is given by

$$K' = \frac{a^2c}{1-a} \approx \frac{\Lambda^2 c}{\Lambda^\infty(\Lambda^\infty - \Lambda)} \quad (2.11)$$

We can get an approximate value of K' from eq. 2.11 by measuring Λ and c. If we consider the effect of concentration on behaviour of dissociated ions, we receive from (2.8):

$$a \approx \Lambda/\left[\Lambda^\infty - (A\Lambda^\infty + A)(ac)^{1/2}\right] \quad (2.12)$$

Generally in liquid electrolyte solutions the conduction is induced by ion migration with respect to outer electric field. In principle positively charged ions or ionic clusters (undissolved or partially dissolved solute) move towards negatively and negatively charged carriers towards positively charged electrode. When the electroneutral molecule or an ionic cluster is exposed to an electric field the charge inside the molecules rearranges with respect to the applied electric field building up an electric dipole (this is called an electron polarization). Electron polarization influences the permittivity of the electrolyte resulting in change of solution reactance (especially in a high frequency region) [1, 35, 36].

2.4.2 Polymer electrolytes (PEs)

In the polymer electrolytes (apply to both; solid and gel polymer electrolytes) the charged carriers are in form of single cations, single anions, or the ion clusters depending on a degree of solubility. Ionic conduction is achieved by the movements of ions associated with polymer segment or through amorphous region with the increased presence of the solvent. The mobility of the charge carriers is determined by their environment. It is a function of interaction with polymer and other ions, the nature of the charge carrier and flexibility of polymer segment.

Number of interpretations has been introduced concerning the ion transfer mechanism inside polymer electrolytes, but there is still no clear picture of the movement of ion inside the polymer electrolyte by now. Armand suggested a hopping mechanism with only cations (Li, Na, K) moving down channels within PEO helical crystalline structure (assuming no anion motion). This model cannot explain the ion motion in amorphous regions [22]. Gray suggested another principle of the ion movement associated with the polymer segmental motions via making and breaking the coordination bonds between cations and polymers, resulting in more free volume for ion migration under the electric field. Considering the ion-ion interaction and different ionic species in polymer electrolyte, she proposed two types of ionic motions (a) the ion motion assisted by polymer chain motion and (b) the ion motion from ionic cluster to ionic cluster with polymer chains acting as anchor points [37].

2.4.3 Gel polymer electrolytes (GPEs)

In the gel polymer electrolyte the conduction is strongly influenced by the presence of immobilized solvent in the polymer matrix. In such polymer-solvent-salt systems, the polymer acts as a stiffener for the solvent which solvates the salt and acts as the conduction medium. Increasing the equivalent weight of a solvent-polymer ratio on behalf of the solvent in the system we create highly amorphous domains permitting fast ion movement through the bulk. It was proved by Bohnke for concentration of PMMA, in the PMMA-$LiClO_4$-PC system, lower than 30-35 wt% the polymer matrix can be considered as a passive element of the conductance. The two conduction paths were postulated; (a) for low concentration of polymer (i.e. lower than 30 wt%) the gel electrolyte can be considered as made of liquid electrolyte encaged in a matrix of polymer (electroactive species can migrate through the solvent domain surrounding the matrix polymer) and (b) for high concentrations of polymer (i.e. higher than 30 wt%) some strong interaction may be created between the polymer chains and the electrolyte [38,39]. The latter case leads to a restricted ion motion resulting in the conductivity decrease. In such case the conductivity would most probably be a product of cumulative contribution of both; ionic motion suggested by Gray and heterogeneous nature of gel polymer electrolyte postulated by Bohnke.

References

[1] GRANQVIST, C. G. *Handbook of Inorganic Electrochromic Materials*. The Netherlands: Elsevier, 1995. 2 sv. (337, 296 s.). ISBN 0-444-89930-8.

[2] AVENDANO, E. Electrochromism in Nickel-based Oxides. Coloration Mechanism and Optimization of Sputter-deposited Thin Films. Sweden: Uppsala University Library, 2004. 125 s. Uppsala University. Dissertation. ISBN 91-554-5996-X.

[3] AZENS, A., et al. Flexible foils with electrochromic coatings: science, technology and applications. In *Material Science and Engineering*. The Netherlands: Elsevier, 2005. B 119. s. 214-223.

[4] NIKLASSON, G.A., GRANQVIST, C.G. Electrochromics for smart windows: thin films of tungsten oxide and nickel oxide, and devices based on these. In *Journal of Material Chemistry*. United Kingdom: RSC Publishing, 2007. 17. s. 127-156.

[5] HECKNER, Karl-Heinz, KRAFT, Alexander. Similarities between electrochromic windows and thin film batteries. In *Solid State Ionics*. The Netherlands: Elsevier, 2002. 152-153. s. 899-905.

[6] GRANQVIST, C.G. *Electrochromism and Electrochromic Devices*. United Kingdom: CRC Press, 1997. The CRC Handbook of Solid State Electrochemistry, s. 587-613. ISBN 0-8493-8956-9.

[7] *Sage Electrochromics – Technology* [online]. [2008] [cit. 2008-09-01]. Available from WWW: <www.sage-ec.com>.

[8] LIN, T.H., HO, K.CH. A complementary electrochromic device based on polyaniline and poly(3,4-ethylenedioxythiophene). In *Solar Energy Materials and Solar Cells*. The Netherlands: Elsevier, 2006. 90. s. 506-520.

[9] SESHADRI, V., et al. Optimization, preparation, and electrical short evaluation for 30 cm^2 active area dual conjugated polymer electrochromic windows. In *Organic Electronics*. The Netherlands: Elsevier, 2007. 8 s. 367-381.

[10] TUNG, T-S, HO, K-CH. Cycling and at-rest stabilities of complementary electrochromic device containing poly(3,4-ethylenedioxythiophene) and Prussian blue. In *Solar Energy Materials and Solar Cells*. The Netherlands: Elsevier, 2006. 90. s. 521-537.

[11] WANG, J-Y, et al. Influence of colouring voltage on the optical performance and cycling stability of a polyaniline-indium hexacyanoferrate electrochromic system. In *Solar Energy Materials and Solar Cells*. The Netherlands: Elsevier, 2008. 92. s. 112-119.

[12] KRAFT, Alexander, et al. Electrodeposition and electrochromic properties of N-ethyl substituted poly(3.4-ethylenedioxypyrrole). In *Electrochimica Acta*. The Netherlands: Elsevier, 2007. 52. s. 5856-5862.

[13] SYRRAKOU, E., et al. Eco-efficiency evaluation of a smart window prototype. In *Science of the Total Environment*. The Netherlands: Elsevier, 2006. 359. s. 267-282.

[14] PAPAEFTHIMIOU, S., et al. Development of electrochromic evacuated advanced glazing. In *Energy and Buildings*. The Netherlands: Elsevier, 2006. 38. s. 1455-1467.

[15] NAGAI, Junichi, et al. Durability of electrochromic glazing. In *Solar Energy Materials and Solar Cells*. The Netherlands: Elsevier, 1999. 56. s. 309-319.

[16] VARSHNEY, P., et al. Photo-polymerized films of lithium ion conducting solid polymer electrolyte for electrochromic windows (ECWs). In *Solar Energy Materials and Solar Cells*. The Netherlands: Elsevier, 2003. 79. s. 449-458.

[17] CINNSEALACH, R., et al. Coloured electrochromic windows based on nanostructured TiO_2 films modified by adsorbed redox chromophores. In *Solar Energy Materials and Solar Cells*. The Netherlands: Elsevier, 1999. 57. s. 107-125.

[18] LIN, Chiao-Fen, et al. A complementary electrochromic system based on a Prussian blue thin film and a heptyl viologen solution. In *4th Advanced Batteries and Accumulators*. Brno: BUT Brno, 2002. s. 16-1-16-4.

[19] JOVANOVSKI, V, LAVRENČIČ ŠTANGAR, U, OREL, B. Urethanosil ionic nanocomposite gel conductors with an ionic liquid: redox electrolytes for electrochemical devices. In *Acta Chimica Slovenica*. Slovenia: Slovenian Chemical Society, 2004. 51. s. 47-57.

[20] ŠURCA VUK, A., et al. In situ resonance micro-Raman and UV-visible spectroelectrochemical studies of an electrochromic device with an I_3^-/I^- redox sol-gel electrolyte. In *Solid State Ionics*. The Netherlands: Elsevier, 2003. 165. s. 247-255.

[21] BYKER, Harlan J. Electrochromic and Polymers. In *Electrochimica Acta*. The Netherlands: Elsevier, 2001. 46. s. 2015-2022.

[22] ARMAND, M.B., CHABAGNO, J.M., DUCLOT, M. *Fast ion Transport in Solids. Electrodes and Electrolytes*. Vashitsha et al. The Netherlands: North Holland Publishers, 1979. Poly-ethers as solid electrolytes, s. 131.

[23] NAIR, J.R., et al. UV-cured methacrylic membranes as a novel gel-polymer electrolyte for Li-ion batteries. In *Journal of Power Sources*. The Netherlands: Elsevier, 2008. 178. s. 751-757.

[24] LIU, X.J., OSAKA, T. Properties of electric double-layer capacitors with various polymer gel electrolytes. In *Journal of Electrochemical Society*. USA: Electrochemical society, 1997. 144. s. 3066-3071.

[25] APARICIO, M., et al. Proton-conducting methacrylate–silica sol-gel membrane containing tungstophosphoric acid. In *Journal of Power Sources*. The Netherlands: Elsevier, 2005. 145. s. 231-236.

[26] JANATA, J., et al. Chemical sensors. In *Analytical chemistry*. USA: ACS, 1998. 70. s. 179-208.

[27] DI MARCO, G., et al. Solid state electrochromic device: behaviour of different salts on its performance. In *Solid State Ionics*. The Netherlands: Elsevier, 2000. 127. s. 23-29.

[28] MACFARLANE, D.R., et al. Polymer electrolytes for electrochromic window applications. In *Solid State Ionics*. The Netherlands: Elsevier, 1996. 86-88. s. 959-964.

[29] STEVENS, J.R., et al. Polyether-PMM adhesive electrolytes for electrochromic applications. In *Solar Energy Materials and Solar Cells*. The Netherlands: Elsevier, 1994. 39. s. 223-237.

[30] AGNIHOTRY, S.A., PRADEEP, SEKHON, S.S. PMMA based gel electrolyte for EC smart windows. In *Electrochimica Acta*. The Netherlands: Elsevier, 1999. 44. s. 3121-3126.

[31] NASEF, M.M., SAIDI, H., DAHLAN, K.Z.M. Preparation of composite polymer electrolytes by electron beam-induced grafting: Proton- and lithium ion- conducting membranes. In *Beam Interactions with Materials and Atoms*. The Netherlands: Elsevier, 2007. B 265. s. 168-172.

[32] ANDREI, M., et al. Highly conductive solid polymer electrolyte for smart windows. In *Polymer*. The Netherlands: Elsevier, 1994. 35. s. 3592-3597.

[33] LU, W. Stable Conducting Polymer Electrochemical Devices Incorporating Ionic Liquids. In *Synthetic Metals*. The Netherlands: E, 2003. 135-136. s. 139-140.

[34] MARCILLA, R., et al. Tailor-made polymer electrolytes based upon ionic liquids and their application in all-plastic electrochromic devices. In *Electrochemistry Communications*. The Netherlands: Elsevier, 2006. 8 s. 482-488.

[35] LANTROPOV, L. I. *Theoretical Electrochemistry*. Russia: Mir Publishers, 1972. 568 s.

[36] IZUTSU, Kosuke. *Electrochemistry in Nonaqueous Solutions*. Germany: Wiley-VCH, 2002. 352 s. ISBN 3-527-30516-5.

[37] GRAY, Fiona M. *Solid Polymer Electrolytes: Fundamentals and Applications*. USA: VCH Publishers, 1991. 237 s. ISBN 3-527-27925-3.

[38] BOHNKE, O., et al. Fast ion transport in new lithium electrolytes gelled with PMMA. 1. Influence of polymer concentration. In *Solid State Ionics*. The Netherlands: Elsevier, 1993. 66. s. 97-104.

[39] BOHNKE, O., et al. Fast ion transport in new lithium electrolytes gelled with PMMA. 2. Influence of lithium salt concentration. In *Solid State Ionics*. The Netherlands: Elsevier, 1993. 66. s. 105-112.

3 The outline of the thesis

The dissertation deals with the research on the gel polymer electrolytes primarily but not solely designed for use in EC devices, but also in other Li-ion applications (e.g. Li-ion batteries). The following goals have been achieved:

- optimization of the composition, and preparation of the new GPEs
- material and electrochemical research of prepared GPEs
- development of new methods for EC device fabrication and its assembly
- optoelectrochemical testing of the prepared EC devices.

The experimental part of the work is structured into 7 main chapters with a partial summary at the end of each section and overall summary in the chapter 10. Starting with Chapter 4 the list of the materials used for GPE and EC device preparation is shown. An overview of the characterization techniques is further given stressing the electrochemical impedance spectroscopy. The ionic conductivity was considered as a crucial parameter for GPE classification thorough the whole work. In order to understand the ion-conduction mechanism correctly the equivalent circuits of prepared GPEs are proposed and their parameters discussed in relation with experimental temperature. The examples of measured data together with their interpretation are shown.

In chapter 5 the optimization of earlier developed GPE based on poly(methyl methacrylate) is discussed. The conduction mechanism was confirmed by mean of laser optical microscopy. The preparation of the new poly(2-ethoxyethyl methacrylate) and poly(ethyl methacrylate) based GPEs using direct UV or thermal polymerization is described. The effect of sample composition and temperature on the electrochemical and mechanical properties of GPEs is discussed.

Chapter 6 introduces the new concept of ionic conductivity improvement; upon addition of electrically inert nanosized aluminium oxides. The electrochemical behaviour of modified poly(methyl methacrylate) based GPEs with immobilized lithium and sodium ions is discussed together with the theoretical explanation of conductivity improvement.

Chapters 7 and 8 are the key chapters of the thesis. They deal with the implementation of prepared polymer electrolytes into electrochromic and hybrid electrochromic devices. The chemical composition of gels was optimized for use in EC devices. The new approach in EC (*in-situ* direct polymerization) and HEC (vacuum bag lamination) cell fabrication is described. The cells were tested by means of coupled optoelectrochemical techniques using customized testing procedures. The comments on long term testing are included.

The Chapter 9 is about mechanical and rheological properties of prepared gel polymer membranes. The special attention is paid to the adhesion of prepared GPEs towards coated or uncoated glass or flexible substrates. The 180° peel test method was employed according to international ASTM and ISO standards. Moreover the comments on thermal and dimensional stability of discussed systems emerge.

4 Experimental procedures and materials

This chapter gives an overview of materials and experimental techniques. The closer look is given on voltammetry and electrochemical impedance spectroscopy (EIS). A conduction mechanism, the ionic conductivity-temperature relation and the method of EIS data interpretation of prepared samples are discussed in detail. An overview of molecular formulas of the chemicals is given in "Symbols and abbreviation" section. The chemicals were supplied by Sigma-Aldrich® (Germany) and are grouped based on their appearance in particular chapters and chemical analogy.

The chapter is organized in the following order: materials (4.1), characterization techniques for morphological studies (4.2.1), cyclic and linear sweep voltammetry (4.2.2), EIS spectroscopy (4.2.3), UV-VIS spectral (4.2.4), and thermal together with techniques for mechanical analysis (4.2.5).

4.1 *Materials*

A battery grade solvents, propylene carbonate (PC) 99.7% was kept under molecular sieve in a desiccator for two weeks prior it was used. The residual water content estimated by 831 Karl Fischer Coulometer (Metrohm AG) after the two weeks was 9.8 ppm and remained unchanged during the storage period. Ethylene carbonate 99% (EC) and Sulfolane (tetramethylene sulfone, TMS) 99% were used as received.

Monomers, methyl (MMA), ethyl (EMA) and 2-ethoxyethyl (EOEMA) methacrylate (all 99%) were twice distilled under reduced pressure. Commercially available oligomeric resin Superacryl® (SA, Spofa-Dental, CZ) was dried at 60 °C prior use. The resin was composed of poly(methyl methacrylate) (PMMA) particles with a mean diameter of 58.88 μm covered by Dibenzoyl peroxides (0.8 – 0.9 wt%) for initiating the polymerization and 0.05 wt% of fumed silica. The maximal declared particle diameter was 130 μm. Cross-linking agents, ethylene dimethacrylate (EDMA) and 1,6-hexanediol dimethacrylate (hexamethylene dimethacrylate, HexadiMA) were used as received. The UV-polymerization initiator, benzoine ethylether (BEE), was recrystallised from chloroform. The polymerization initiator for heat initiated processes, 2,2'-azobis(isobutyronitrile) (AIBN), was recrystallised from chloroform. All monomers and the initiator were stored at 4 °C. Prior to storage in the glove box, the monomers were purged by argon for 30 minutes, the initiator was pulverised and dried in a vacuum at 25 °C for 2 hours. The synthetisation of unhydrolyzed organic-inorganic precursor ICS-PPG (3-isocyanatopropyltriethoxy silane and poly(propyleneglycol)-bis-(2-amino-propyl)ether) was described elsewhere [1]. The acetic acid ≥ 99.5% (EtOH) was used as received.

An inorganic lithium and sodium perchlorates ($LiClO_4$, $NaClO_4$) and were dried in vacuum for 48 h at 110 °C and stored in a desiccator (all ≥ 99.95%). Lithium iodide (LI) and iodine (I_2) (all ≥ 99.99%) were used as received.

A redox couple, ferrocene/ferrocenium $[Fe(\eta^5\text{-}C_5H_5)_2]/[Fe(\eta^5\text{-}C_5H_5)_2]^+$ ≥ 99.99% was used without pretreatment.

The nanosized fillers, aluminium (Al_2O_3) oxides were dried at 150 °C for 24 hours. The Al_2O_3 was used in the two modifications; whiskers 2–4 nm (diameter) and nanopowder with the particle size up to 47 nm.

A 2B methyl violet indicator for microscopy was used as received.

4.2 *Characterization Techniques*

4.2.1 Morphological Studies

The distribution of the nanosorbent in the bulk of Gel polymer Electrolytes (GEPs) was monitored by monocular optical microscope (OM) Ecovision BP-20/400 (HELAGO, CZE) with 4×, 10× and 40× achromatic and 10(16×) eyepiece objectives. The microscope was interconnected via USB port with PC.

The surface morphology, the layer-substrate intersection and the thickness of the evaporated electrochemical layers were studied using Confocal Laser Scanning Microscope (CLSM) Olympus LEXT 3000 (Olympus, Japan) with the total magnification of 120× to 14400× and 0.12 μm resolution. The sample was illuminated by semiconductor laser ($\lambda = 408\pm5$ nm) and halogen lamp with dichroic (heat shielding) mirror.

The study of miscibility and surface morphology of the GPEs and the superficial morphology of electrochromic layers together with the shape of nanosized oxides were done on the Scanning Electron Microscope (SEM) Philips XL30 CP. Accelerating voltage ranged from 5 to 25 kV, depending on the thickness of the deposited layer and the size of particles.

The dimensional modifications of nanosized oxides were distinguished and confirmed using High-resolution Transmission Electron Microscopy (HRTEM) carried out on a JEOL JEM 3010 microscope operated at 300 kV (LaB_6 cathode, point resolution 1.7Å). Images were recorded on a CCD camera with resolution 1024x1024 pixels using the Digital Micrograph software package.

4.2.2 Voltammetry

Voltammetry is a term used to include all the methods that measure current-potential curves (voltammograms) at small indicator electrodes other than dropping mercury electrode (DME).

The techniques involve perturbing the initial zero-current condition of an electrochemical cell by imposing a change in potential to the working electrode and observing the fate of the generated current as a function of time (or, in some cases, by imposing a current and observing the potential). The most popular types of voltammetric indicator electrodes are disc electrodes. The materials used for disc electrodes are platinum, gold, graphite, glassy carbon (GC), carbon paste, boron-doped diamond, etc. The major benefits of using other than mercury electrode are wide potential window especially on the positive side and the possibility of electrode surface modification.

In principle voltammetry provides information on (a) the kinetics of the electron transfer processes and (b) the thermodynamics of such electron transfer allowing us to understand the redox behaviour of electroactive species [2,3].

Linear sweep voltammetry (LSV)

In linear sweep voltammetry (LSV), a static indicator electrode (A cm^2 in area) is used and its potential is scanned at constant rate v (V.s^{-1}) from an initial value (E_i) in the positive or negative direction (see Fig. 4.1). A typical linear sweep voltammogram is shown in Fig. 4.2. After reaching a peak, the current decreases again.

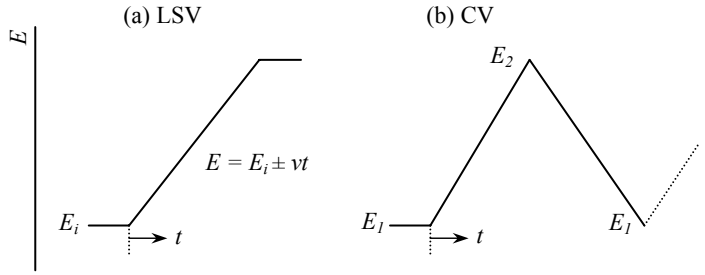

Fig. 4.1 Applied voltage in linear sweep voltammetry (a) and cyclic voltammetry (b) [3].

For a reversible reduction process, the peak current i_p is expressed by Randles-Ševčík equation:

$$i_p = 2.69 \cdot 10^5 \cdot n^{\frac{3}{2}} \cdot A \cdot D_0^{\frac{1}{2}} \cdot c \cdot v^{\frac{1}{2}} \tag{4.1}$$

where i_p is peak current (A), n number of transferred electrons, A area of the electrode, D_o apparent diffusion coefficient (cm^2.s^{-1}), c concentration of the species (mol.cm^{-3}) and v potential scan rate (V.s^{-1}). The constant 2.69×10^5 is calculated for 25 °C measurement temperature.

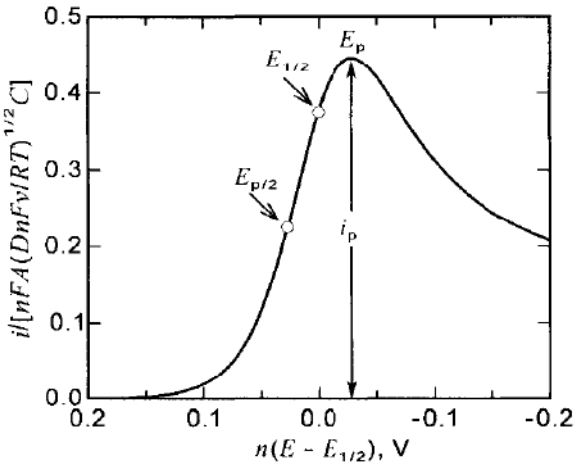

Fig. 4.2 Linear sweep voltammogram for a reversible process; E_p peak potential; $E_{p/2}$ half-peak potential, $E_{1/2}$ half-wave potential, i_p peak current [3].

The peak potential E_p and the half-peak potential $E_{p/2}$ are related to the half-wave potential $E_{1/2}$ in DC polarography [3] by following equations:

$$E_p = E_{1/2} - 1.11\frac{RT}{nF} = E_{1/2} - \frac{0.0285}{n}, \tag{4.2}$$

$$Ep_{/2} = E_{1/2} + 1.09\frac{RT}{nF} = E_{1/2} + \frac{0.0285}{n}, \tag{4.3}$$

$$\left|E_p - Ep_{/2}\right| = 2.20\frac{RT}{nF} = \frac{0.0565}{n} \tag{4.4}$$

where i_p and E_p [V] (or $E_{p/2}$) give quantitative and qualitative information on the electroactive species. i_p is proportional to $v^{1/2}$ (v = voltage scan rate), while the charging current i_{cc} is proportional to v. Thus, the i_p/i_{cc} ratio decreases with v. The constants 0.0285 and 0.0565 are calculated for 25 °C measurement temperature.

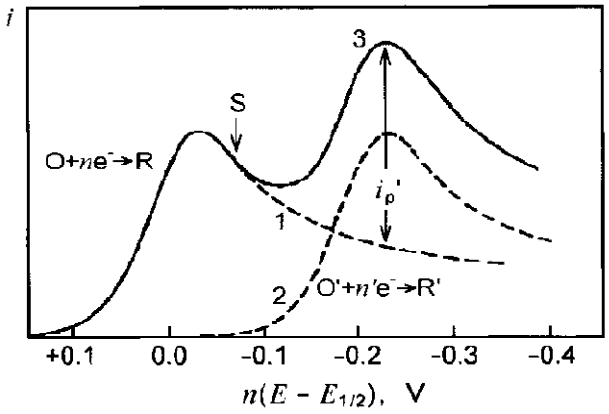

Fig. 4.3 Linear sweep voltammogram for a two-component system [3].

For a totally irreversible reduction process (see Fig. 4.3) the following equations apply:

$$i_p = (2.99 \cdot 10^5) \cdot n(\alpha n_a)^{\frac{1}{2}} \cdot A \cdot D_0^{\frac{1}{2}} \cdot c \cdot v^{\frac{1}{2}} , \tag{4.5}$$

$$E_p = E^{0\prime} - \left(\frac{RT}{\alpha n_a F}\right)\left[0.780 + ln\left(\frac{D_0^{1/2}}{k_s}\right) + ln\left(\frac{\alpha n_a F v}{RT}\right)^{1/2}\right], \tag{4.6}$$

$$\left|E_p - Ep_{/2}\right| = 1.857\frac{RT}{\alpha n_a F} = \frac{0.0477}{\alpha n_a} \tag{4.7}$$

where α is the transfer coefficient, n_a is the number of electrons that participate in the rate-determining step, $E^{0'}$ is the formal potential, k_s is the standard rate constant, and RT/F = 0.0257 at 25 °C. For an irreversible process, the value of i_p depends on α, and, if α = 0.5, it is about 20% smaller than that for a reversible process. The peak potential, E_p, depends on the scan rate (v) and becomes ($30/\alpha\, n_a$) mV more negative for each ten-fold increase in v.

In this method, a wide range of scan rate (v) is possible, i.e. from 10^{-3} V.s^{-1} to 10^3 V.s^{-1} with a conventional apparatus, and up to 10^6 V.s^{-1} or more with a combination of a sophisticated apparatus and an ultra-microelectrode [3].

Cyclic voltammetry (CV)

In cyclic voltammetry (CV), the potential is linearly scanned forward from E_1 to E_2 and then backward from E_2 to E_1, giving a triangular potential cycle (see Fig. 4.1b). Figure 4.4 shows some examples of cyclic voltammograms for the process $Ox + ne^- \leftrightarrow Red$, where only Ox is in the solution. Curve 1 is when the process is reversible. In the forward scan, a cathodic peak is obtained by the reduction of Ox to Red, as in LSV. In the backward scan, an anodic peak appears, due to the re-oxidation of the Red, which was generated during the forward scan. For a reversible process, the cathodic (reverse) and anodic (forward) peak currents are equal in magnitude ($|i_{pc}| = |i_{pa}|$ or $|i_{pr}| = |i_{pf}|$) and the cathodic peak potential E_{pc} (E_{pr}) is ($58/n$) mV more negative than the anodic peak potential E_{pa} (E_{pf}). Moreover, the half-wave potential, which is used to obtain the formal redox potential, is obtained by $E_{1/2} = (E_{pc}+E_{pa})/2$. By decreasing the reversibility, the

difference between the two peak potentials increases. Curve 2 represents considerably irreversible process. Compared with curve 1, the cathodic peak appears at much more negative potential, the anodic peak at much more positive potential. If the process is completely irreversible, the anodic peak does not appear in the measurable potential region. From the irreversible CV curve, we can obtain kinetic parameters (rate constant and transfer coefficient) for the electrode reaction, usually by a simulation method. Curve 3 is for the case in which $Ox \leftrightarrow Red \overset{k}{\rightarrow} A$, i.e. Red can be reversibly re-oxidized to Ox but, before the re-oxidation, some part of the Red is converted to non-electroactive species A. The cathodic peak appears in the same way as in curve 1, but the anodic peak current is smaller than that in curve 1. From the decrease in the anodic peak current, we can get the rate constant k.

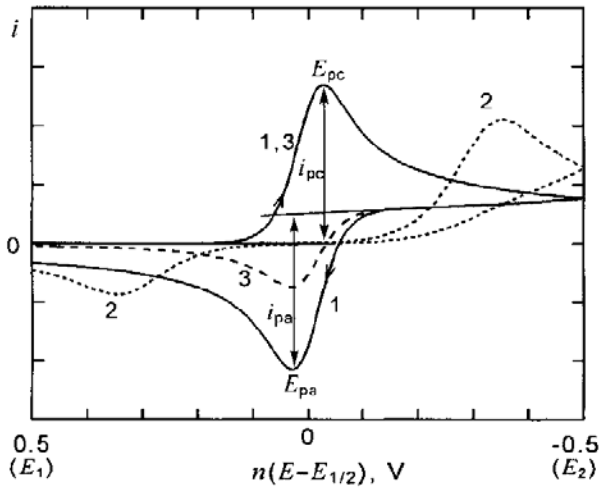

Fig. 4.4 Cyclic voltammograms for the electrode reaction $\boldsymbol{Ox + ne^- \leftrightarrow Red}$, which is reversible (curve 1), irreversible but $\alpha = 0.5$ (curve 2), and reversible but accompanied by a conversion of Red to an electro-inactive species (curve 3). $E_{1/2}$ is for reversible process [3].

In CV, the voltage scan rate can be varied over a wide range, the highest scan rate reaching 10^6 $V.s^{-1}$ or more. Thus, the CV method is applicable to study electrode processes, even when the products or intermediates are very short-lived (< 10 μs). The CV method is often used in non-aqueous solutions [3].

CV and LSV instrumentation

The potentiogalvanostats PGSTAT 12 (30) or 10 μAutolab (both Eco Chemie, The Netherlands) were used for electrochemical measurements. The measuring procedures and data analysis (e.g. magnitude of oxidative and reductive current waves, current peak position, half-wave potential, etc) were managed using the General Purpose System (GPES) module supplied with the potentiogalvanostats.

The electrochemical measurements of liquid systems were performed in a three electrode arrangement [2] with a glassy carbon or platinum electrode (Metrohm; 2.7 mm diameter) as a working and platinum rod as an auxiliary/counter electrode. As a reference electrode a Saturated calomel electrode (SCE; Metrohm) or homemade PMMA-Cd-Cd^{2+} electrode were used. The Cd/Cd^{2+} system was developed in our laboratory for electrochemical investigation of liquid and polymer aprotic systems ($E(Cd/Cd^{2+}) = 2.66$ V vs. Li/Li^+) [4].

Solid-state electrochemical measurements were conducted in the PTFE cell (see APPENDIX A^1 to A^4), based on design earlier proposed by Vondrák and Klápště,

used for investigation of prepared polymer electrolytes. A gold (1.6 mm in diameter) or glassy carbon (3 mm in diameter) rods served as a working electrode (both BASi, USA), a glassy carbon as a counter, and PMMA-Cd-Cd^{2+} solid-state as a reference electrode. The surface of working and counter electrode was polished by abrasives (0.3 alumina, Metroohm, CH) and soft cloth after each measurement.

4.2.3 A.C. Electrochemical Impedance Spectroscopy

Electrochemical impedance Spectroscopy (EIS) is a powerful tool, based on impedance measurements, which can be applied to a variety of electrochemical systems, including those involved in corrosion, electrodeposition, polymer films, and semiconductor electrodes.

This method involves the application of a small perturbation of applied potential or current. The response to the applied perturbation, which is generally sinusoidal, can differ in phase and amplitude from the applied signal. Comparison is made between the electrochemical cell and an equivalent electrical circuit that contains combinations of resistances and capacitances.

A frequently used circuit, called the Randles equivalent circuit, is shown in Fig. 4.5. There is a component representing transport by diffusion (Z_f), a component representing kinetics (R_Ω), and another representing the double layer capacity (C_d). The parallel elements are introduced because the total current through the working interface is the sum of distinct contributions from the faradaic process, i_f, and double-layer charging, i_c. The double-layer capacitance is nearly a pure capacitance; hence it is represented in the equivalent circuit by the element C_d. The faradaic process must be considered as general impedance, Z_f. All of the current passes through the solution resistance; therefore R_Ω is inserted as a series element to represent this effect in the equivalent circuit.

The faradaic impedance can be represented as a pure resistance, R_{ct} the charge-transfer resistance, separated from another general impedance, Z_W, the Warburg impedance, which represents a difficulty of a mass transfer of electroactive species [5,6].

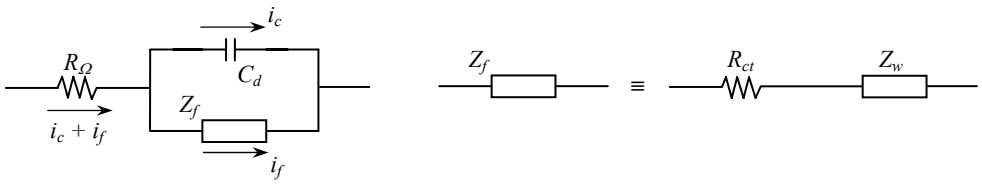

Fig. 4.5 Equivalent circuit of an electrochemical cell (a); subdivision of Z_f into R_{ct} and Z_W (b) [6].

The ionic conductivity of studied polymer systems

The ionic conductivity of polymer electrolyte can be determined by direct current measurements and the alternating current measurements. Alternating current measurement method is a more popular approach because ionic conducting polymers possess both the bulk resistivity, R_b and capacitance capability, C_b. Polymer electrolyte systems are usually quite complicated because they are heterogeneous with both amorphous and crystalline regions and non-uniform salt concentration distribution. The factors have to be considered: the effective pathway of the current is a tortuous

pathway, which is longer than the distance between the two electrodes; higher resistance barriers may exists between the interfaces of the different phases; and the potentially mobile ions are not completely dissociated from each other or free to migrate. All these factors make it difficult to interpret the A.C. measurement data.

Under the assumption that the polymer electrolyte systems are homogeneous and all the mobile ions were assumed to be free to migrate, which did not intimately interact with each other we can make an ideal simplification of real polymer. Since the a.c. response of polymer electrolytes varied with mobile species in polymer electrolyte and electrodes used in the experiment, the polymer electrolytes can be divided into two types according to the mobile species; (a) only one kind of ionic species was mobile and (b), more than one kind of ionic species were mobile. Also the electrodes used in the measurement can be divided into two types: blocking electrodes (the mobile species do not participate in any electrode reaction, such as the platinum electrodes); and non-blocking electrodes (there is finite electrode reaction, such as the lithium electrodes).

The following is the typical A.C. responses of idealized polymer electrolyte under the above mentioned assumption. The migration of the ions and the dielectric polarization of the polymer chain can be represented by a resistor, R_b and a capacitor, C_b, respectively. At the same time each electrode acts like a parallel-plate capacitor, so it can be represented by a capacitor, C_e. For the cells of type (a) or type (b) polymer electrolyte sandwiched between two blocking electrodes, the equivalent circuit can be simplified as shown in Fig. 4.6a. The total impedance of the cell can be expressed by following equation:

$$Z^*_{total} = R_b \left[\frac{1}{1+(\omega R_b C_b)^2}\right] - j\left(R_b \left[\frac{\omega R_b C_b}{1+(\omega R_b C_b)^2}\right] + \frac{1}{\omega C_e}\right) \quad (4.8)$$

where Z^*_{total} is a complex impedance (consisting of a real and imaginary part, $Z^* = Z' - jZ''$), j is a complex number operator ($j = \sqrt{-1}$) and ω is an angular frequency ($\omega = 2\pi f$). The plot of the real part of impedance against the imaginary part gives a Nyquist Plot, as shown in the right part of the following figure. The advantage of Nyquist representation is that it gives a quick overview of the data which allows making qualitative interpretations.

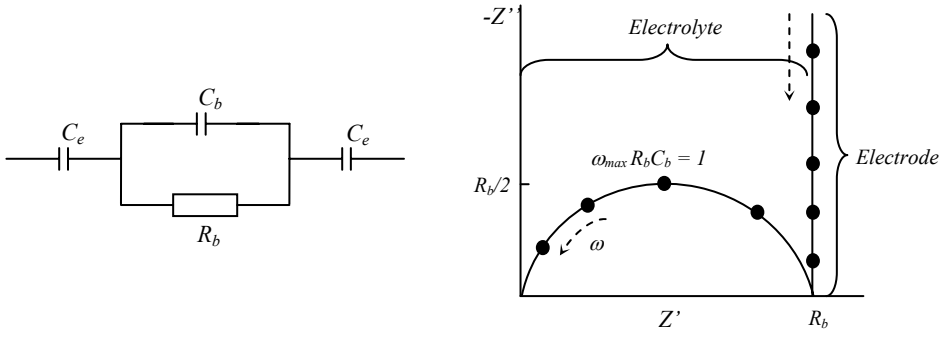

(a) (b)

Fig. 4.6 (a) Schematic representation of a polymer electrolyte/blocking electrode cell, R_b electrolyte resistance; C_b electrolyte capacitance; C_e electrode capacitance and (b) simulated complex impedance plot for the circuit in (a) [7].

Figure 4.6b illustrates the impedance plot from the low frequencies to the high frequencies. At high frequencies, the circuit can be reduced to a parallel R_b, C_b combination and the impedance plot is a semicircle in the complex plane. At low frequencies, the circuit can be reduced to a series R_b and C_b combination and the

impedance plot is a vertical spike displaced by a distance R_b along the real axis. At very low frequency, the circuit can be simplified to the electrode capacitance C_e only.

All the fundamental electrical properties of the polymer electrolytes and the cell such as R_b, C_b and C_e, can be obtained through the following calculations based on the impedance data: R_b (geometry dependent physical term) is determined from the intersection point of the impedance curve with the x axis except the origin; C_b is calculated from

$$C_b = \frac{1}{\omega_{max} R_b} \tag{4.9}$$

at the maximum of the semicircle in impedance plot; C_e is obtained through

$$C_e = \frac{1}{Z'' \omega} \tag{4.10}$$

from any point on the spike.

The specific ionic conductivity σ is dimensional irrelative and describes the material properties. The relationship of the specific ionic conductivity σ with R_b can be represented by a simple form as an equation (4.11) for the measurement setup with polymer electrolytes film sandwiched between two electrodes:

$$\sigma = \frac{l}{R_b A} \tag{4.11}$$

where l (cm) represents the separation distance of the electrodes, A (cm^2) is the area of the electrode and σ ($S.cm^{-1}$) is the specific conductivity.

The above interpretations are all derived from the idealized polymer electrolytes. However, in the impedance spectrum of the real polymer electrolytes, semicircles are significantly broadened and electrode spikes are distinctly non-vertical. The departure of the real A.C. response from the idealized models is attributed to the following factors: surface layers on the electrodes; dielectric relaxation and ion trapping; inhomogeneities in polymer electrolytes; ion and ion interaction; rough electrodes, etc [5-7].

EIS instrumentation

The electrochemical impedance measurements were performed using the Frequency response analyzer (FRA) module of the potentiostat Autolab 12 (Eco Chemie, The Netherlands). The frequency ranged from 100 kHz to 1 mHz depending on the temperature and the nature of the sample. A single sine operation mode of sine wave with the amplitude of 10 mV superimposed onto D.C. polarization potential was used. The impedance response was typically measured over the range -70 to 70 °C (gel polymer electrolytes) and 25 to 60 °C (liquid electrolytes). For measurement at low temperatures the samples were placed in a cylindrical Dewar flask and cooled using solid carbon dioxide. For measuring at a temperature over 25 °C we used thermostated bath (MEMMERT WB 10, Germany). To avoid direct contact with the cooling or heating medium (distilled water in thermostated bath or ethanol in Dewar flask) the electrodes were placed into a silica glass beaker.

For liquid electrolytes, the standard conductivity cell (dimensional constant 0.85 cm^{-1}; Verkon, Czech Republic) with an integrated temperature sensor was used.

The thin membranes of polymer electrolytes were placed between two stainless steel blocking electrodes (A = 1 cm^2) with mechanically polished surface and fixed in a nylon holder. A Pt micro-tip temperature probe attached to the membrane was used to

verify the bulk temperature of the sample. The thickness (l) of the samples varied from 0.4 to 0.9 mm and was measured using a micrometer screw.

The obtained impedance spectrum was analyzed by the Fit&Simulation tool, option of the FRA software, used to simulate the response and produce the values of equivalent circuit parameters [8]. The computation was done based on the non-linear least square method, an approach first published by Boukamp [9].The ohmic resistance (R_b) was pre-determined from the intersection point of the impedance curve with the Z' axis using either a linear or circle approximation. The resulting value was used during the fitting and further converted into a value of specific conductivity according to the equation (4.11).

Ionic conductivity and equivalent circuits of liquid and gel polymer electrolytes at t > 0 °C

Figure 4.7 shows an impedance spectrum of a polymer electrolyte (apply also to the liquid samples). In the chart the two impedance plots of the membrane measured at 60 and 70 °C are displayed. Despite the conventional equivalent circuit, as proposed by Bruce [7], only one non-vertical spike appears regarded to the electrode impedance.

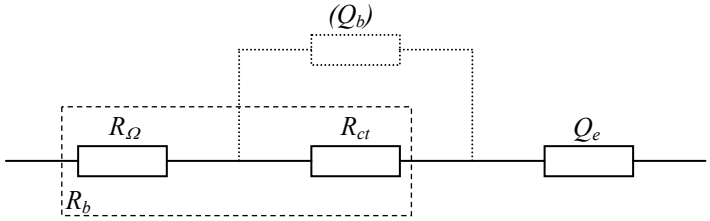

Fig. 4.7 Equivalent circuit for liquid and gel polymer electrolytes measured at t > 0 °C, R_b, the bulk resistance comprises of R_Ω solution and R_{ct} charge transfer resistance, Q_e is the electrode CPE.

At the high frequencies, a typical impedance semicircle assigned to the bulk impedance is surpassed by a R_b element, which encompasses the polymer (solution) resistance (R_Ω) and the charge transfer resistance (R_{ct}), the resistance to the charge carriers driven by the migration forces (see an equivalent circuit in Fig. 4.7). At a very low frequencies, the equivalent circuit can be reduced to R_Ω and Q_e in series appearing as a non-vertical spike displaced by R_b along the real axis. From Figure 4.7, the Q_e is a specific circuit element called a Constant phase element (CPE), which is associated with current and potential distribution over an inhomogeneous electrode surface [10]. The impedance of CPE is defined as:

$$Z = \frac{1}{(j\omega C)^n} \tag{4.12}$$

where C (F) is the ideal capacitance and n is an empirical constant, $0 \leq n \leq 1$. When $n = 1$, CPE acts as an ideal capacitor.

At the temperatures above 0 °C, the equivalent circuit from Fig. 4.7 can be reduced to the serial combination of R_b and Q_e. We propose that the R_{ct} component of R_b is surpassed by R_Ω which means that the overall resistivity is rather induced by the heterogeneous (polymer-solvent) or electrolyte medium than the pure-faradaic charge transfer resistance. Using the FRA software we applied proposed equivalent circuit from Fig. 4.7 to the impedance spectrum (60 °C) from Fig. 4.8 and we received the following circuit parameters; R_b = 62.41 Ω, $Q(Q_e)$ = 2.3 × 10^{-6} S proportional to $\omega^{0.97}$.

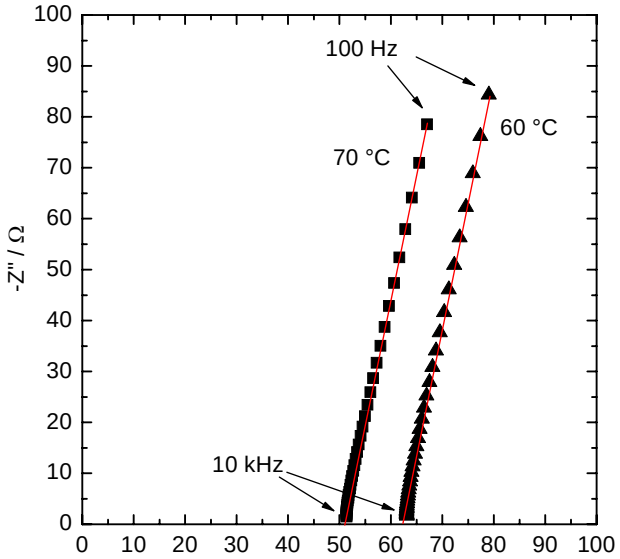

Fig. 4.8 Nyquist plot of MMA/SA gel containing $LiClO_4$ in PC with fitted equivalent circuit impedance (red curves), frequency range from 10 kHz to 100 Hz, measurement temperature 60 and 70 °C.

Ionic conductivity and equivalent circuits of the gel polymer electrolytes at t < 0 °C

The impedance spectrum of the polymer electrolyte measured at -60 °C is shown in Figure 4.10. As the temperature decreases, an impedance spectrum converts to the semicircle at the high frequency region followed by the non-vertical spike at the low frequency region. At the same time the equivalent circuit is transformed into a parallel combination of Q_b and R_{ct} in series with R_Ω and Q_e. The mutual contribution of R_Ω and R_{ct} to the overall sample resistivity can be again bundled into R_b component. The new CPE element Q_b (bulk capacity) represents the dielectric properties of the sample.

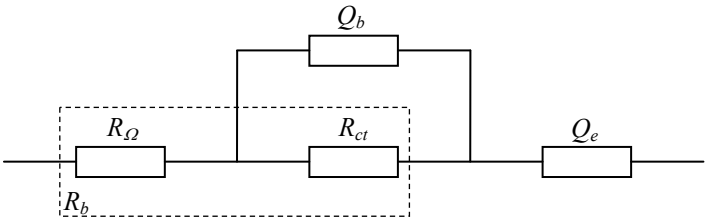

Fig. 4.9 Equivalent circuit for gel polymer electrolytes measured at t < 0 °C, R_b, the bulk resistance comprises of R_Ω solution and R_{ct} charge transfer resistance, Qb is a bulk CPE and Q_e is the electrode (double-layer) CPE.

At high frequencies where the impedance of bulk resistance and capacitance are of the same magnitude the equivalent circuit is reduced to parallel $R_{ct}Q_b$ combination displaced by the R_Ω along the real axis. The Q_b impedance is small but rises as the frequency diminishes. For low frequency the Q_b gives a high reactance but the current passes predominantly through R_{ct} increasing Z' and diminishing Z'', which results in

reduction of the equivalent circuit to a series combination of R_bQ_e giving a rise to the vertical spike. The high reactance of the Q_b (bulk CPE) is a result of a dielectric relaxation caused either by trapped ions (the pathways through the polymer are not available), by the inhomogeneities (uneven salt distribution) or by dipole-dipole interactions. It is important to declare that all later introduced electrolytes are both cationic and anionic conductors. This means that neither cation nor anion covalent bonding to the polymer chain is anticipated.

At the temperature below 0 °C the magnitude of the R_Ω is becoming less significant compared to R_{ct}. Further, when the temperature is decreased under -20 °C the ability of charge carriers to move through the bulk is strongly reduced by the solidification of polymeric network which is remarkable at approx. -55 °C followed later by a solvent's melting point [11]. A closer look at this phenomenon will be presented in chapters 5, 6 and 7. When the equivalent circuit from Fig. 4.9 is applied to the impedance spectrum in Fig. 4.10, we receive the following values; R_b = 53.57 kΩ, $Q(Q_b)$ = 2.19 × 10^{-9} S proportional to $\omega^{0.82}$, and $Q(Q_e)$ = 7.7 × 10^{-6} S proportional to $\omega^{0.78}$.

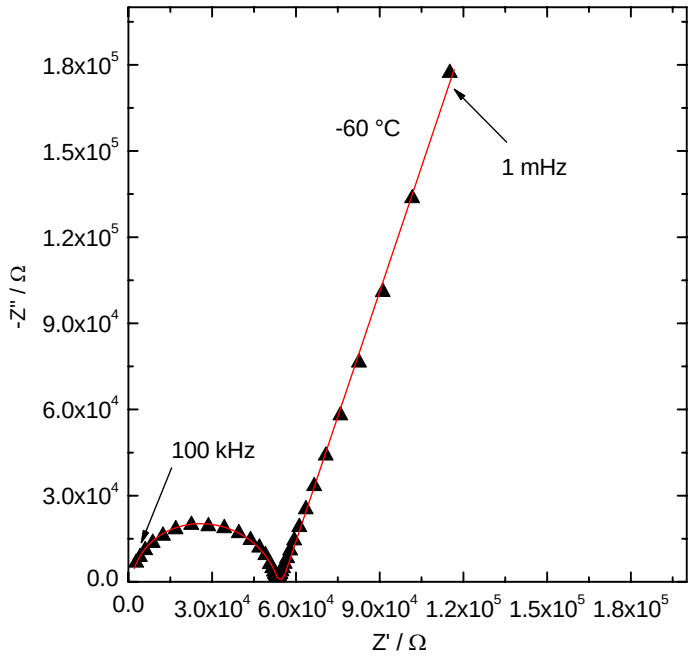

Fig. 4.10 Nyquist plot of MMA/SA gel containing $LiClO_4$ in PC with fitted equivalent circuit impedance (red curve), frequency range from 100 kHz to 1 mHz, measurement temperature -60 °C.

The red abscissas and semicircle in the Nyquist plots (Fig. 4.8 and 4.10) are the results obtained from the Fit&Simulation module of the FRA software. The maximal deviation of modelled impedance response is up to 5% of the experimental values. Usually the individual component parameters are fitted with the minimal 99.5% accuracy.

The specific conductivity-temperature relation and the conductivity data interpretation

The ionic conductivity of polymer electrolytes is strongly dependent on temperature. The conductivity increases with increasing temperature which indicates an activated process. The empirical relationships were developed to fit extensive ionic conductivity data of various electrolytes at different temperatures, which include

Arrhenius law equation, Vogel-Tamman-Fulcher (VTF) equation, Williams, Landel and Ferry (WLF) equation, etc [7].

In the thesis the data are processed using the first two quoted equations. The *Arrhenius law equation* was used to fit the temperature conductivity-dependency of liquid electrolytes and gel polymer electrolytes in a defined temperature range (usually above 0 °C). Arrhenius law equation as shown in equation (4.13) is a basic relationship, which describes the linear relationship of $ln\ \sigma_0$ with 1/T as follows:

$$\sigma = \sigma_0 exp\left(-\frac{E_A}{RT}\right) \tag{4.13}$$

where σ_0 is conductivity at the absolute temperature $T = 0$ K, E_A is the apparent activation energy [J.mol^{-1}], and R is the gas constant.

In order to correlate easier the data with the literature we preferred to use the decadic logarithm expression of Arrhenius formula

$$log_{10}\sigma = \frac{A}{T} + B \tag{4.13.1}$$

where A and B are constants. The Arrhenius activation energy for conduction E_A is then accessible from the parameter k using the formula:

$$E_A = -2.303 \cdot k \cdot R \tag{4.13.2}$$

where k is a slope of a straight line obtained from a linear regression.

Figure 4.11 presents the relationship between the ionic conductivity and temperature of gel polymer electrolyte with $NaClO_4$ salt dissolved in PC. The data are plotted in Arrhenius coordinates (specific conductivity is plotted as a decadic logarithm versus $1000.T^{-1}$ [K^{-1}]). The conductivity data were fitted in the 3 temperature domains; (1) from +70 to 0 °C, (2) from 0 to -70 °C, and (3) from +70 to -70 °C. The activation energies and fitted constants for the system from Fig. 4.11 are summarized in Table 4.1.

Table 4.1 Fitted constants A, r^2 (correlation coefficient) and E_A (Apparent activation energy) obtained from conductivity data for MMA/AIBN gel electrolyte containing $NaClO_4$ in PC and nanosized Al_2O_3 at temperatures ς between -70 and 70°C.

t (°C)	A (K)	r^2	E_A (kJ.mol^{-1})
70 < ς < 0	-1.249	0.993	23.92
0 < ς < -70	-3.402	0.961	65.14
70 < ς < -70	-2.494	0.94	47.76

Within the first region (green line) the conductivity fully obeys Arrhenius law, with the apparent activation energy $E_{A(70 < ς < 0)}$ = 23.92 kJ.mol^{-1} and correlation factor (r^2) approaching 1. The compliance of measured and fitted data continues down to -20 °C where the first change in the slope is observed. This characteristic was observed in all studied systems (PMMA, PEMA and PEOEMA based polymer matrixes) as an endothermic peak during differential scanning calorimetry (DSC). At this point (still above glass transition temperature, T_g) the polymer structure is being transformed from amorphous to more crystalline, accompanied by a steep increase in resistivity. The second region (blue line) hence encompasses two changes in the conductivity curvature. The first one at -20 °C, known as a transformation point [11], and the second one at -55 °C connected with the melting point of plasticizer (PC) which

results an even steeper increase of resistivity. The value of apparent activation energy increases to $E_{A(0 < \varsigma < -70)} = 65.14$ kJ.mol^{-1} and the correlation factor decreases to $r^2 = 0.961$ (see. Table 4.1). For the temperature from +70 to -70 °C the correlation factor reaches the minimal value $r^2 = 0.961$ and the apparent activation energy $E_{A(70 < \varsigma < -70)} = 47.76$ kJ.mol^{-1} .

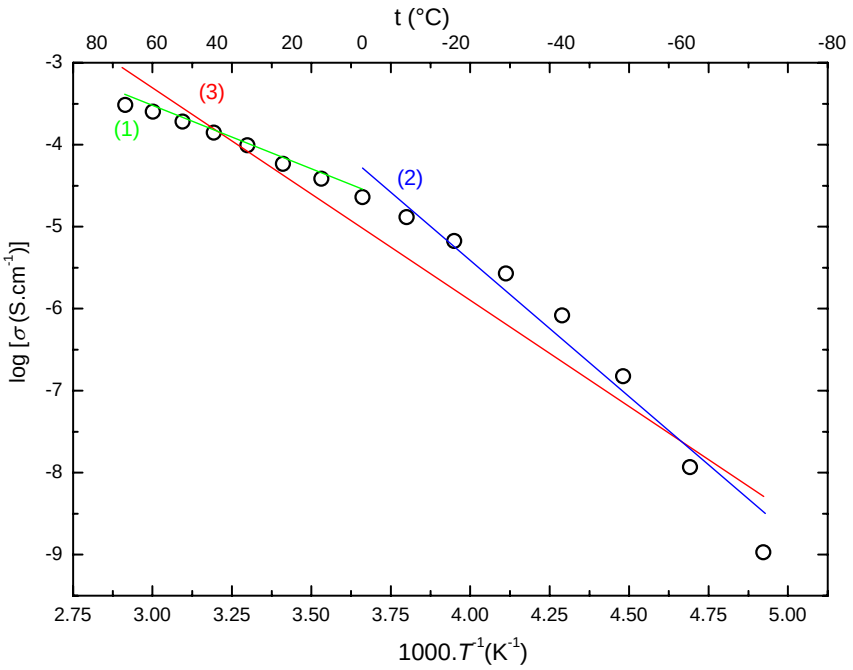

Fig. 4.11 Fitted conductivity of MMA/AIBN gel electrolyte containing 0.1M $NaClO_4$ in PC (black dots) plotted according to the Arrhenius equation using parameters given in Table 4.1. The linear regression was performed in the 3 temperature domains: (1) 70 < ς < 0 (green); (2) 0 < ς < -70 (blue) and (3) 70 < ς < -70 °C (red line).

It is obvious, From Fig. 4.11, that the Arrhenius relationship is *not applicable* within 70 and -70 °C temperature range, particularly when heterogeneous polymers or highly viscous electrolytes are examined. We conclude; (I) from Table 4.1: there are three parts of the conductivity curve that correspond with three Arrhenius relations with three different activation energies; (II) the limiting temperature for PMMA, PEMA and PEOEMA based gel polymer electrolytes are found to be ς ≥ -20 °C ($r^2 \approx 1$) in order to receive satisfactory results. Above this temperature or when fitted separately, the single rate constant Arrhenius law can provide a reliable output.

Though, the accurate description of conductivity-temperature dependence (70 < ς < -70 °C) for afore mentioned polymer systems can be realized by applying the *Vogel-Tamman-Fulcher (VTF) equation* in the following form:

$$ln\left(\sigma T^{\frac{1}{2}}\right) = -\frac{B}{R(T-T_0)} + lnA \qquad (4.14)$$

where A, B and T_0 are fitted constants. The empirical constant A is a pre-exponential factor, which is determined by the transport coefficient and is proportional to the number of charge carriers. T_0 (K) is the temperature at which the free volume disappears and corresponds to an ideal glass transition temperature at the thermodynamic equilibrium. Finally, B is proportional to activation energy of conduction and is accessible from the parameter A using the formula:

$$E_A = -A \cdot R \qquad (4.14.1)$$

here A is a slope of a straight line obtained from a linear regression and R is a gas constant. The glass transition temperature was determined by Dynamic mechanical analysis (DMA), $T_{g(MMA/AIBN)}$ = 193.15 K further discussed in chapter 9.

Figure 4.12 shows the relationship between the ionic conductivity and temperature of gel polymer electrolyte with $NaClO_4$ salt dissolved in PC. This time the data are plotted according VTF coordinates. From the linear regression (Fig. 4.12) and correlation factor $r^2 = 0.999$ (Table 4.2), we assume that the gel polymer electrolytes discussed in the thesis fully obey the VTF temperature-conductivity relationship.

Table 4.2 Fitted constants T_0, A, r^2 (correlation coefficient) and E_A (Apparent activation energy) obtained from conductivity data for MMA/AIBN gel electrolyte containing $NaClO_4$ in PC and nanosized Al_2O_3 at temperatures ς between -70 and 70°C.

t (°C)	T_g (K)	T_0 (K)	A (S.cm^{-1}K$^{1/2}$)	r^2	E_A (kJ.mol^{-1})
70 < ς < -70	183.15	155	-2.632	0.999	21.88

The $E_{A(70 < ς < 0)} = 21.88$ kJ.mol^{-1} from Table 4.2 quantitatively corresponds to $E_{A(70 < ς < -70)}$ = 23.92 kJ.mol^{-1} from Table 4.1 which confirms that the Arrhenius equation is applicable under above specified conditions.

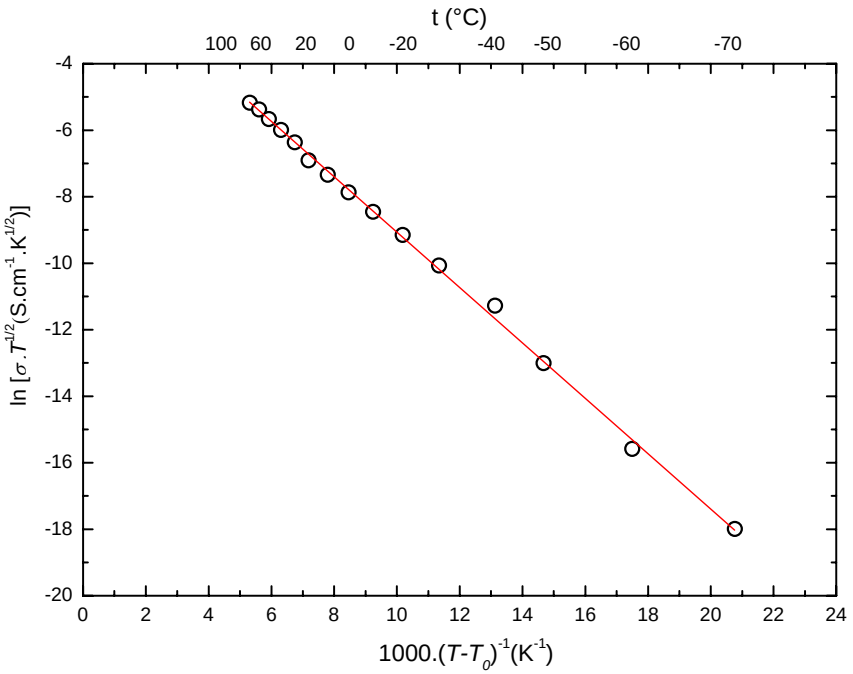

Fig. 4.12 Fitted conductivity of MMA/AIBN gel electrolyte containing 0.1M $NaClO_4$ in PC (black dots) plotted according to the Vogel-Tamman-Fulcher equation using parameters given in Table 4.2. The linear regression was performed within 70 < ς < -70 °C (red line).

The conductivity data in the thesis are displayed in Arrhenius coordinates for easier comparison with the literature. The apparent activation energy data are accompanied by a reference to the temperature region from which the data were taken so to be comparable mutually [10].

4.2.4 UV-VIS Spectral Analysis

UV-visible absorption spectra of the ECDs or the electrodes were conducted either on the Perkin Elmer Lambda 35 UV/VIS or the HP 8452A diode array spectrophotometer. In-situ, UV-visible spectroelectrochemical measurements were made on the same UV/VIS spectrophotometers coupled with the potentiogalvanostat PGSTAT 12 or 30.

4.2.5 Thermal and mechanical analysis

Thermal stabilities of polymer electrolytes were studied by a Thermal Advantage Q500 (TA Instruments, USA) modulated thermogravimetric analyzer (TGA). Samples were carefully weighed to about 20±2 mg in a platinum pan. Both the weight loss curves and the derivative thermogravimetric (DTGA) scans were recorded at a rate 5 or 10 °C/min under a nitrogen atmosphere from room temperature to 600 °C.

Thermal transition temperature and crystalline melting behaviour of the acrylic based GPEs were investigated using a Thermal Advantage Q2000 Differential Scanning Calorimeter (DSC). Samples were scanned in the range of -90 to 250 °C. All the DSC thermograms were recorded at a scan rate of 5 °C/min. All the samples were run twice. After first thermal scanning, samples were quenched to -90 °C using liquid nitrogen and immediately the second thermal scan was performed with the same temperature range as by the first run. The cooling/heating temperature rate was controlled by Refrigerated Cooling System RCS 90.

The visco-elastic (Young Modulus) behaviour and the thermal transition temperatures (Tg) were obtained from Thermal Advantage Q800 Dynamic Mechanical Analyzer (DMA) operating in an isostrain mode. The constant strain was applied with frequency of 1 Hz and amplitude 20 μm. The temperature in the chamber increased from -150 to 150 °C by 5 °C/min. The sub-ambient temperatures were controlled by liquid nitrogen cooling system.

The DMA, DSC and TGA experiments were remotely controlled via universal TA Instrument software. A Glass Transition Temperature (Tg) of studied samples was obtained either as an onset out of the storage modulus (E') curve or as a peak value of the loss modulus (E'') using a peak search tool embedded in the programme. Young's modulus was displayed as a stress versus strain values from a sample displacement.

The tensile properties of polymer electrolyte films were characterized by Twin column Material Testing Machine LS100*Plus* (Lloyd Instruments) with 100 kN load. The gauge length, pre-load and crosshead speed differed among the experiments and were automatically controlled by computer. The approximate values of crosshead speed and pre-load were 50 mm/min and 0.05 N respectively. The experiments were conducted with respect to the international ASTM D903-98 and ISO 8510-2:2006(E) standards for a 180° Peel test.

A viscosity of the liquid electrolyte solutions was measured by Brookfield Viscometer DV-II+ Pro (Brookfield, USA). The spindle number „0“ or „1“ was immersed into a solution and rotates at a constant speed of 60 revolutions per minute. The viscosity and the shear rate/stress were monitored. The torque measurement accuracy was kept below 20% of the scale.

References

[1] LAVRENČIČ ŠTANGAR, Urška, et al. Proton-conducting sol–gel hybrids containing heteropoly acids. In *Solid State Ionics*. 145th edition, 2001. s. 109-118.

[2] ZANELLO, Piero. *Inorganic Electrochemistry: theory, practice and application*. United Kingdom: The Royal Society of Chemistry, 2003. 634 s. ISBN 0-85404-661-5.

[3] IZUTSU, Kosuke. Electrochemistry in Nonaqueous Solutions. Germany: Wiley-VCH, 2002. 352 s. ISBN 3-527-30516-5.

[4] REITER, J., VONDRÁK, J., MIČKA, Z. Solid-state Cd/Cd^{2+} reference electrode based on PMMA gel electrolytes. In *Solid State Ionics*. 177th edition, 2007. s. 3501-3506.

[5] BRETT, Ch. M. A., BRETT, A. M. O. *Electrochemistry: Principles, Methods, and Applications*. New York: Oxford University Press, 1994. 444 s. ISBN 0-19 855388-9.

[6] BARD, A. J., FAULKNER, L. R. *Electrochemical Methods*: *Fundamentals and Applications*. 2nd rev. edition. New York: John Wiley&Sons, 2001. 850 s. 2. ISBN 0-471-04372-9.

[7] MACCALLUM, J. R., VINCENT, Colin A. *Polymer Electrolyte Reviews 1*. Germany: Springer, 1987. 368 s. ISBN 1851660712.

[8] ECO CHEMIE B.V., The Netherlands, Utrecht, Kanaalweg 29-G, *Modular electrochemical instruments (GPES – General Purpose Electrochemical System, FRA – Frequency Response Analyzer System)*, 2001, 115 s.

[9] BOUKAMP, Bernard A. A package for impedance/admittance data analysis. In *Solid State Ionics*. The Netherlands: Elsevier, 1986. 18. s. 136-140.

[10] KREJZA, Ondřej, et al. The presence of nanostructured Al_2O_3 in PMMA-based gel electrolytes. In *Journal of Power Sources*. The Netherlands: Elsevier, 2008. 178. s. 774-778.

[11] VONDRÁK, Jiří, et al. Ion-conductive polymethylmethacrylate gel electrolytes for lithium batteries. In *Journal of Power Sources*. The Netherlands: Elsevier, 2005. 146. s. 436-440.

5 Liquid and gel polymer electrolytes with Li and Na perchlorates

Section 5.1 deals with the liquid $LiClO_4$-PC and $NaClO_4$-PC based systems. The preparation and electrochemical characterization of poly(methyl methacrylate) based gel polymer electrolytes (GPEs) is discussed in section 5.2. The new poly(2-ethoxyethyl methacrylate) and poly(ethyl methacrylate) based GPEs are introduced in section 5.3. The effect of material composition, temperature, cross-linking agent or salt concentration on the electrochemical and mechanical properties of GPEs is discussed with the stress on the ionic conductivity. Finally the results on conductivity and electrochemical stability of acrylic based GPEs are summarized in section 5.4.

5.1 *Propylene carbonate based liquid electrolytes*

A non-aqueous organic solvent, Propylene carbonate (PC), was chosen for its good physical and electrochemical properties. Among others; high dielectric constant ($\varepsilon = 44.14$), low melting point (MP = -48.8 °C), high boiling point (BP = 242 °C) and low toxicity. From electrochemical properties; broad accessible potential window (from -3.5 to +2.5 V vs Fc/Fc^+ electrode; $E(Fc/Fc^+) = +0.39$ V vs SHE) and good compatibility with lithium solutes (e.g. perchlorates, tetrafluoroborates and hexafluorophosphates) and acrylic acids [1-3, 6].

The PC/Li-ion systems are desirable for most of Li-ion based "rocking chair" applications, such as electrochemical Supercapacitors, Lithium-ion batteries or Electrochromic devices [1, 4, 5]. In this work we focused mainly on systems with mobile Li and Na cations. Together with lithium ($LiClO_4$) and sodium ($NaClO_4$), the results on magnesium ($Mg(ClO_4)_2$), zinc ($Zn(CLO_4)_2$) and cadmium ($Cd(ClO_4)_2$) systems were reported [10].

5.1.1 Preparation and appearance

The liquid electrolytes (LEs) were prepared by dissolving exact amount of inorganic perchlorates in PC. The solution was then thoroughly stirred and stored in desiccator. Usually the samples were examined immediately after the preparation in order to prevent contamination with aerial moisture. Prepared solutions were transparent, hygroscopic and odourless. The viscosity, η [cP], of 1M $LiClO_4$ in PC solution at RT (25 °C) was determined at 1.58 cP within 17% of the scale (using spindle #1). The water content was kept below 10 ppm (measured by Karl-Fischer).

5.1.2 Specific conductivity of liquid electrolytes with Li^+ and Na^+ ions

Figure 5.1 shows the conductivity values of $LiClO_4$-PC system with different lithium ion concentration. Basically an increase in conductivity is induces by increase of $LiClO_4$ in the system (see Fig. 5.1A). The impedance measurements showed, that almost three-order increase of conductivity can be caused by addition of lithium into PC in comparison to the samples with pure PC (1.2×10^{-6} see. Table 5.1). The conductivity

increases steadily until it reaches its maximal value $\kappa = 6.1$ mS.cm^{-1} for 1 mol.l^{-1} of $LiClO_4$. Above 1M concentration the conductivity starts to decrease. This is probably caused by insufficient lithium salt dissolution resulting in ion-ion forming. The strong ion-ion pairs or electrically neutral ionic clusters do not further participate on conduction which results in conductivity decrease. A threshold, the concentration of $LiClO_4$ or $NaClO_4$ in PC at which the ionic conductivity begins to fade was found between 0.75 and 1 mol.l^{-1}. Using the equation (2.7) the specific conductivity values were transformed into molar conductivity and plotted versus square root of $LiClO_4$ concentration (see Fig. 5.1B). The molar conductivity data decreases linearly with increasing electrolyte concentration, due to increased ion-ion interactions.

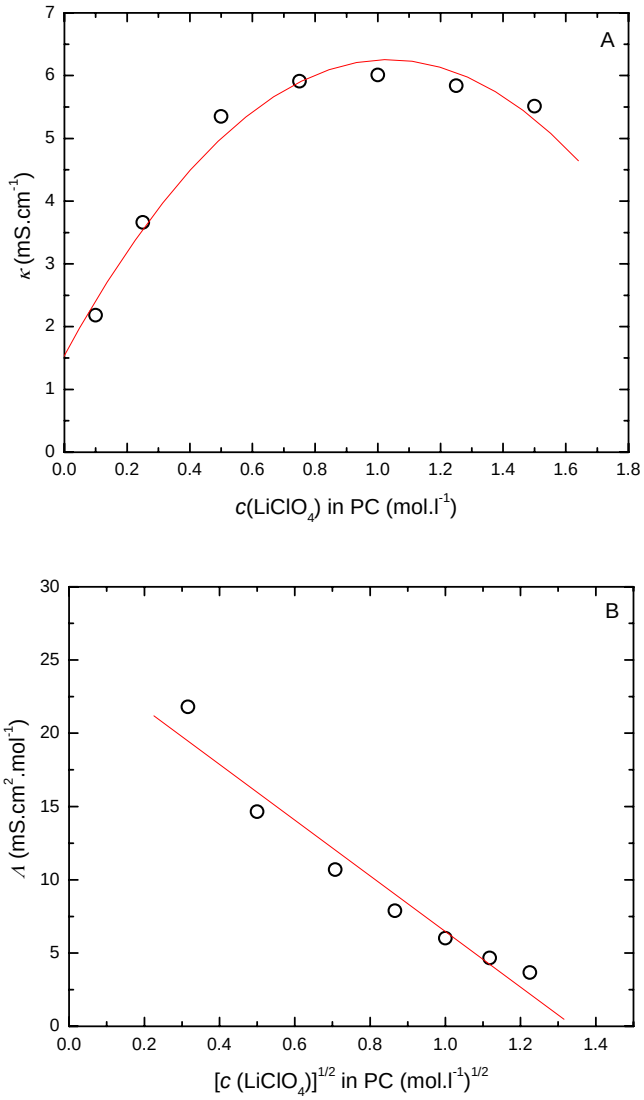

Fig. 5.1 Specific (A) and molar (B) conductivity plot of $LiClO_4$ in PC at a different molar concentrations; red curves represents a polynomial or linear fit for κ-c and Λ-$c^{1/2}$ respectively, measured at RT.

The Arrhenius plot of 0.75M Li and Na perchlorates in PC is shown in Fig. 5.2. Apparently the Li electrolyte shows overall higher conductivity than the one with Na ions. Both curves obey the Arrhenius relationship with apparent activation energies for $LiClO_4$ and $NaClO_4$ in PC to be 12.96 kJ.mol^{-1} and 13.47 kJ.mol^{-1} respectively.

The maximal conductivity values for Li and Na based electrolytes measured at +60 °C were 10.7 mS.cm^{-1} and 9.4 mS.cm^{-1} respectively.

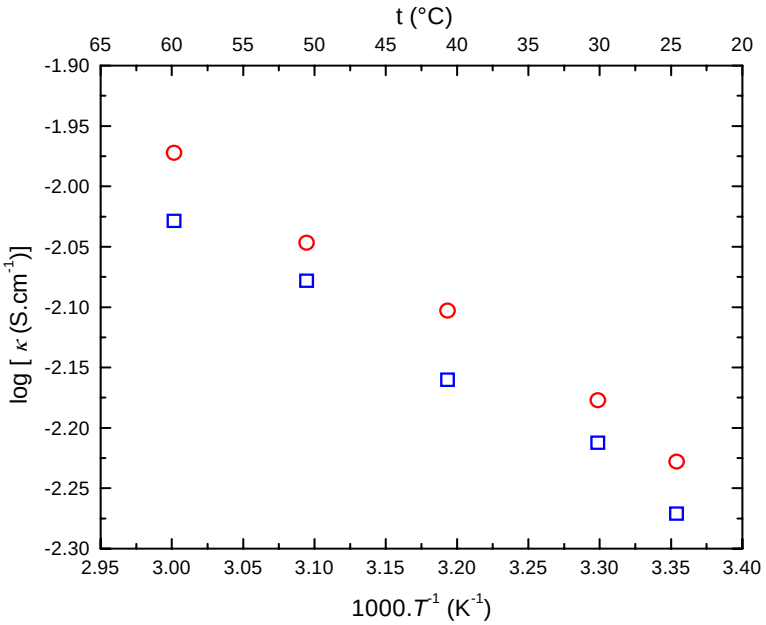

Fig. 5.2 Arrhenius plot of the specific conductivity for 0.75M $NaClO_4$ (squares) and $LiClO_4$(circles) in PC, measured from 25 to 60°C.

In Table 5.1 the overview of specific conductivities for LE with Li and Na ions of is given. We can conclude from Tab. 5.1 and Fig. 5.2 that the electrolyte with dissolved ions of smaller radii demonstrates higher ionic conductivities whereas the movement of Na ions with bigger ionic radii is probably hindered by their surroundings. In our earlier work the systems with dissolved Mg^{2+}, Zn^{2+} and Cd^{2+} ions in the PC were reported [10].

Table 5.1 Specific conductivities of Li and Na perchlorates dissolved in PC, $c_{(Li,Na)}$ = 0.5 mol.l^{-1}, the conductivity of plain PC is included for reference, measured at RT.

Electrolyte composition	κ (S.cm^{-1})
PC only	1.2×10^{-6}
PC-$LiClO_4$	5.4×10^{-3}
PC-$NaClO_4$	4.9×10^{-3}

5.2 *PMMA based GPEs*

Since 1997 our research team has been extensively dealing with an electrochemical research on 3rd generation, poly(methyl methacrylate) (PMMA) based gel polymer electrolytes for several aprotic applications [11,12]. It is a heterogeneous system with a liquid electrolyte entrapped in the polymer network. The host polymer, composed of poly(methyl methacrylate) (PMMA), is swollen by the solvent with mobile Li or Na ions. The diversity of proposed material is given by the preparation method involving commercial available product called Superacryl® (Spofa-Dental, Czech Republic). The gel polymer electrolytes prepared from Superacryl® precursor

demonstrate high ionic conductivity (10^{-3} $S.cm^{-1}$ at RT) and good mechanical properties.

Our earlier work was dedicated to fundamental electrochemical research of PMMA-PC-salt based systems [11,12]. The application of the redox PMMA-PC-LiI-I_2 system in Hybrid electrochromic devices (HECDs) (see chapter 7) was reported [13]. Recently, the incorporation of nanosized oxides (see chapter 6) along with the new techniques of preparation by the means of UV initiation or vacuum-bag lamination of PMMA based GPEs were proposed [14]. Moreover the electrochemical nature of PMMA-PC-Na and PMMA-PC-Li systems is being verified with a Magnetic Resonance Spectroscopy (NMR) or by optical means using methyl violet indicator [15-20].

5.2.1 Preparation

Basically the two *thermally-initiated* and one *UV-initiated* methods of formation the PMMA based GPEs with mobile Li or Na ions were proposed:

PMMA based GPEs prepared from Superacryl® precursor (further referred as ***MMA/SA***)

1. $LiClO_4$ or $NaClO_4$ were carefully weighed and dissolved in propylene carbonate (PC) to receive desired molar concentration.
2. The electrolyte solution was mixed with monomer - methyl methacrylate (MMA) and stirred.
3. Corresponding amount of oligomeric Superacryl® precursor was added to initiate the polymerization.
4. The vial with a solution was shortly shaken in a hand and poured into a Petri dish.
5. The *heat initiated polymerization process* was then finished in an oven at 80 °C for 90 minutes.
6. Alternatively the polymerization can be accomplished by resting the solution in a digester for one week.

PMMA based GPEs prepared by direct MMA thermal initiation (further referred as ***MMA/AIBN***)

1. A polymerization initiator 2,2'-azobis(isobutyronitrile) (AIBN) was dissolved in a mixture of monomer (MMA) and cross-linking agent ethylene dimethacrylate (EDMA).
2. $LiClO_4$ or $NaClO_4$ were carefully weighed and dissolved in PC to receive desired molar concentration.
3. The electrolyte was mixed with the MMA/EDMA/AIBN solution and bubbled with nitrogen for 2 minutes.
4. The vial with a solution was poured into a Petri dish and placed into an oven.
5. The *polymerization process* was then *heat initiated* in the oven tempered at 80 °C and terminated after 100-120 minutes.

PMMA based GPEs prepared by direct MMA UV initiation (further referred as ***MMA/BEE***)

1. $LiClO_4$ or $NaClO_4$ were carefully weighed and dissolved with PC at desired molar concentration.
2. The electrolyte was mixed with the MMA/EDMA solution and bubbled with nitrogen for 2 minutes.
3. The exact amount of polymerization initiator benzoine ethylether (BEE) was added.
4. The solution was covered in order to prevent UV-light exposure and stirred until the BEE was completely dissolved.
5. The solution was injected with the syringe into the custom-made mould comprising of two parallel plates made of glass and poly propylene (PP) distanced by the 0.5 or 1 mm thick silicon spacer (defining the membrane's thickness – l) and secured with clamps (the mould was purged by nitrogen prior filling).
6. The *UV-initiated polymerization process* was terminated after 4 - 4.5 hours under the 2 × 15 W UV-mercury lamp.

It will be seen later that the amount and ratio of initial components determines mechanical properties and influences the chemical stability of the gel. Therefore the optimal composition of PMMA based membranes strongly varied depending on particular membrane utilization. Following table summarizes standard chemical compositions for the PMMA-acrylic systems. In case of MMA/SA based membranes the weight percentage (wt%) is used due to presence of chemically undefined (M_r(SA)) commercial resin. For other systems (MMA/AIBN and MMA/BEE) the initial component ratio is expressed in molar percentage (mol%).

Table 5.2 The chemical composition of PMMA based GPEs with 0.5M $LiClO_4$-PC electrolyte.

Gel Polymer Electrolyte	Chemical composition[1] (mol%) / (wt%)*	Polymer matrix composition (mol%) / (wt%)*
MMA/SA	MMA/PC/$LiClO_4$ 62.9/35.5/1.6*	MMA/SA 66.7/33.3*
MMA/AIBN	MMA/PC/$LiClO_4$ 57.7/40.5/1.7	MMA/EDMA/AIBN 98.7/0.3/1
MMA/BEE	MMA/PC/$LiClO_4$ 57.5/40.7/1.7	MMA/EDMA/BEE 98.7/0.3/1

[1] MMA expresses the contribution of the host matrix in the overall sample composition

5.2.2 Basic material characterisation

In the gel polymer electrolytes, the polymer matrix-solvent ratio determines the mechanical and electrochemical properties. We found the amount over 40 mol% of MMA to be sufficient to create self-supporting gel polymer electrolyte with reasonable electrochemical properties. Incoherent gel with high viscosity was received when the amount of MMA decreased below 30 mol%. During preparation, the MMA/AIBN system is virtually homogenous while the Superacryl® prepared gel shows high inhomogeneities caused by dispersed PMMA particles originating from the precursor. The PMMA particles, clearly visible by naked eye immediately after preparation, diminish with no visible residues during the polymerization. Except the surface unevenity of MMA/SA membranes there are no visible differences in between both; heat and UV-initiated systems. In MMA/SA based membranes the polymer linkage was

applied to increase the mechanical stability (see 5.2.5). Following the preparation procedure from 5.2.1 we receive the elastic and sticky membranes of a thickness between 0.5 and 1 mm. The gels show the transmittance of 90 – 93% in a visible spectrum. No visible change in their appearance (i.e. yellowing) was observed when exposed to UV light. The gel is indifferent to water and does not absorb aerial moisture although contains hygroscopic perchlorates. Elasticity and consistence is kept for months, required foils can be easily cut out with no remaining on glass or other tools. When kept on air the PMMA based membranes suffer from solvent evaporation lowering their elasticity and hindering the specific conductivity (detailed in 5.2.3).

5.2.3 The evolution of specific conductivity during polymerization

The evolution of MMA/SA gel conductivity in time is shown in Fig. 5.3. The conductivity and the weight loss were monitored during one week after preparation. The initial conductivity of the blend decreased 2 to 3 times in two days and then remained almost constant. At the end of the investigation the slight increase of conductivity was observed, however, not exceeding 10% of the ultimately monitored value. Apparently, the initial decrease is a result of a sluggish polymerization which is retarded by the presence of PC based liquid component.

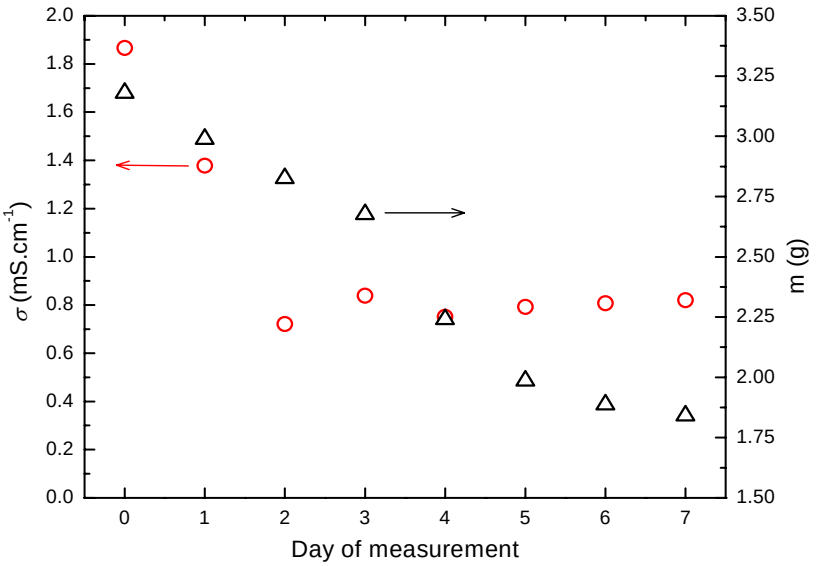

Fig. 5.3 The specific conductivity and bulk weight development of the MMA/PC/$LiClO_4$= 62.9/35.5/1.6 (wt%) gel, 0.5M $LiClO_4$ in PC, measured at RT.

Along with the sample conductivity the weight loss of almost 50% (with respect to its initial value) was recorded. The weight loss is probably connected with the evaporation of solvent commenced when exposed to air. The solvent evaporation diminishes the both; elasticity and conductivity of the gel.

In order to report the impact of storage period on specific conductivity the PMMA based GPEs with both Li and Na ions were examined one week after preparation and then after 16 months of storage in a shelf. The specific conductivity of gels with following composition was measured and the results are summarized in Table 5.3.

Table 5.3 The chemical composition of PMMA based GPEs with 0.1M $LiClO_4$ and $NaClO_4$ in PC, measured at RT.

GPE	Chemical composition (mol%) / (wt%)*	σ(1st week) (S.cm^{-1})	σ(64th week) (S.cm^{-1})
MMA/SA	[1]MMA/PC/$LiClO_4$ 63.7/36.0/0.3*	1.58×10^{-4}	0.72×10^{-4}
MMA/SA	[1]MMA/PC/$NaClO_4$ 63.7/36.0/0.4*	1.78×10^{-4}	0.85×10^{-4}
MMA/AIBN	MMA/PC/$LiClO_4$ 58.5/41.1/0.4	0.22×10^{-4}	0.14×10^{-4}
MMA/AIBN	MMA/PC/$NaClO_4$ 58.5/41.1/0.3	0.38×10^{-4}	0.08×10^{-4}

[1] MMA expresses the contribution of the host matrix in the overall sample composition

We conclude, from Table 5.3, the conductivity decay was more pronounced in MMA/SA (46.7%) than in case of MMA/AIBN (42.1%) gels. At the same time the decrease in conductivity for gels containing $LiClO_4$ was higher (54.7%) than that with $NaClO_4$ (34.1%). In the real applications the electrolyte is encapsulated in order to minimize direct contact with the surroundings.

5.2.4 The dependency of specific conductivity on monomer-solvent ratio

We suggest that the threshold for maximal concentration of inorganic Li and Na perchlorates (as shown in fig. 5.1) is not affected by the presence of methyl methacrylate (MMA). The less polar monomer does not influence the solubility of salt in the system. Therefore the optimal salt-solvent ratio from fig. 5.1 can be adapted also for PMMA based systems.

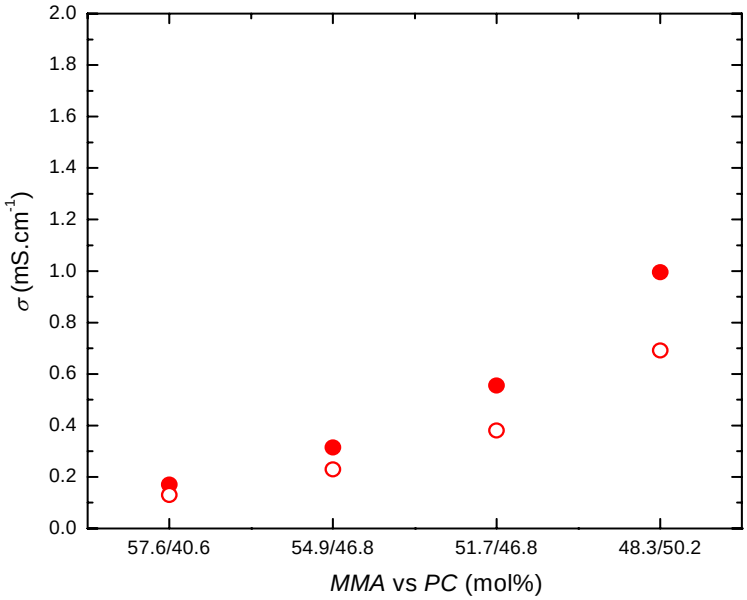

Fig. 5.4 The specific conductivity of MMA/AIBN (full circles) and MMA/BEE (empty circles) gels with different monomer-solvent ratio, 0.5M $LiClO_4$ in PC, measured at 30 °C.

An influence of monomer-solvent ratio on mechanical properties of gels was discussed in chapter 5.2.2. Here the conductivity of 0.5M $LiClO_4$-PC electrolyte with different solvent-monomer ratio was measured and the results are displayed in Fig. 5.4. We found almost exponential increase of conductivity when the monomer-solvent ratio is increased on behalf of PC. The specific conductivity of MMA/AIBN increased almost 6 times from initial 0.17 $mS.cm^{-1}$ at MMA/PC=57.6/40.6 (mol%) to 0.99 $mS.cm^{-1}$ at MMA/PC=48.3/50.2 (mol%). In case of MMA/BEE the conductivity increased more than 5 times from initial 0.13 $mS.cm^{-1}$ at MMA/PC=57.6/40.6 (mol%) to 0.69 $mS.cm^{-1}$ at MMA/PC=48.3/50.2 (mol%). However the composition of both gels was the same, different only in the method of polymer formation, the conductivity of thermal polymerized MMA/AIBN membrane at MMA/PC=48.3/50.2 (mol%) concentration was remarkably higher than that of UV polymerized MMA/BEE membrane.

In the 3rd generation GPEs, the polymer serves as a stiffener raising the viscosity and enhancing mechanical properties. On the other hand the liquid phase is suppressed which results in restricted free-ion movement and consequent decrease of conductivity. Pronounced increase of conductivity in MMA/AIBN system might originate from less-uniform polymer matrix when compared to MMA/BEE (discussed in detail in the chapter 5.2.6).

5.2.5 The effect of cross-linking on the specific conductivity

It is known that the reactive groups in polymers can facilitate cross-linking, thus enhances the physical and chemical integrity. Such changes in mechanical properties with increasing amounts of cross-linking agent appeared to be affected by the chain length and flexibility of the cross-linking agents used. The flexibility of polymer structures formed by dimethacrylates, such as ethylene dimethacrylate (EDMA), increases with an increase in length of the central repeating ethoxy groups. Together with higher tensile strength and improved high temperature mechanics of polymers the Tg is increased.

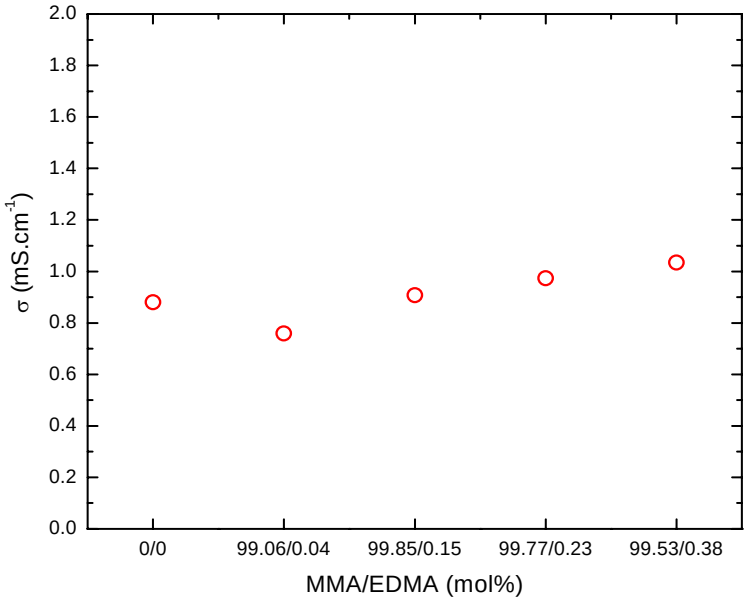

Fig. 5.5 The specific conductivity of MMA/SA gels with different monomer-cross-linker ratio, 0.5M $LiClO_4$ in PC, measured at 30 °C.

The conductivity of 0.5M $LiClO_4$-PC electrolyte with different monomer-cross-linking agent ratio was measured and the results are displayed in Fig. 5.5. The change in the membrane's composition is connected only with polymer matrix; therefore the concentration of MMA/EDMA is expressed in molar percentage. The increase of conductivity to 1.03 $mS.cm^{-1}$ at 0.38 mol% of EDMA vs. MMA solution was observed (initially it was 0.88 $mS.cm^{-1}$).

It has been earlier reported that the high concentration of cross-linking agent in PMMA and 2-hydroxyethyl methacrylate (HEMA) based polymers results in the formation of a close polymer network structure difficult to be swollen by water absorption [7]. Adapted to our system we assume that cross-linking (up to 0.5 mol%) of EDMA decreases polymer chain solubility, positively influences cohesive forces and the stiffness of the polymer matrix (refer to Young modulus values of cross-linked GPEs in 9.2). The polymer is then capable to harbour more solvent, resulting in the slight increase of conductivity, while retaining good structural stability.

5.2.6 Heterogeneity of PMMA based GPEs

From the definition of GPE, a liquid electrolyte immobilized in polymer matrix is believed to create an amorphous system with joint liquid and solid phase. Figure 5.6 shows the Arrhenius plot of the two PMMA based membranes with dissolved 0.1M $LiClO_4$ in PC measured from -70 to 70 °C. Thermally polymerized membranes were prepared in chemical compositions; MMA/PC/$LiClO_4$=62.7/36.0/0.3 for MMA/SA and MMA/PC/$LiClO_4$=58.3/41.5/0.4. Surprisingly higher conductivity was observed in case of MMA/SA than in MMA/AIBN however, the latter had higher amount of PC in monomer-solvent ratio (see Fig. 5.6).

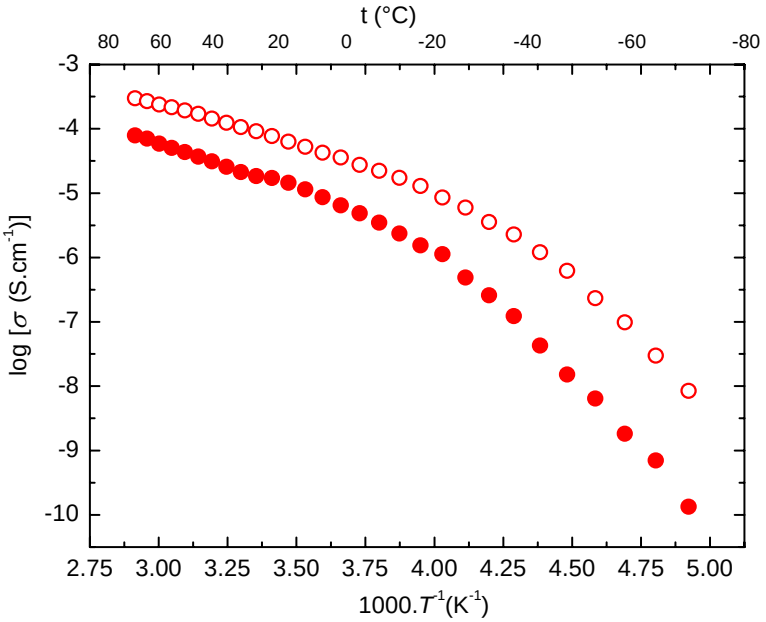

Fig. 5.6 The comparison of MMA/SA (empty circles) and MMA/AIBN (full circles) gels, 0.1M $LiClO_4$ in PC, measurement temperature from -70 to +70 °C.

The apparent activation energy was estimated from linear section (0 to +70 °C) of the curves where both systems appeared to obey single reaction rate constant dependency. Visible change of slope in conductivity curve, due to polymer host solidification appeared at around -20 °C. Using simplified Arrhenius equation (4.13.2),

we received $Ea_{-70<\zeta<70}$(MMA/SA) = 23.9 kJ.mol^{-1} and $Ea_{-70<\zeta<70}$(MMA/SA) = 26.8 kJ.mol^{-1}.

In order to be distinguished in the bulk properties we have added 2B methyl violet in a trace amount into both samples. The methyl violet dye is first evenly dispersed in the blend and lately inhibited during polymerization. Prepared thin slices were checked with optical microscope working in reflected light mode, the scans are displayed in Fig. 5.7. The formation of channels with low PMMA resp. high solvent-salt concentration along the PMMA particles (dispersed white spots) was clearly visible. On the other hand the MMA/AIBN sample showed excellent bulk homogeneity (Fig. 5.7 on the right) with suppressed liquid phase and rather reduced conductivity.

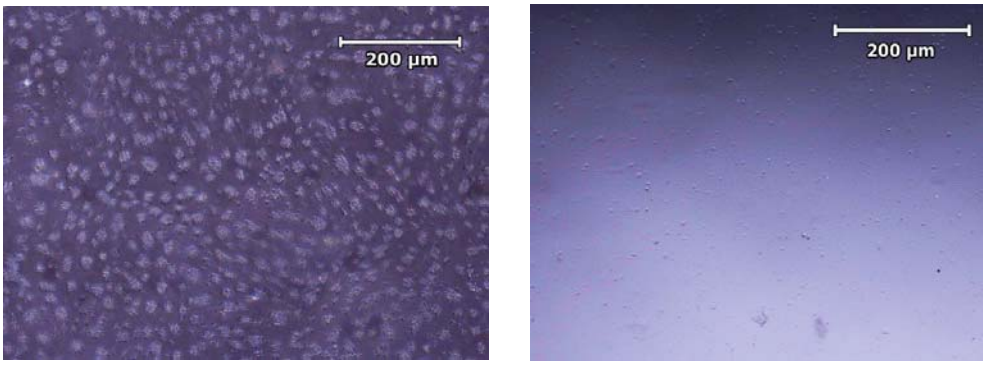

Fig. 5.7 The scan of a typical cross-section of MMA/SA (left) and MMA/AIBN (right) based GPEs with a trace element of 2B methyl violet.

We assume that the gels differ in their properties in several points which indicate the benefit of MMA/SA gels; (a) the specific conductivity is considerably higher (b) formation of conducting channels with high PC concentration between solid PMMA particles must be expected in this case. The nature of Superacryl® based gels seems to be in an agreement with a number of literature definitions of gels as submicroscopic colloidal systems [24,25]. Not only the polymer content, but also the solvent-salt ratio influences both Ea and bulk conductivity. When the activation energies for liquid systems from chapter 5.1.2 are compared with PMMA based electrolytes we see remarkable Ea–sample's nature dependency.

5.2.7 Electrochemical stability on glassy carbon electrodes

The electrochemical stability of GPEs is crucial for the practical use, especially in electrochemical power sources where high energy density, cycle stability and exceptional lifetime is a need (i.e. Li-ion batteries and Supercapacitors).

Voltammetrical measurements of 1M $LiClO_4$ in PC-MMA is shown in fig. 5.8. Higher concentration of supporting electrolyte was chosen to reduce the IR drop (solution resistivity) of the electrolyte. Voltammogram from Fig. 5.8 shows no peaks of either PC decomposition into propane or H_2 or the oxidation of the solvent with CO_2 product. The potential window of MMA/SA gels was estimated to 2V, no irreversible faradaic reaction observed in between -0.2 V to +1.5 V vs $CdCd^{2+}$ reference electrode. Though, when the potential is reduced down to -2 V vs $CdCd^{2+}$ the irreversible faradaic response was recorded (not shown in Fig. 5.8). Most probably the onset for reduction of O_2 or H_2O impurities occurs at -0.5 and -2 V respectively, followed by creation of solid electrolyte interface (SEI) -like passivating layer common in Li-ion batteries (i.e. Li_2CO_3 layer on anode) [6,8].

We believe that the H_2O or O_2 traces originate from Superacryl® resin. During the subsequent cycles within -0.5 and 1.5 V vs $CdCd^{2+}$, no further shift occurred suggesting that there is no further charge transfer within the specified potential window.

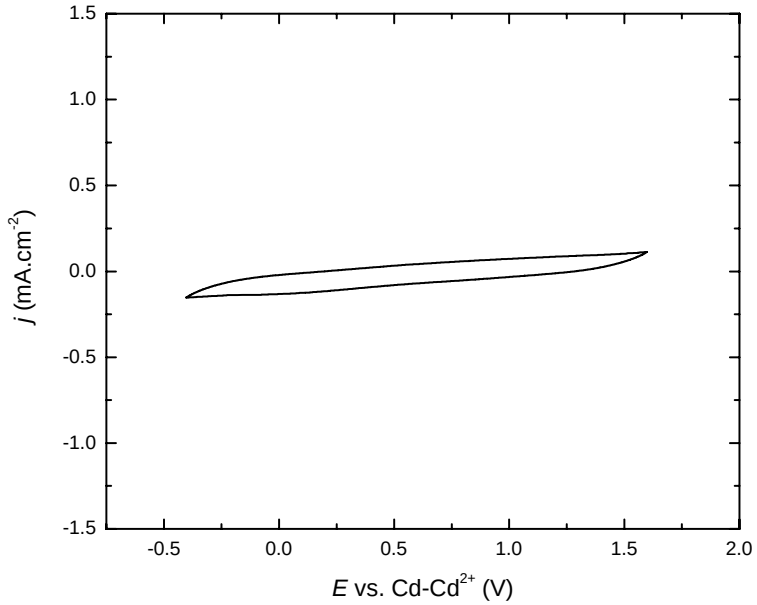

Fig. 5.8 The cyclic voltammogram of 1 M $LiClO_4$ in MMA/SA gel, MMA/PC/$LiClO_4$=61.9/35.0/3.1 (wt%), WE and CE glassy carbon, PMMA-Cd-Cd^{2+} reference electrode, scan rate 10^{-3} $V.s^{-1}$, 5th scan, measured at RT

5.3 *EOEMA and EMA based GPEs*

The new gel polymer electrolytes based on poly(ethyl methacrylate) (PEMA) and poly(2-ethoxyethyl methacrylate) (PEOEMA) polymers prepared by direct radical polymerization are proposed to fulfil requirements of the technology of Li-ion batteries [5] and Electrochromic devices [1]. It is a 3rd generation heterogeneous system with mobile Li and Na ions in an aprotic solvent entrapped in the amorphous PEMA and PEOEMA matrixes. The matrixes are composed of two different monomers: ethyl methacrylate (EMA) and 2-ethoxyethyl methacrylate (EOEMA). The main difference is in polarity of monomers; on the contrary to MMA the EOEMA methacrylate dissolves inorganic salts itself and allows preparation of polymer electrolytes with higher salt content (5.3.3), whereas the EMA based gels show high specific conductivity and less volatility than formerly proposed MMA system (5.4). The UV-initiated polymerization ensures well defined and uniform structure of prepared membranes [21, 22].

The latest results from application of *in-situ* polymerized PEOEMA and PEMA based GPEs in an electrochromic device assembly are described in chapter 8 [23]. Here the electrochemical properties with a stress on electrochemical stability are discussed.

5.3.1 Preparation

The PEOEMA and PEMA based gels were prepared by *UV-initiated* polymerization comprising several preparation steps:

The GPEs prepared by direct EMA and EOEMA polymerization (further referred as ***EMA*** *and* ***EOEMA*** *based GPEs respectively*)

1. $LiClO_4$ or $NaClO_4$ were carefully weighed and dissolved with PC at desired molar concentration.
2. The electrolyte was mixed with either ethyl methacrylate (EMA) and ethylene dimethacrylate (EDMA) or 2-ethoxyethyl methacrylate (EOEMA) and 1,6-hexanediol dimethacrylate (HexadiMA) solution and bubbled with nitrogen for 2 minutes.
3. The exact amount of polymerization initiator BEE (1 mol% of monomer) was added.
4. The solution was covered in order to prevent UV-light exposure and stirred until the BEE dissolved thoroughly.
5. The solution was injected with the syringe either into (a) the mould made of glass and poly propylene (PP) distanced by the 0.5 or 1 mm thick silicon spacer (defining the membrane's thickness – l) and secured with clamps, or (b) between the two electrodes in case of *in-situ* polymerized ECD (see chapter 8.2.2) both purged with nitrogen prior filling.
6. The *UV-initiated polymerization process* was for both above-mentioned assemblies terminated after 4 - 4.5 hours under the 2 × 15 W UV-mercury lamps.

The optimal ratio of initial components differs upon desired mechanical and electrochemical properties. Following table summarizes standard chemical compositions for the PEMA and PEOEMA based gels addressed to obtain high ionic conductivity values. A particular component concentration is expressed in molar percentage (mol%).

Table 5.4 The chemical composition of PEMA and PEOEMA based GPEs with 1M $LiClO_4$-PC electrolyte.

Gel Polymer Electrolyte	Chemical composition (mol%)	Polymer matrix composition (mol%)
EMA	EMA/PC/$LiClO_4$ 39.2/56.0/4.8	EMA/EDMA/BEE 98.7/0.3/1
EOEMA	EOEMA/PC/$LiClO_4$ 35.5/59.4/5.1	EOEMA/ HexadiMA /BEE 98.7/0.3/1

5.3.2 Basic material characterisation

The UV polymerized electrolytes are elastic and homogeneous membranes of a thickness corresponding to the thickness of the silicon spacer in the preparation cell. All used chemicals are colourless; therefore the prepared membranes are highly transparent. The optical transparency was found to be over 93% in the visible part of spectra. The polymer membranes are also stable either stored in desiccator or exposed to air. The long-term storage of PEMA-PC-$LiClO_4$ in air (over 6 months) did not cause phase-separation of the sample or any visible changes of the homogeneity or mechanical properties. Neither PEOEMA nor PEMA based membranes suffered from yellowing

when exposed to direct UV-light. The required foils can be easily cut out and the membranes are well sticky, but do not leave any traces on glass or electrode after removal. The adhesion of PEMA and PEOEMA based GPEs towards plain glass, glass-WO_3 or ITO (SnO_2:In) coated poly(ethylene terephthalate) (PET) foil is detailed in chapter 9.1. An influence of monomer-solvent ratio on mechanical and electrochemical properties is discussed in chapter 5.3.4.

5.3.3 The specific conductivity of EOEMA based GPEs with different salt concentration

On contrary of MMA and EMA, EOEMA is a polar monomer with a large dipole moment. The presence of an ethoxyethyl group in the molecule allows us to prepare GPEs with higher concentration of Li or Na ions. Figure 5.9 shows the conductivity dependency of PEOEMA based GPE on different $LiClO_4$-PC concentration. In case of LEs the maximal conductivity corresponds to approx. 0.75 mol.l^{-1} of $LiClO_4$ in PC (see Fig. 5.1). Here, the threshold at which the conductivity begins to fade due to ion-ion pairing is shifted above 1.2 mol.l^{-1} followed by remarkable decrease in conductivity when the concentration of $LiClO_4$ exceeds 1.8 mol.l^{-1}. An attempt was made to prepare PEOEMA electrolytes with a higher content of $LiClO_4$ (c. 25 mol%), but at temperatures under 50 °C the sample exhibited a lower conductivity than expected [22]. Also a lower optical transparency of this sample was observed when the electrolyte was slightly opaque. Both results imply that $LiClO_4$ is partially segregated from the electrolyte.

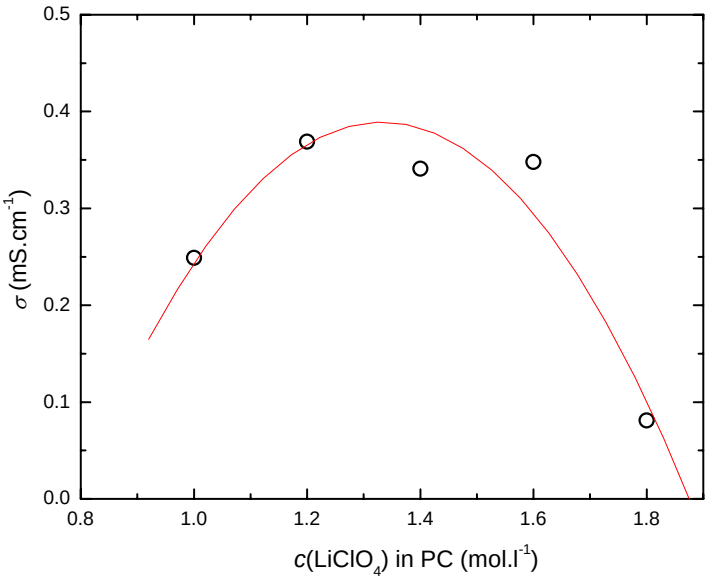

Fig. 5.9 Dependence of the specific conductivity of PEOEMA based GPE on the concentration of $LiClO_4$ in PC; initial composition: EOEMA/PC=48.3/45.5 mol%; red curve is the polynomial fit; measurement temperature 30 °C.

5.3.4 The specific conductivity of EOEMA based GPEs with different monomer-solvent ratio

An influence of the solvent content in the PEOEMA based membrane is displayed in Figure 5.10. The salt concentration in the system was 1.6 mol.l^{-1}. Similarly to MMA/AIBN and MMA/BEE gels (see Fig. 5.4) the steep in conductivity (more than 10 times) was observed. An increase of PC from initial 30.7 to 46.0 mol% (see fig. 5.10)

raised the specific conductivity from 0.031 mS.cm^{-1} (EOEMA/PC=64.2/30.7) to 0.328 mS.cm^{-1} (EOEMA/PC=48.0/46.0). The conductivity increase was remarkably higher in case of PEOEMA than that of PMMA based gels. Owing to the partial cross-linkage of the network the sample keeps its toughness and elasticity even with a lower content of the polymer.

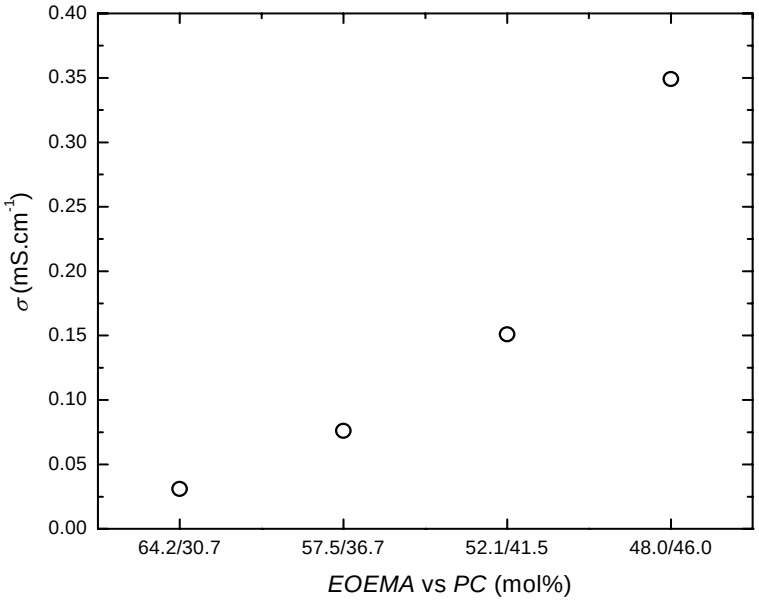

Fig. 5.10 Dependence of the specific conductivity of EOEMA/PC gel on different monomer-solvent ratio; 1.6M $LiClO_4$ in PC; measurement temperature 30 °C.

5.3.5 Electrochemical stability on glassy carbon electrodes

For the investigation of PEMA and PEOEMA electrolytes the samples with the chemical composition; EMA/PC/$LiClO_4$=50.5/44.7/4.8 and EOEMA/PC/$LiClO_4$= 41.2/37.5/21.3 mol% were chosen. Initial voltammetry measurements did not show any electrochemical reaction in the potential range from 0.1 to 1.5 V vs. Cd/Cd^{2+} (Fig. 5.11 – 5th scan).

The potential limit at the positive side (over 1.5 V) was assigned to the oxidation of propylene carbonate [6, 8]. If the potential range was enlarged down to -2.2 V, an irreversible cathodic wave appeared at the potential approx. -0.5 V during the first cycle implying that O_2 were being reduced (Fig. 5.11 and 5.12 – 6th scan). Further cycling caused rapid decrease of the wave and it almost disappeared within 3 – 5 cycles (Fig. 5.11 and 5.12 – 56th scan). The voltammograms did not change during the further cycling.

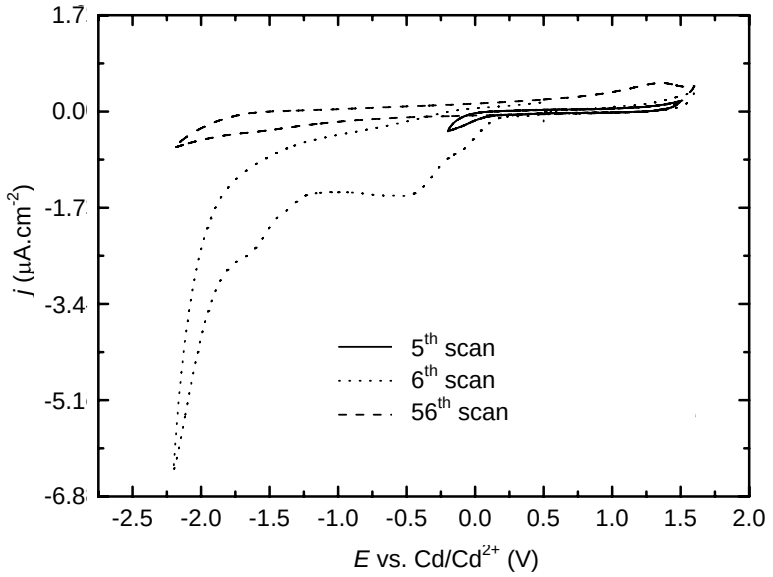

Fig. 5.11 Cyclic voltammograms of PEMA based GPE; composition EMA/PC/$LiClO_4$=50.5/44.7/4.8 mol%; WE and CE glassy carbon, PMMA-Cd-Cd^{2+} reference electrode; scan rate 5 $mV.s^{-1}$, measured at RT.

The irreversible wave attributed to the oxygen reduction is greatly reduced in the second and subsequent scans due to the LiO_2 and Li_2O_2 film creation. The wave of the irreversible reduction of water was also observed at ca. -1.7 V in both PEMA and PEOEMA gel electrolytes, consequently strongly reduced within 3 – 5 cycles.

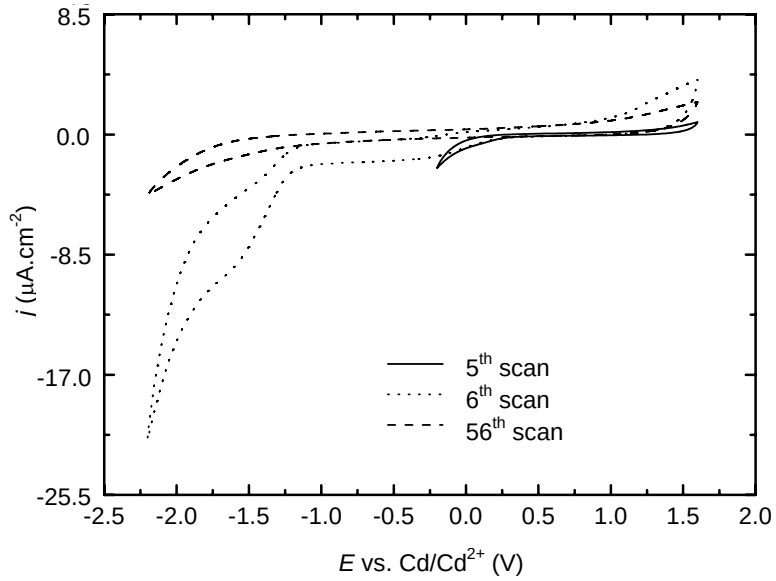

Fig. 5.12 Cyclic voltammograms of PEOEMA based GPE; composition EOEMA/PC/$LiClO_4$= 41.2/37.5/21.3 mol%; WE and CE glassy carbon, PMMA-Cd-Cd^{2+} reference electrode; scan rate 5 $mV.s^{-1}$, measured at RT.

5.3.6 Electrochemical stability on gold electrode

Figures 5.13 and 5.14 show the cyclic voltammograms of the PEOEMA (EOEMA/PC/LiClO4=41.2/37.5/21.3 mol%) and PEMA (EMA/PC/$LiClO_4$=

38.9:56.2:4.9 mol%) electrolytes on the gold electrode done in argon atmosphere. Comparing with the voltammetrical measurements of liquid PC-based electrolytes done in argon-filled glove box, we found that the electrochemical stability of the polymer electrolytes is limited by the properties of propylene carbonate. At potentials around -1.2 V we found an irreversible cathodic wave accordant with formation of a protective layer similar to the solid electrolyte interface (SEI) formation on graphite electrodes and followed by reversible reduction and oxidation of lithium at -2.6 V. On contrary to the real SEI layer described in lithium-ion batteries, the cathodic wave of the protective layer content is visible on each scan, what can conclude, that the layer is recovered during every cycle.

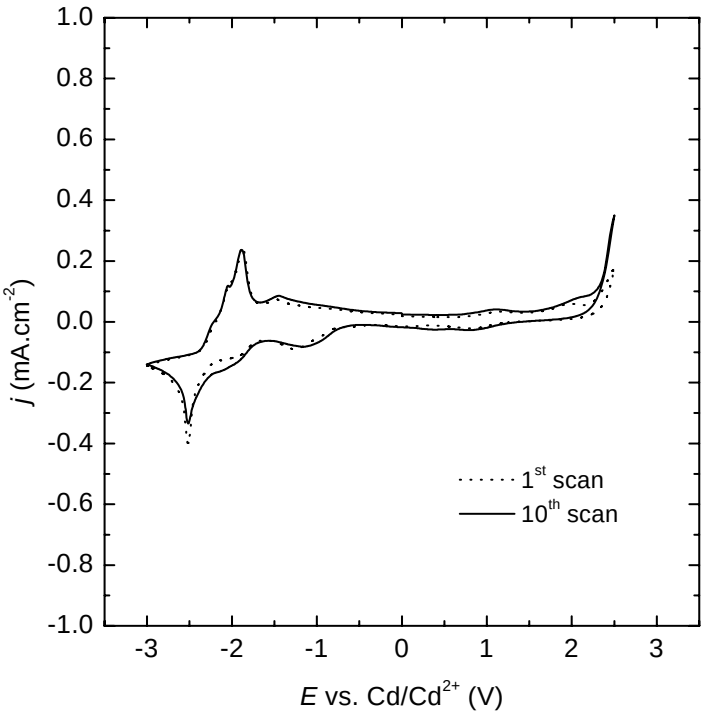

Fig. 5.13 Cyclic voltammograms of PEMA based GPE; composition EMA/PC/$LiClO_4$= 38.9:56.2:4.9 mol%; 1st (dot line) and 10th (solid line) scan; gold (WE), glassy carbon (CE), PMMA-Cd-Cd^{2+} (RE); scan rate 10 $mV.s^{-1}$; measured at RT.

Both the PEMA and PEOEMA electrolytes exhibit a similar anodic behaviour when propylene carbonate is oxidized above 2.5 V vs. Cd/Cd^{2+}. The linear sweep voltammograms on glassy carbon (Fig. 5.15) showed an anodic wave at 2.3 V that does not appear on gold electrode under the same conditions. This peak can be possibly attributed to pre-oxidation of PC [9]. If the cyclic voltammogram is measured up to 3 V, a cathodic wave around 2.4 V appears both on gold and glassy carbon electrode.

From comparison with literature and also from our voltammetrical measurements of liquid PC electrolytes we can conclude that the present polymer lowers the reactivity of the electrolyte perhaps by influencing the reaction rate and possibly enlarges the accessible potential window, which is important for recent testing in lithium-ion batteries [9].

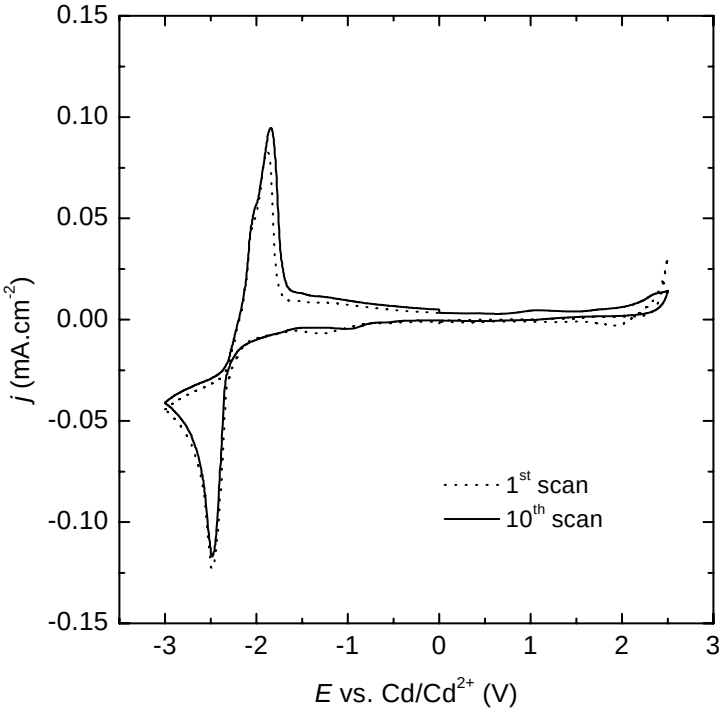

Fig. 5.14 Cyclic voltammograms of PEOEMA based GPE; composition EOEMA/PC/$LiClO_4$= 48.3:45.5:6.3 mol%; 1st (dot line) and 10th (solid line) scan; gold (WE), glassy carbon (CE), PMMA-Cd-Cd^{2+} (RE); scan rate 1 $mV.s^{-1}$; measured at RT.

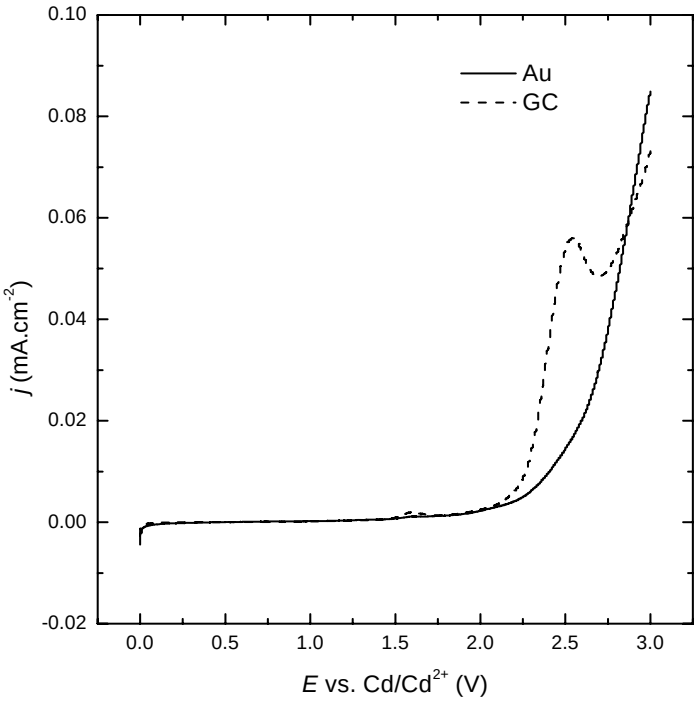

Fig. 5.15 The linear sweep voltammograms of the PEOEMA based GPE on gold (solid line) or glassy carbon (dash line) as a working electrode; composition EOEMA/PC/$LiClO_4$=48.3:45.5:6.3 mol%; platinum (CE), PMMA-Cd-Cd^{2+} (RE); scan rate 1 $mV.s^{-1}$; measured at RT.

5.4 *Comparison of ionic conductivities of acrylic based GPEs*

Figure 5.16 presents the specific conductivity of PMMA, PEMA and PEOEMA based gel polymer electrolytes measured at 30 °C. The membranes are divided into two groups according to the method of polymer matrix formation (UV or heat cured). In the term of host polymer matrix we can divide the resulting conductivity values from Fig. 5.16 into the conductivity of PMMA, PEOEMA and PEMA membranes. The conductivity data for both, Li and Na containing systems are displayed. The perchlorate concentration was 0.5 mol.l^{-1} for PMMA and 1 mol.l^{-1} for EOEMA and EMA gels. The higher salt concentration in the case of EOEMA gels was chosen with respect to its positive impact on salt solubility. In order to receive comparable results within the later two matrixes the EMA based gels with 1 mol.l^{-1} Li and Na concentration were prepared. Absolute conductivity values of all systems (as shown in Fig. 5.16) together with their chemical composition are summarized in Tab. 5.5. It is important to say that the composition of all membranes was kept the same as it was defined in chap. 5.2.3 (PMMA) and 5.3.1 (PEOEMA and PEMA).

Scrutinizing the results from Fig. 5.16 and Tab. 5.5 we conclude; (a) on contrary of the LE, Na containing gels are more conductive than those with Li ions, most probably it is due to higher affinity of smaller Li ion with dense charge to make a covalent bond with carboxyl groups in polymer chain; (b) higher conductivity of the gel with Na over Li ions was pronounced in case of MMA/SA due to its rather amorphous nature as discussed in 5.2.6; (c) employing direct initiation technique for PMMA based GPEs resulted in major conductivity deterioration, though the mechanical properties improved; (d) with comparable dimensional and mechanical stability the EMA and EOEMA based GPEs exhibit appreciably higher conductivities than MMA/BEE.

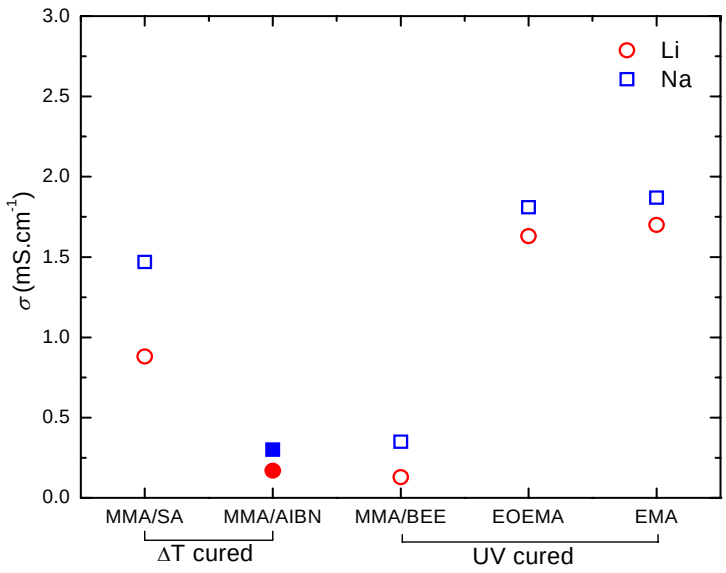

Fig. 5.16 Dependency of specific conductivity of GPEs with Li (circles) and Na (squares) ions on the membrane composition and preparation method; measurement temperature 30°C.

We showed that increased content of the solvent and salt improves the material conductivity. On the other hand, when the excess amount of an organic solvent is added to the polymer matrix, the material has not enough strength to keep a solid film. Another parameter to be considered is the uniformity of chemical composition and the electrochemical stability. However the MMA/SA gels showed high ionic conductivities

they proved rather poor electrochemical stability on GC electrodes. Nevertheless, directly polymerized gels (by heat MMA/AIBN or UV MMA/BEE) exhibit vast decrease of conductivity values. The limitation of PMMA material is mainly in the area of negative potentials, where several irreversible cathodic waves of oxygen reduction were observed.

Table 5.5 Overview of PMMA, PEMA and PEOEMA based GPEs containing Li and Na perchlorates in PC in 0.5 or 1 mol.l^{-1} concentration, their chemical composition and specific conductivity values, measurement temperature 30 °C.

Gel Polymer Electrolyte	Chemical composition[1] (mol%) / (wt%)*	Salt concentration (mol.l^{-1})	σ (S.cm^{-1})
MMA/SA	[1] MMA/PC/$LiClO_4$ 62.9/35.5/1.6*	0.5	0.9×10^{-3}
	[1] MMA/PC/$NaClO_4$ 62.7/35.5/1.8*		1.5×10^{-3}
MMA/AIBN	MMA/PC/$LiClO_4$ 57.7/40.5/1.7	0.5	1.7×10^{-4}
	MMA/PC/$NaClO_4$ 57.7/40.5/1.7		3.0×10^{-4}
MMA/BEE	MMA/PC/$LiClO_4$ 57.5/40.7/1.7	0.5	1.3×10^{-4}
	MMA/PC/$NaClO_4$ 57.5/40.7/1.7		3.5×10^{-4}
EMA	EMA/PC/$LiClO_4$ 39.2/56.0/4.8	1	1.7×10^{-3}
	EMA/PC/$NaClO_4$ 39.2/56.0/4.8		1.9×10^{-3}
EOEMA	EOEMA/PC/$LiClO_4$ 35.5/59.4/5.1	1	1.6×10^{-3}
	EOEMA/PC/$NaClO_4$ 35.7/59.8/4.5		1.8×10^{-3}

[1] MMA expresses the contribution of the host matrix in the overall sample composition

The accessible electrochemical window of both PEMA and PEOEMA polymer electrolytes was estimated from -2.1 V to 1.5 V vs. Cd/Cd^{2+} on GC, and up to 5.1 V vs. Li/Li^{+} on gold electrodes. The highest conductivity among Li containing system was 0.9 mS.cm^{-1} for MMA, 1.6 mS.cm^{-1} for EOEMA and 1.7 mS.cm^{-1} for EMA based gel polymer electrolyte.

Further, we found that PMMA based GPEs should contain at least 40 mol% of polymer but on the other hand in case of EOEMA and EMA gels less, but partially cross-linked polymer can deliver enhanced toughness and elasticity while retaining good ionic conductivity. Moreover, the advantage of direct UV-polymerization of electrolyte inside the device was considered for the proposed practical application of the new method of ECD preparation (see chapter 8.2.2).

References

[1] GRANQVIST, C. G. *Handbook of Inorganic Electrochromic Materials*. The Netherlands: Elsevier, 1995. 2 sv. (337, 296 s.). ISBN 0-444-89930-8.

[2] MARCUS, Y. *The Properties of Solvents: Wiley Series in Solution Chemistry: Volume 4*. England: Wiley&Sons, 1999. 399 s. ISBN 0-471-98369-1.

[3] SONG, J.Y., WANG, Y.Y., WAN, C.C. Review of Gel-type Polymer Electrolytes for Lithium-ion Batteries. In *Journal of Power Sources*. The Netherlands: Elsevier, 1999. 77. s. 183-197.

[4] CONWAY, Brian E. *Electrochemical Supercapacitors: Scientific Fundamentals and Technological Applications*. Kluwer Academic/Plenum Publishers, 1999. 736 s. ISBN 0306457369.

[5] SCHALKWIJK, Walter A., SCROSATI, B. *Advances in Lithium-Ion Batteries*. New York: Kluwer Academic/Plenum Publishers, 2002. 513 s. ISBN 0-306-47356-9.

[6] HAHN, M., et al. Gas Evolution in Activated Carbon/propylene carbonate Based Double-layer Capacitors. In *Electrochemistry Communications*. The Netherlands: Elsevier, 2005. 7 s. 925-930.

[7] ARIMA, T., HAMADA, T., McCABE, J. F. The Effects of Cross-linking Agents on Some Properties of HEMA-based Resins. In *Journal of dental research*. USA: International & American Associations for Dental Research, 1995. s. 1597-1601.

[8] MOSHKOVICH, M., GOFER, Y., AURBACH, D. Investigation of the Electrochemical Windows of Aprotic Alkali Metal (Li, Na, K) Salt Solutions. In *Journal of Electrochemical Society*. USA, 2001. 148. s. 155-167.

[9] GEORÉN, P., LINDBERGH, G. On the use of Voltammetric Methods to Determine Electrochemical Stability Limits for Lithium Battery Electrolytes. In *Journal of Power Sources*. The Netherlands: Elsevier, 2003. 124. s. 213-220.

[10] KREJZA, Ondřej, et al. Specific Conductivity of PMMA Based Gel Electrolytes Containing Cadmium, Magnesium or Lithium Salts. In *4th Advanced Batteries and Accumulators*. Brno: BUT-Brno, 2003. s. 50-51. ISBN 80-214-2298-0.

[11] VONDRÁK, Jiří, et al. Ion-conductive polymethylmethacrylate gel electrolytes for lithium batteries. In *Journal of Power Sources*. The Netherlands: Elsevier, 2005. 146. s. 436-440.

[12] VONDRÁK, Jiří, et al. Polymer Gel Electrolytes for Electrochromic Devices. In *Electrochimica Acta*. The Netherlands: Elsevier, 1999. 44. s. 3067-3073.

[13] ŠURCA VUK, A., KREJZA, O., JEŠE, R., et al. Comparison of Hybrid Electrochromic Cells Employing Sol-Gel and Polymeric I_3^-/I^- Redox Electrolytes. In *6th International Meeting on Electrochromism*. Brno: BUT-Brno, 2004. s. 150-151. ISBN 80-214-2622-5.

[14] KREJZA, Ondřej, et al. The presence of nanostructured Al_2O_3 in PMMA-based gel electrolytes. In *Journal of Power Sources*. The Netherlands: Elsevier, 2008. 178. s. 774-778.

[15] KREJZA, Ondřej, et al. A Study of PMMA Based Electrolytes with the Methyl Violet Dyes. In *11th International Symposium on Polymer Electrolytes*. Ofir: University of Minho, 2008. s. 125-125.

[16] KREJZA, Ondřej, et al. Heterogeneity of PMMA-PC Based Gel Electrolytes. In *9th Advanced Batteries and Accumulators.* Brno: BUT-Brno, 2008. s. 73-75. ISBN 978-80-214-3659-6.

[17] KREJZA, Ondřej, et al. The Ionic Mobility in Gel Polymer Electrolytes Studied by NMR Spectroscopy. In *Polymer Batteries and Fuel Cells: PBFC 2007*. Rome, 2007. s. 203-204.

[18] KREJZA, Ondřej, et al. Resistivity and NMR of PMMA Based Gel Electrolytes. In *58th Annual Meeting of the International Society of Electrochemistry*. Banff: ISE, 2007. s. 1-1.

[19] KREJZA, Ondřej, et al. Mobility of Ions in PMMA Gel Polymers Studied by NMR. In *11th International Symposium on Polymer Electrolytes*. Ofir: University of Minho, 2008. s. 67-67.

[20] VOGNAR, J., MACALÍK, M., BARTUŠEK, K., ŠPIČÁK, P., VONDRÁK, J., NOVÁK, V., KREJZA, O. A Study of PMMA based Electrolytes Containing Na^+ Ions by Nuclear Magnetic Resonance. In *9th Advanced Batteries and Accumulators*. Brno: BUT-Brno, 2008. s. 66-70. ISBN 978-80-214-3659-6.

[21] REITER, Jakub, et al. Poly(ethyl methacrylate) and poly(2-ethoxyethyl methacrylate) Based Polymer Gel Electrolytes. In *Journal of Power Sources*. The Netherlands: Elsevier, 2006. 158. s. 509-517.

[22] KREJZA, O., REITER, J., VONDRÁK, J. Methacrylate-based Polymer Electrolytes for Electrochromic Devices and Lithium-ion Batteries. In *8th Advanced Batteries and Accumulators: [A.B.A. -8]*. Brno: BUT-Brno, 2007. s. 76-78. ISBN 978-80-214-3424-0.

[23] REITER, J., KREJZA, O., SEDLAŘÍKOVÁ, M. Electrochromic Devices Employing Methacrylate-based Polymer Electrolytes. In *Solar Energy Materials and Solar Cells*. The Netherlands: Elsevier, 2009. 93. s. 249-255.

[24] BOHNKE, O., et al. Fast ion transport in new lithium electrolytes gelled with PMMA. 1. Influence of polymer concentration. In *Solid State Ionics*. The Netherlands: Elsevier, 1993. 66. s. 97-104.

[25] BYKER, Harlan J. Electrochromic and Polymers. In *Electrochimica Acta*. The Netherlands: Elsevier, 2001. 46. s. 2015-2022.

6 PMMA based GPEs incorporating nanostructured Al_2O_3 additives

Section 6.1 describes the morphology of nanostructured aluminium oxides used as electrically inert additives in liquid and gel polymer electrolytes. The specific conductivity (6.2.1) and the behaviour of Fc/Fc^+ metallocene complex (6.2.2) in $LiClO_4$-PC based liquid electrolytes (LEs) with Al_2O_3 additives are discussed in section 6.2. The influence of dispersed nanosized Al_2O_3 on the ionic conductivity of PMMA based GPEs with Li and Na ions is detailed in section 6.3.

6.1 *Morphology of nanosized aluminium oxides*

Various methods have been applied to increase the conductivity of polymer electrolytes. One of the approaches relies upon the addition of nanocomposite sorbents. The positive influence of electrically inert nanoparticles on either the specific conductivity or mechanical properties of plasticized LiX/PMMA and LiX/PEO based binary systems has been announced [1-3]. Johansson and Jacobsson [4] reported the conductivity enhancement in the LiX/PEO based system ascribing the phenomenon to specific surface interactions subsequently confirmed by Ahmad et al. on PMMA-LiTf-TiO_2 based electrolytes [5].

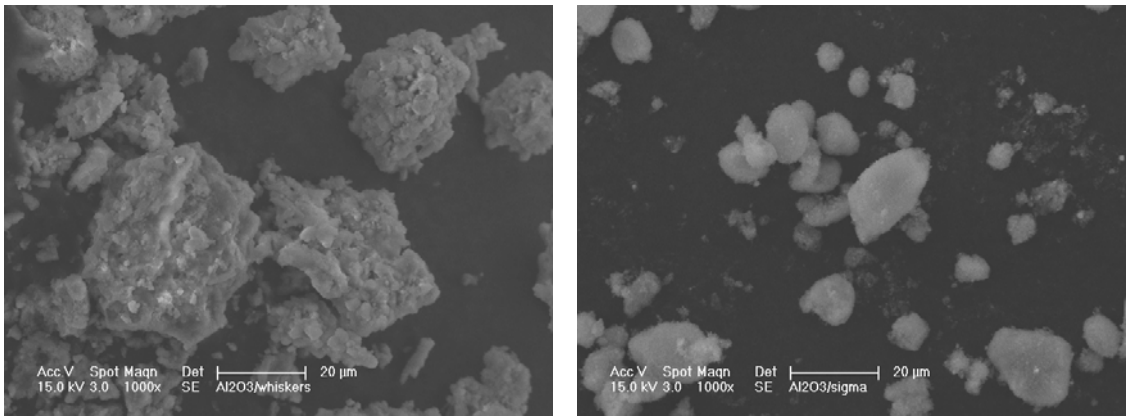

Fig. 6.1 SEM micrographs of Al_2O_3 in whiskers (left) and nanopowder (right) modifications.

In a modern electrochemical cell microporous inorganic fillers such as fumed silica, alumina or titanium oxide are widely used. A large surface area of the sorbent increases the host polymer porosity and enhances electrolyte retention, hence increases conductivity. Moreover the electrically inert additives are used to react with the products of the side reactions occurring mainly on negative electrode in Li-ion based battery application thus extending the cell's lifetime and enhancing the charge capacity [6,7].

The liquid and gel polymer electrolytes with Al_2O_3 additives of the particle size between 40 and 47 nm "nanopowder" and 2-4 nm "whiskers" were examined (see Fig. 6.1 and 6.2). The SEM micrographs from Fig. 6.1 show a formation of sharp edged

agglomerates on the left and pulverized rather separate powder on the right. A nanopowder modification was a white flake-like powder with apparent spherical shape when magnified (see Fig. 6.1 and 6.2 on the right). In the whiskers modification the Al_2O_3 appeared as a fine grain but rather dense clay characterized by gray colour and fast sedimentation when dispersed in a blend (see Fig. 6.2 on the left).

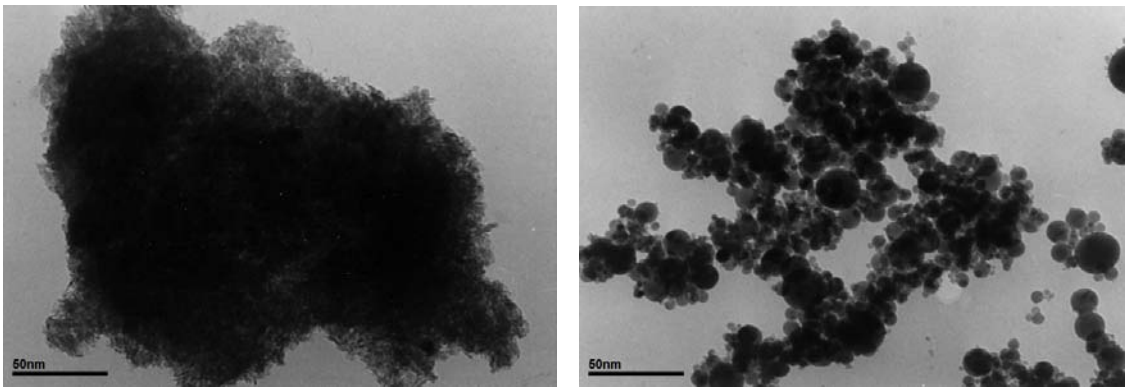

Fig. 6.2 High Resolution TEM micrographs of Al_2O_3 in whiskers (left) and nanopowder (right) modifications.

For a TEM analysis the powder samples were dispersed in ethanol and the suspension was treated in ultrasound for 10 minutes. A drop of very dilute suspension was placed on a holey-carbon-coated copper grid and allowed to dry by evaporation at ambient temperature.

6.2 *$LiClO_4$-PC-Al_2O_3 based LEs*

First of all the electrochemical behaviour of Al_2O_3 additives in a liquid environment was observed. The initial tests with the whiskers modification revealed partial or complete matter settlement during both, CV and EIS experiments. Therefore, only the results from the nanopowder modification of alumina are discussed.

6.2.1 Specific conductivity measurements

For the initial conductivity measurements the liquid electrolytes were prepared from 0.1 mol.l^{-1} $LiClO_4$ in PC and certain amount of alumina additives. The concentration of supporting electrolyte was chosen with respect to the experiments subsequently performed in the polymer electrolyte environment (chapter 6.3). The contribution of the filler was 0, 3.46, 7.17 and 10 wt% of the sample. The prepared electrolytes were sonicated to keep the alumina particles evenly distributed. In order to eliminate the oxygen content the solution was bubbled by argon for 2 minutes prior each impedance scan. In order to minimize the exposure time (aprotic LE with inorganic perchlorates are strongly sensitive to moisture uptake) only single impedance spectrum within 10 kHz and 100 Hz was recorded. The impedance measurements were performed using a standard 2-electrode conductometry cell within the 25 and +60 °C temperature range. Figure 6.3 shows the conductivity values of $LiClO_4$-PC-Al_2O_3 electrolytes. At a room temperature the conductivity of a pure $LiClO_4$-PC solution was 1.87 mS.cm^{-1}. As we expected the conductivity decreased when the nanopowder was introduced into the system. The lowest conductivity value of the system containing 3.46 wt% of Al_2O_3 was 1.57 mS.cm^{-1}.

Compared to TiO_2 with a relatively high dielectric constant (ε = 180), the Al_2O_3 with ε = 9.8 is expected to be rather aggravating the solubility of Li salt in PC (ε = 64.5) [7]. Hence, the observed decrease of conductivity values in liquid electrolytes with respect to increasing volume of Al_2O_3 in a blend was in perfect agreement with the results reported by Chen [1] (refer to Fig. 6.3). Another reason for resistivity decrease might be mutual interaction of free Li cation and dispersed Al_2O_3 particles [12,15].

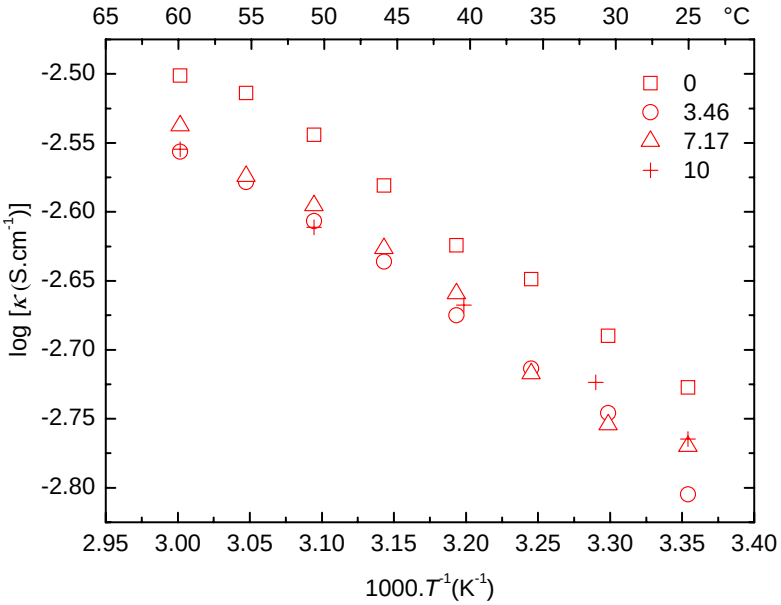

Fig. 6.3 Arrhenius plot of the specific conductivity of PC-$LiClO_4$ based liquid electrolytes with corresponding content of Al_2O_3 in wt. %, measurement temperature from 25°C to 60°C.

6.2.2 Incorporation of the transition metal complex

Under assumption of restricted Li-ion movement in a liquid environment incorporating Al_2O_3 additives, the investigation of electrochemical behaviour of a transition metallocene complex was involved. For the suitable electrochemical properties ferrocene/ferrocenium (Fc/Fc^+) redox couple was chosen. One of the main characteristics of ferrocene is its capacity to lose an electron without the molecule being broken-up, following the reaction:

$$Fc \leftrightarrow Fc^+ + e^- \tag{6.1}$$

thereby generating the corresponding ferrocenium ion. Electrochemical redox reaction of Fc/Fc^+ is diffusion controlled and can be assumed as electrochemically reversible one or Nernstian using specific diagnostic criteria, from chapter 4.2.2, that can be subdivided as follows:

Properties of the potential

» the potential of the forward peak, E_{pf}, is independent of the scan rate;

» the separation between the potentials of the forward and reverse peaks (called peak-to-peak separation), ΔE_p at 25 °C, defined as:

$$\Delta E_p = E_{pf} - E_{pr} = \frac{2.3 \cdot R \cdot T}{n \cdot F} \tag{6.2}$$

where *n* is the number of electron exchanged per molecule of Fc/Fc^+, is equal to 59/*n* mV and such value maintains constant with scan rate but is dependent on the temperature.

Properties of the current

- the ratio between the current of the forward peak and the square root of the scan rate, $i_{pf}/v^{1/2}$, is constant with the scan rate;
- the current ratio between the reverse and the forward peaks, i_{pr}/i_{pf}, is constant and equal to 1 if diffusion coefficients of both species are equal.

Beside qualitative description of the complex behaviour we included determination of the apparent diffusion coefficients using Randles-Ševčík equation (4.1) [8,9].

For voltammetrical measurements the starting solution of 1 $mol.l^{-1}$ $LiClO_4$ in PC was prepared. The higher concentration of supporting electrolyte was chosen to minimize the IR drop. Further the ferrocene in 5×10^{-3} $mol.l^{-1}$ concentration was added into the system. The cyclic voltammetry was performed in electrochemical cell on platinum disc electrode as the working and platinum rod as the auxiliary electrode. The potential step applied to a working electrode was balanced against SCE reference electrode at 10, 20, 30, 40 and 50 $mV.s^{-1}$ scan rates. Each experiment comprised of five scans while only the data from the 5th scan are presented.

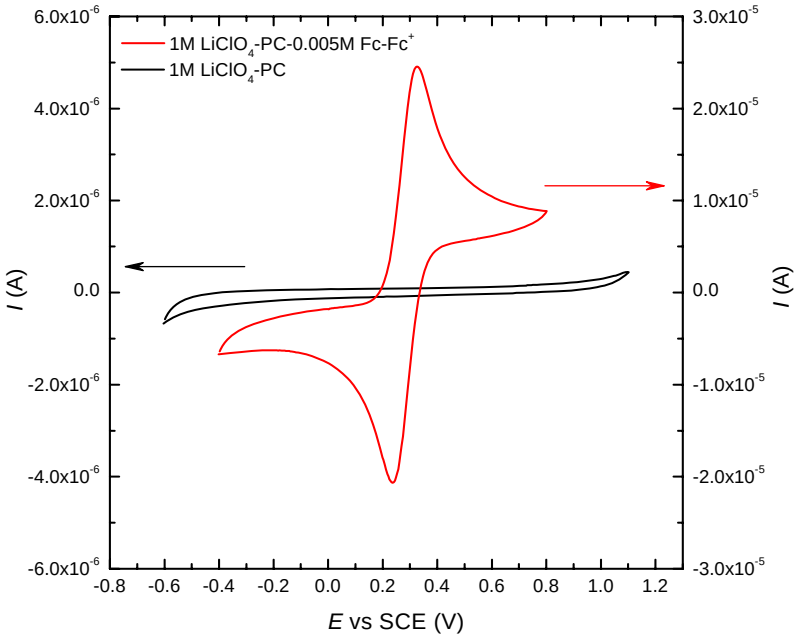

Fig. 6.4 The cyclic voltammograms of 1M $LiClO_4$-PC (black curve) and 1M $LiClO_4$-PC with 0.005M $Fc\text{-}Fc^+$ solutions; WE- Pt disc, CE- Pt rod, RE-SCE, scan rate 50 $mV.s^{-1}$, 5th scan.

Cyclic voltammograms of the starting solution are displayed in figure 6.4. The potential scan of 1M $LiClO_4$ in PC revealed no faradaic activity within -0.6 and 1.1 V potential range. Upon addition of 0.005M ferrocene the oxidative pulse at +0.322 mV appeared followed by reductive peak at +0.241 mV versus SCE. The peak-to-peak separation value ΔEp was found to be 82 mV. However this value is evidently higher than above mentioned 59 mV of electrochemically reversible processes, in measuring the peak-to-peak separation, a departure of 10-20 mV from the theoretical value

(especially at relatively high scan rates) was found not compromise the criterion of reversibility. In that the eventual presence of solution resistances, however suppressed by higher $LiClO_4$ concentration tends to lay down the forward/reverse peaks system, thus increasing the relative ΔE_p value [8,9]. The positions of both forward and reverse peaks remained unchanged even at slower scan rates. Slightly lower apparent diffusion coefficient of uncharged ferrocene molecule was calculated from the reverse current peak magnitude. The current ratio between the reverse and forward peak approached unity suggesting the reversibility of the process. Experimental data of starting solution with $Fc\text{-}Fc^+$ redox couple together with the conductivity value are displayed in the first row of tab. 6.1.

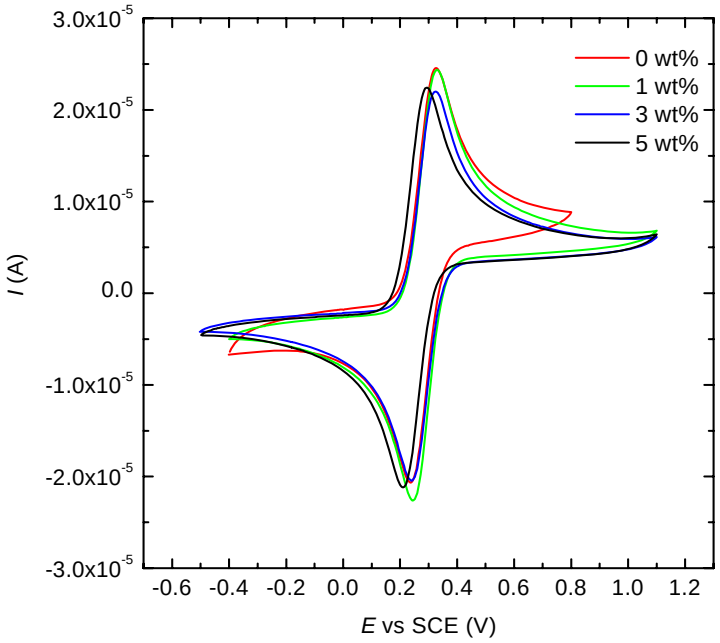

Fig. 6.5 The cyclic voltammograms of 1M $LiClO_4$-PC-0.005M $Fc\text{-}Fc^+$ solutions with 0, 1, 3 or 5wt% of Al_2O_3; WE- Pt disc, CE- Pt rod, RE-SCE, scan rate 50 $mV.s^{-1}$, 5^{th} scan

The comparison between 1M $LiClO_4$-PC-0.005M $Fc\text{-}Fc^+$ and the same solution enriched with 1, 3 or 5 wt% of Al_2O_3 additives is shown in Fig.6.5. Sedimenting of the nanosorbent containing samples was accelerated when ferrocene was introduced into the system. In order to prevent the particle settlement all samples were bubbled by argon for 2 minutes prior each measurement. During the measurement only migration and diffusion forces took place. Voltammograms were recorded at 50 $mV.s^{-1}$ and the 5^{th} scan was used for data interpretation and further analysis. The electrode arrangement remained unchanged. The working electrode surface was carefully cleaned, from the alumina residues, with abrasives (0.3 alumina, Metrohm, CH) and soft cloth between each measurement.

The experimental data of analyzed solutions with Al_2O_3 are introduced in table 6.1. When we look at the voltammograms from fig. 6.5 we see only minor changes when comparing to the solution plain of alumina (red curve). The scans with 1 and 3 wt% of the filler are almost identical whereas only a slight shift towards more negative potentials of both E_{pf} and E_{pr} of the 5 wt% are observed. On the other hand the value of peak-to-peak ratio of the same sample was found the closest to theoretical 59 mV as described above. From the quantitative point of view an amount of oxidized and subsequently reduced ferrocene-ferrocenium couple was the highest for the 1 wt%

sample, reflected in increased apparent diffusion coefficient. Contrary to the theoretical assumption the $i_{pf}/v^{1/2}$ ratio linearly increased with the scan rate indicating a diffusion controlled process. Finally, the impedance check of the 1M $LiClO_4$- PC-Al_2O_3 solutions revealed approx. 5% increase of the conductivity values upon the Ferrocene addition Tab 6.1.

Table 6.1 The peak potentials, apparent diffusion coefficients and peak currents of 0.005M Fc/Fc^+ complex in 1M $LiClO_4$-PC with Al_2O_3 additives (scan rate 50 $mV.s^{-1}$, 5^{th} scan, Ep confidence interval ± 0.003 V)

$m(Al_2O_3)$ (wt%)	E_{pf} (mV)	E_{pr} (mV)	ΔE_p (mV)	i_{pf} (μA)	i_{pr} (μA)	i_{pr}/i_{pf} (-)	D_{0f} ($cm^2.s^{-1}$)	D_{0r} ($cm^2.s^{-1}$)	κ ($S.cm^{-1}$)
0	323	241	82	22.30	22.57	1.01	1.10×10^{-6}	1.13×10^{-6}	6.20×10^{-3}
1	330	247	89	24.67	24.34	0.98	1.35×10^{-6}	1.31×10^{-6}	6.09×10^{-3}
3	321	239	82	22.21	22.17	1.00	1.09×10^{-6}	1.09×10^{-6}	5.97×10^{-3}
5	293	214	79	22.79	22.66	0.99	1.15×10^{-6}	1.14×10^{-6}	5.93×10^{-3}

With respect to conductivity diminution, observed during initial impedance analysis, we believed that the presence of inert Al_2O_3 nano-additives would increase the mutual interactions with the redox couple influencing an apparent diffusion coefficient. Nevertheless, only a slight deviation from the reversibility criterion (ΔE_p) in case of 1 wt% of the sorbent had been observed. In other words; expected quasi-reversible behaviour of the liquid system incorporating Al_2O_3 additives and Fc/Fc^+ complex was not confirmed under above mentioned experimental conditions. Moreover, the shift of the peak potentials suggesting enhanced solvatation of Fc/Fc^+ couple by the presence of Al_2O_3 (5 wt%) was noticed. Following the experimental data we propose that the dipole moment of Al_2O_3 molecule can to some extend participate in solvation process of ferrocene. Similar effect can be expected also in case of supporting electrolyte which means that the number of free ions would increase. It is important to note that the diameter of used ferrocene cation is 1.44 nm, which is higher than that of lithium or sodium perchlorate.

6.3 *$LiClO_4$-PC-Al_2O_3 and $NaClO_4$-PC-Al_2O_3 based GPEs*

The behaviour of Al_2O_3 additives in the gel polymer electrolytes was examined using electrochemical impedance spectroscopy. Similar to liquids, fast particle settlement of the whiskers modification occurred also in the presence of gel. Unfortunately, the electrochemical characterization is not included due to observed phase separation in gel samples with Fc/Fc^+ redox couple. Therefore, only the conductivity results from the nanopowder modification of alumina are discussed.

6.3.1 Preparation and experimental setup

Basically, four sets of samples were prepared based on the preparation method described in chapter 5.2.1. The gels were thermally initiated MMA/SA, and cross-linked MMA/AIBN based membranes in combination with embedded Li or Na ions. The concentration of electrolyte was 0.1 $mol.l^{-1}$ in PC. The 40-47 nm Al_2O_3 in the nanopowder modification was represented in 0, 3.46, 7.17, 10 and 12 wt% in both mentioned systems. Following table summarizes the chemical compositions of all studied membranes.

The mixture of the components from table 6.2 in a suitable ratio was poured in a Petri dish (Ø 5 cm) and placed in an oven. The polymerization process of MMA/SA and MMA/AIBN gels was finished by warming for 1.5 h / 90 °C and 2 h / 80 °C respectively. Solutions on MMA/AIBN basis were bubbled in argon for 2 minutes before inserting into oven. Gels prepared in this way were kept in a desiccator.

Table 6.2 The chemical composition and overview of GPEs containing Al_2O_3 nanoparticles with electrolytes based on 0.1mol.l^{-1} Li and Na perchlorates dissolved in PC.

Gel polymer electrolytes[1]		Al_2O_3 (40-47 nm) nanopowder content				
type	components	0 wt%	3.46 wt%	7.17 wt%	10 wt%	12 wt%
MMA/SA	MMA/PC/$LiClO_4$	63.7/36.0/0.33	61.5/34.5/0.32	59.1/33.4/0.31	57.3/32.4/0.30	56.0/31.7/0.29
	MMA/PC/$NaClO_4$	63.7/36.0/0.36	61.5/34.7/0.35	59.1/33.4/0.34	57.3/32.4/0.33	56.0/31.7/0.32
MMA/AIBN	MMA/PC/$LiClO_4$	58.3/41.1/0.38	56.3/39.9/0.37	54.1/38.4/0.36	52.4/37.2/0.34	51.3/36.4/0.33
	MMA/PC/$NaClO_4$	58.2/41.3/0.42	56.2/39.9/0.40	54.1/38.4/0.39	52.4/37.2/0.38	51.3/36.4/0.37

[1] The chemical composition of all GPEs is expressed in wt%

The impedance measurements were performed using the impedance module of the potentiostat Autolab 12 within the frequency range of 100 kHz to 1 mHz for lower temperatures and 10 kHz to 100 Hz for temperatures above 0 °C. The membranes of a thickness from 0.4 to 0.9 mm were cut out from Petri dishes and fastened between two stainless steel blocking electrodes. The impedance response was measured over the range -70 to 70 °C.

6.3.2 Morphology and appearance

The GPEs without ceramic sorbent were superficially homogeneous transparent membranes with transmittance over 90%, easy to cut out from the Petri dish. We found the transparency to be strongly depending upon alumina content. Optical observation of the samples revealed that the Al_2O_3 nanopowder was not evenly distributed. In all membranes, prepared from 3.46 wt% of Al_2O_3, the nanopowder was attracted to both surfaces in comparison to the whole membrane volume (see Fig. 6.6). However the recorded impedance spectra did not demonstrate any multilayer behaviour usually represented by several adjacent impedance loops (C‖R combinations). A further increase of alumina over 3.46 wt% caused that the bulk distribution was fully homogeneous. Increasing the content of Al_2O_3 over 7.17 wt% we received a deep white, non-transparent membrane.

Fig. 6.6 Typical cross-section of the MMA/SA based GPE containing 3.46 wt% of Al_2O_3 nanoparticles, OM 100× magnified.

The surface morphology was studied using SEM. The micrographs from Fig. 6.7 show grooved surface of the MMA/SA membrane with 7.17 wt% alumina content. When magnified the white path of nanosorbent appears (Fig. 6.7 on the right) suggesting that the sorbent was evenly distributed in the bulk. At the same time the visible traces signify the insolubility of alumina in the PC.

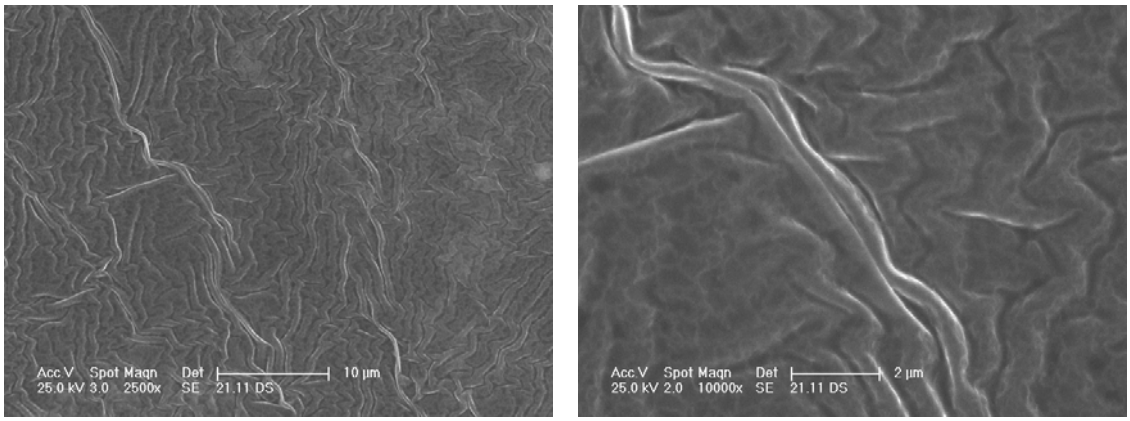

Fig. 6.7 SEM micrographs of MMA/SA based GPE containing 7.17 wt% of Al_2O_3 nanoparticles.

Figure 6.8 represents the micrographs of MMA/AIBN based gel electrolyte with 10 wt% of alumina. Generally in all MMA/AIBN based membranes we observed better surface homogeneity which is also visible when the images on the left of figures 6.7 and 6.8 are compared. Contrary to MMA/SA based gels the degree of Al_2O_3 dispersion in a bulk of MMA/AIBN based membranes was somehow suppressed probably due to their higher homogeneity. We assume that the more amorphous nature of MMA/SA based gels with higher amount of the free solvent enhances the distribution of alumina in the bulk. This assumption is also supported by the presence of Al_2O_3 clusters (white aggregates visible in Fig. 6.8 on the right) in case of all MMA/AIBN gels under investigation.

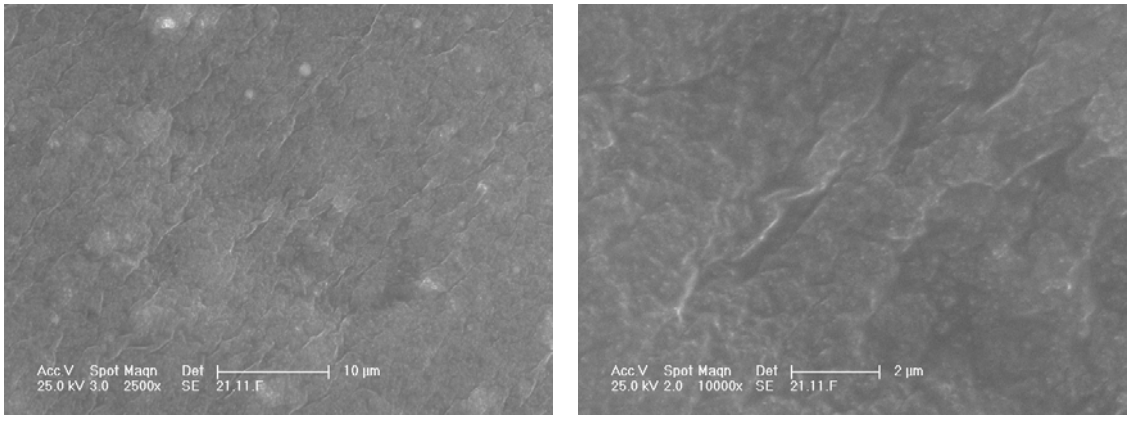

Fig. 6.8 SEM micrographs of MMA/AIBN based GPE containing 10 wt% of Al_2O_3 nanoparticles.

6.3.3 Specific conductivity measurements

Figure 6.10 demonstrates that the specific conductivity of gels with Li ions in the MMA/SA system increases linearly with increasing the volume of Al_2O_3 up to 7.17 wt% (0.37 $mS.cm^{-1}$). In case of Na ions the conductivity decreases following the increasing of Al_2O_3 volume up to 7.17 wt% (0.12 $mS.cm^{-1}$). The overall highest

conductivity of 0.39 mS.cm^{-1} was surprisingly achieved for the gel containing Na ions at 10 wt% of Al_2O_3 content, while a further increase of alumina up to 10 and 12 wt% for both, Li and Na ions containing membranes, means conductivity decrease.

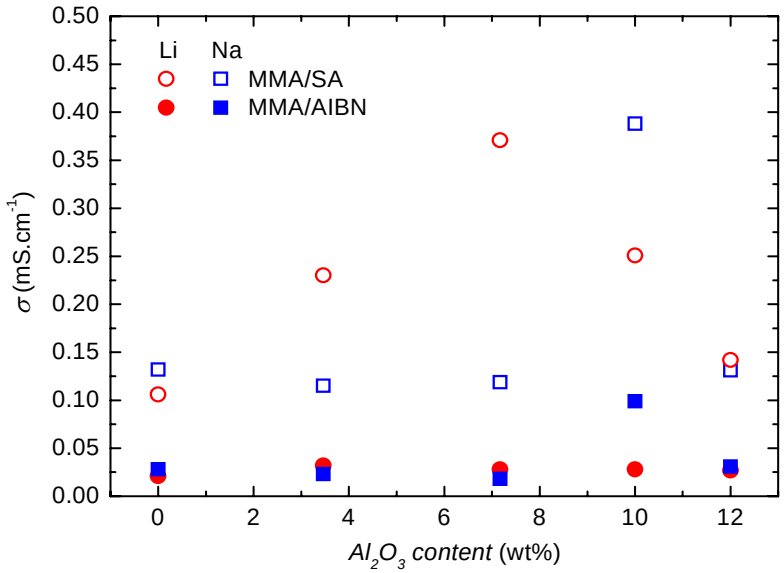

Fig. 6.9 Specific conductivity versus Al_2O_3 content for MMA/SA and MMA/AIBN based gel electrolytes containing Li or Na ions, measurement temperature 30°C.

Using specific conductivity values, with respect to Al_2O_3 content, we compared the MMA/SA and MMA/AIBN based polymer matrixes. Following Figure 6.10, we observed a higher dispersion of measured data, over 380 % for PMMA-PC-$LiClO_4$ at 25°C, resulting in higher conductivity values in case of MMA/SA based electrolytes. Figure 6.10 confirms the presumption of a two-phase heterogeneous system consisting of a polymeric matrix with immobilized solvent [10]. A similar behaviour, though less expressive, was also observed in gels with the MMA/AIBN polymer matrix and Na ions. On the contrary, conductivity values of samples prepared from the MMA/AIBN with dissolved Li ions were not in agreement with values measured in MMA/SA based membranes. The highest conductivity of 0.03 mS.cm^{-1} was achieved in case of MMA/AIBN based GPE with Li ions and 3.46 wt% of Al_2O_3.

Table 6.2 Properties of GPEs based on MMA/SA polymer with 0.1M $LiClO_4$ in PC. Apparent activation energy values E_A obtained from parameter A of Arrhenius plot (at temperatures ς between -70 and 70°C.

Al_2O_3 wt. %	A (K)	$E_{A(0<\varsigma<70\,°C)}$ (kJ.mol^{-1})	A (K)	$E_{A(0<\varsigma<-70\,°C)}$ (kJ.mol^{-1})
0	-1.249	23.9	-2.874	55.0
3.46	-1.045	20.0	-2.607	49.9
7.17	-1.035	19.8	-2.34	44.8
10	-0.997	19.1	-2.544	48.7
12	-0.921	17.6	-2.679	51.3

An example of Arrhenius plot of the specific conductivity of MMA/SA based GPEs with immobilized Li ions and Al_2O_3 nanoparticles is shown in Fig. 6.11 The specific conductivity values from Fig. 6.11 were separately fitted within a temperature range from 70 to 0 °C and 0 to -70 °C in Arrhenius logarithmic scale. Arrhenius slope A

was used to calculate the apparent activation energy derived from equation 4.13.2. Resulting E_A values of GPEs based on MMA/SA polymer with 0.1M $LiClO_4$ in PC are summarized in Table 6.2.

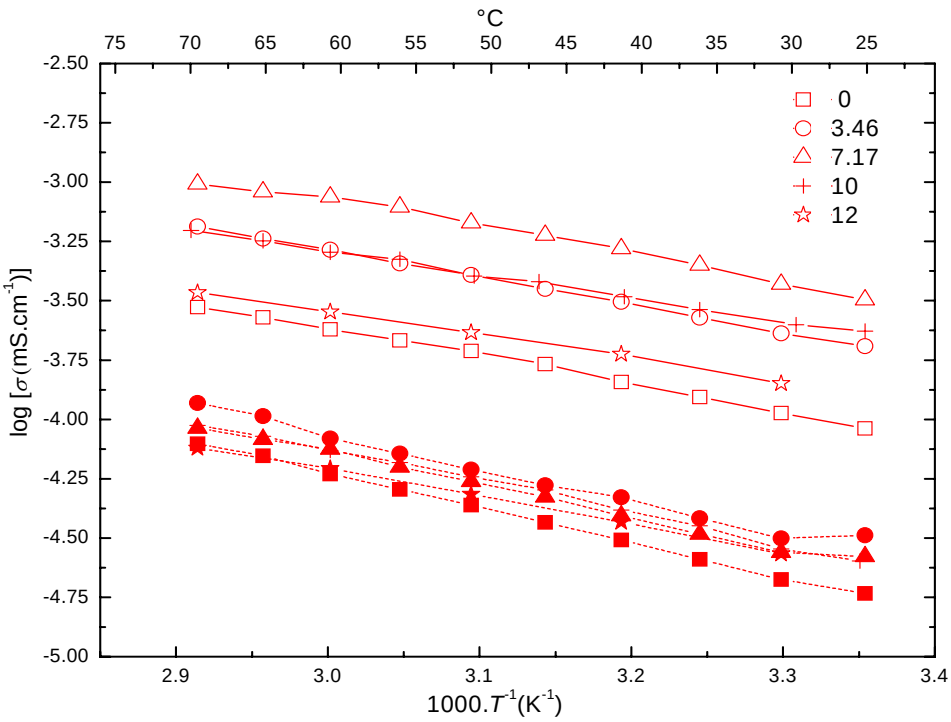

Fig. 6.10 Arrhenius plot of the specific conductivity of MMA/SA (solid line) and MMA/AIBN (dashed line) based gel electrolytes containing immobilized Li ions and denoted wt% of Al_2O_3 sorbent, measurement temperature 25 °C – 70 °C.

In our previous work, we found the possible application of MMA/SA based gel electrolytes reasonable at a temperature above -25 °C, the so called transformation point [11]. At this temperature, disposable changes of polymeric structure, inducing a strong increase of its resistivity, were observed. Figure 6.11 shows slight flattering of conductivity curves. Unlike the gel without alumina filler, the transformation point is lowered by Al_2O_3 addition to values below -25°C. It is important to note that all Li containing samples with alumina exhibited higher conductivities than the membrane plain of Al_2O_3. The conductivity flattering was pronounced especially at lower temperatures. This explanation is supported by apparent activation energy values given in Table 6.2. The $E_{A(0 < \varsigma < 70\ °C)}$ of gel with 10 wt% of the alumina content suggests better conducting system however the highest specific conductivity value exhibits 7.17 wt% Al_2O_3 gel. This discrepancy can be attributed to inaccurate interpolation of the Arrhenius plot as discussed in chapter 4.2.3. Due to unknown T_g values of examined membranes were unable to apply a VTF equation. Still, when the correlation factor is considered the E_A values from Tab. 6.2 give valuable information on the temperature-conductivity dependency especially in the region of $0 < \varsigma < 70$ °C (for detail information on data presentation see chapter 4.2.3).

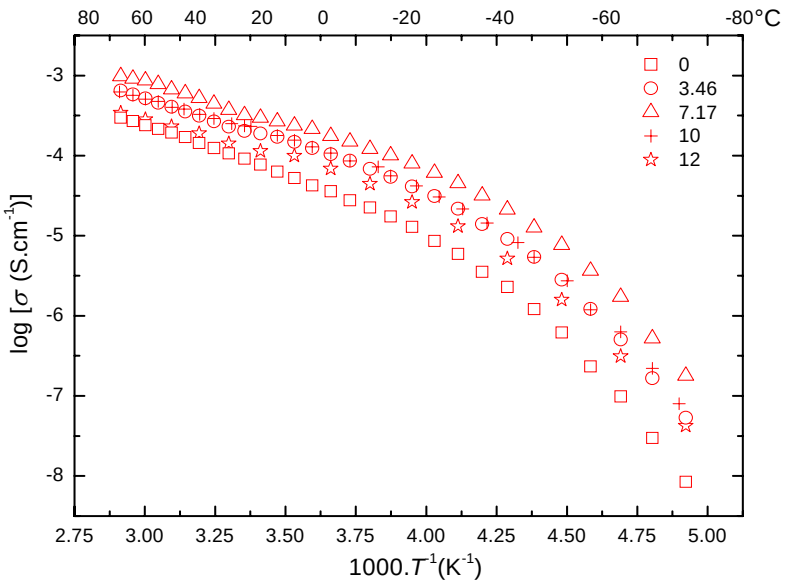

Fig. 6.11 Arrhenius plot of the specific conductivity of MMA/SA based gel electrolytes with immobilized Li ions and Al_2O_3 nanoparticles in wt%, measurement temperature from -70 °C to 70 °C.

We can assume that the conductivity of liquid electrolytes is decreased by the addition of alumina in all Al_2O_3 concentrations. Incorporation of the redox couple suggests that the inhibition of conductivity in liquid electrolytes can be assigned to increased interactions between free charge carriers and dispersed nanoparticles. On the other hand, a remarkable increase of conductivity of almost by one half-order of magnitude at room temperature was observed for MMA/SA based gel electrolytes containing dissolved $NaClO_4$ in PC. The behaviour of Fc/Fc^+ redox couple indicates that the dipole moment of Al_2O_3 molecule can participate in solvation process.

However, understanding of alumina's role in ion-solvating process would need more complex physical effects to be considered, i.e. electrostatic interactions due inductive effects, or to instantaneous dispersion forces (i.e. van der Waal's bonds), or to formation of hydrogen bonds, etc [8,9]. Concerning mechanical properties, a slight enhancement upon addition of Al_2O_3 was achieved. Moreover, we found an increased content of alumina fillers giving a good contrast to PMMA based gel electrolytes, hence making them prospective for electrochromic display application [12-15].

References

[1] CHEN, H. W., LIN, T. P., CHANG, F. CH. Ionic conductivity enhancement of the plasticized PMMA/$LiClO_4$ polymer nanocomposite electrolyte containing clay. In *Polymer*. The Netherlands: Elsevier, 2002. 43. s. 5281-5288.

[2] ADEBAHR, J., et al. Enhancement of ion dynamics in PMMA-based gels with addition of TIO_2 nano-particles. In *Electrochimica Acta*. The Netherlands: Elsevier, 2003. 48. s. 2099-2103.

[3] AHN, J. H., et al. Nanoparticle-dispersed PEO polymer electrolytes for Li batteries. In *Journal of Power Sources*. The Netherlands: Elsevier, 2003. 119-121. s. 422-426.

[4] JOHANSSON, P., JACOBSSON, P. TiO_2 nano-particles in polymer electrolytes: surface interactions. In *Solid State Ionics*. The Netherlands: Elsevier, 2004. 170. s. 73-78.

[5] AHMAD, Shahzada, et al. The effect of nanosized TiO_2 addition on poly(methylmethacrylate) based polymer electrolytes. In *Journal of Power Sources*. The Netherlands: Elsevier, 2006. 159. s. 205-209.

[6] AHMAD, Shahzada, AHMAD, Sharif, AGNIHOTRY, S. A. Nanocomposite electrolytes with fumed silica in poly(methylmethacrylate): thermal, rheological and conductivity studies. In *Journal of Power Sources*. The Netherlands: Elsevier, 2005. 140. s. 151-156.

[7] WALLS, H. J., et al. Fumed silica-based composite polymer electrolytes: synthesis, rheology, and electrochemistry. In *Journal of Power Sources*. The Netherlands: Elsevier, 2000. 89. s. 156-162.

[8] ZANELLO, Piero. *Inorganic Electrochemistry: theory, practice and application*. United Kingdom: The Royal Society of Chemistry, 2003. 634 s. ISBN 0-85404-661-5.

[9] BARD, A. J., FAULKNER, L. R. *Electrochemical Methods*: *Fundamentals and Applications*. 2nd rev. edition. New York: John Wiley&Sons, 2001. 850 s. 2. ISBN 0-471-04372-9.

[10] KREJZA, Ondřej, et al. A Study of PMMA Based Electrolytes with the Methyl Violet Dyes. In *11th International Symposium on Polymer Electrolytes*. Ofir: University of Minho, 2008. s. 125-125.

[11] VONDRÁK, Jiří, et al. Ion-conductive polymethylmethacrylate gel electrolytes for lithium batteries. In *Journal of Power Sources*. The Netherlands: Elsevier, 2005. 146. s. 436-440.

[12] KREJZA, O., ŠILHÁN, Z., SEDLAŘÍKOVÁ, M. Measurements of the PMMA Based Electrolytes Containing Al_2O_3 Nanoparticles. In *7th Advanced Batteries and Accumulators – ABA-2006*. Brno: BUT-Brno, 2006. s. 55-57. ISBN 80-214-3181-4.

[13] KREJZA, Ondřej, et al. The presence of nanostructured Al_2O_3 in PMMA-based gel electrolytes. In *Journal of Power Sources*. The Netherlands: Elsevier, 2008. 178. s. 774-778.

[14] KREJZA, Ondřej, et al. The Presence of Nanostructured Al_2O_3 in PMMA Based Gel Electrolytes. In *7th International Meeting on Electrochromism*. Istanbul, 2006. s. 42-42. ISBN 975-561-281.

[15] KREJZA, Ondřej, et al. Redox Processes in PMMA/PC Gels Prepared by Different Methods. In *11th International Symposium on Polymer Electrolytes*. Ofir: University of Minho, 2008. s. 124-124.

7 Hybrid Electrochromic Devices incorporating PMMA and ICS-PPG 4000 based I_3^-/I^- redox electrolytes

In section 7.1 the electrochemical properties of MMA/SA based GPEs with Li and Na ions designed for use in hybrid electrochromic (HEC) device are discussed. The redox pair was introduced in electrolytes with the dissolution of I_2 and one of the lithium iodide (LiI). Furthermore the comparative sol-gel electrolyte incorporating I_3^-/I^- redox couple and its electrochemical properties are summarized in section 7.2. Section 7.3 elucidates the way of HEC device fabrication and describes in the detail the method of vacuum bag *in-situ* assembly of HEC cell with MMA/SA based electrolyte. The experimental methods for *in-situ* HEC cell testing are detailed in section 7.4. Finally the results from coupled UV-VIS optoelectrochemical tests performed on HEC cells are discussed in section 7.5.

7.1 *MMA/SA based GPEs*

For HEC device assembly the MMA/SA based gel polymer electrolytes with embedded iodide-iodine system were designed. Contrary to gels with $LiClO_4$ and $NaClO_4$ the optional component was represented by LiI or NaI and I_2 dissolved in PC. The ratio 10:1 iodide-iodine in the system was chosen following the previous results [1], potassium iodide was not used due to the low solubility in PC. Thus the concentration was 1.22 M iodide and 0.12 M iodine. The polymeric PMMA electrolytes were prepared the same way as described in chapter 5.2.1. The chemical composition of prepared gels is given in Tab 7.1 together with the specific conductivity values.

Table 7.1 The chemical composition and specific conductivity of MMA/SA based GPEs containing LiI or NaI and I_2 in PC, measurement temperature 30 °C.

Optional component	Chemical composition[1] (wt%)	$c(XI:I_2)$ ($mol.l^{-1}$)	σ ($S.cm^{-1}$)
PC-LiI-I_2	MMA/PC/LiI/I_2 60.3/34.1/4.7/0.9	1.22:0.12	0.36×10^{-3}
PC-NaI-I_2	MMA/PC/NaI/I_2 60.0/33.9/5.2/0.9	1.22:0.12	1.06×10^{-3}

[1] MMA expresses the weight contribution of the host matrix in the overall sample composition

After preparation the samples were stored in Petri dish in an empty desiccator, but one from each system was kept unprotected on air at the room temperature to observe chemical changes due to the effect of the aerial moisture. Prepared gels were brown and produce slight odour of iodine. Stored in Petri dish on air, drops of brown liquid appeared on their surface during several weeks since preparation. FT-IR measurements showed propylene carbonate with a small content of water (less than 3 wt%). It was mentioned earlier that MMA/SA gels with hygroscopic perchlorates exhibit long-term chemical stability without any exclusion of liquid from the structure. Gels stored in a desiccator with silica gel are stable, no liquid is excluded from the material and mechanical properties do not change within more than 9 months.

7.1.1 Specific conductivity measurements

The impedance measurements were performed within the frequency range of 100 kHz to 1 mHz for lower temperatures and 10 kHz to 100 Hz for temperatures above 0 °C. The membranes of a thickness from 0.4 to 0.9 mm were cut out from Petri dishes and fastened between two stainless steel blocking electrodes. The impedance response was measured over the range -70 to 70 °C. The Arrhenius plot of specific conductivity vs. temperature is shown in Fig. 7.1.

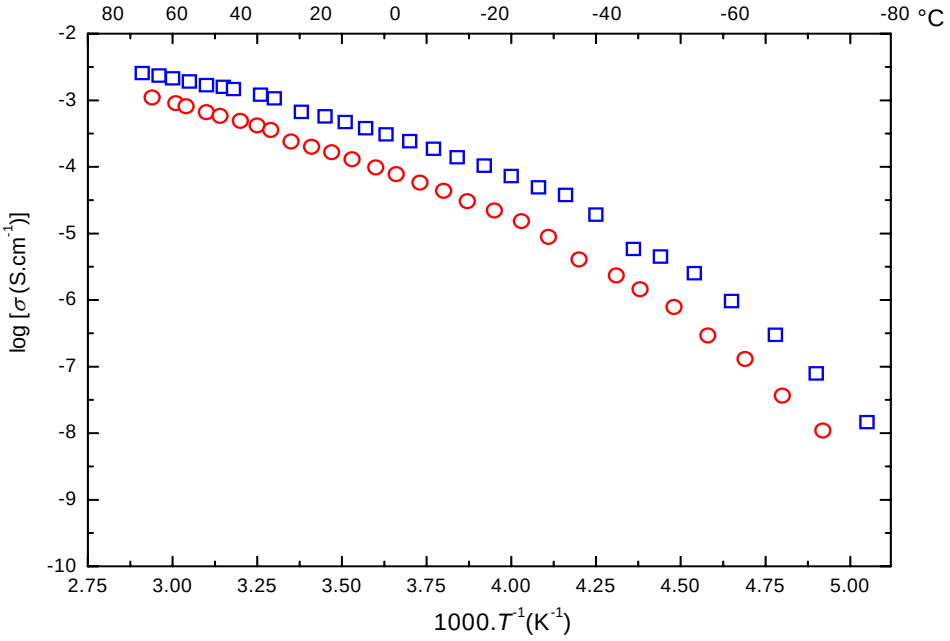

Fig. 7.1 Arrhenius plot of the MMA/SA based gels with NaI/I_2 (squares) and LiI/I_2 (circles), measurement temperature -70 to 70 °C.

From the whole temperature region in Fig. 7.1 one may note that the resistivity is always lower for the sodium iodide-iodine gel than for the gel with lithium salt. Moreover both Li-I_2 and NaI-I_2 systems feature change of the slope at ca. -25 °C (corresponding to $1000.T^{-1} \approx 4.1$) characteristic for heterogeneous PC-PMMA gels, induced by structural change of the polymeric network from elastomeric (less organized, less restrictive towards ions motion) to crystalline (more organized, more restrictive towards ion motion). This structural change is associated with significant decrease of conductivity followed by the second change of the slope at approx. -55 °C (melting point of the solvent). Above this temperature the PC is solidified and the motion of ions in the structure of gel is strongly restricted. Hence from the view of practical application, the operating temperature range is above -25 °C.

The impedance measurements suggested high ionic conductivity of prepared gels. The ionic conductivities of LiI-I_2 and NaI-I_2 gels measured at 30 °C are summarized in Table 7.1. When compared with previously prepared gels with inorganic perchlorates from Tab. 5.5 we see that the specific conductivity of gel with sodium cations is approximately 2 to 3 times higher than the conductivity of lithium gels. The mobility of larger sodium cation is higher than the mobility of lithium cation, whose motion is probably more restricted by the interaction with the polymeric network. The values of conductivity of gels with iodide-iodine system are similar to the values of gels with perchlorates, however the concentration of perchlorates is approximately half of iodide (compare Tab. 5.5 and 7.1).

7.1.2 Electrochemical behaviour

In our earlier work we have investigated the electrochemical behaviour of transition metal complexes in the MMA/SA based gel electrolytes. The redox reaction reversibility and kinetics of Fc/Fc^+ couple were studied using cyclic voltammetry technique and compared with those in liquid, propylene carbonate, medium. Furthermore the apparent diffusion coefficients of the redox couple were determined during polymer matrix formation [2].

From the behaviour of Fc/Fc^+ probe in the liquid PC solution and the MMA/SA based gel electrolyte we conclude; (a) the peak-to-peak separation value (ΔE_p) was found in both PC and MMA/SA close to the value theoretically expected for a reversible process (see chapter 6.2.2); (b) the reversibility of redox reaction was almost unaffected by inhibiting the Fc/Fc^+ couple in the polymer, ΔE_p of Fc/Fc^+ in the gel lied between 60 and 90 mV; (c) no significant influence of supporting electrolyte, Na or Li perchlorates, was recorded; (d) the almost three order decrease of the diffusion coefficients for Fc and Fc^+ during polymerization was observed; D_{0f} in liquid decreased from 6.5×10^{-6} $cm^2.s^{-1}$ to 2.2×10^{-9} $cm^2.s^{-1}$ in the gel medium.

7.2 *ICS-PPG 4000 based sol-gel electrolyte*

For the comparison in HEC device we choose, based on our mutual cooperation, the organo-inorganic electrolyte developed by Orel et al. from National Institute of Chemistry in Ljubljana, Slovenia. Their sol-gel electrolyte is based on unhydrolyzed organo-inorganic precursor ICS-PPG with variable PPG chain length. In our case the molar weight of the PPG was estimated at 4000. The redox electrolyte was made by addition of LiI and I_2 in molar ratio 10:1 to the mixture of ICS-PPG and tetramethylene sulfone (TMS), followed by addition of acetic acid. Co-solvent TMS was chosen because of the high boiling point preventing its evaporation from the HEC device. The electrolytes catalyzed with AcOH gelled in 5 to 7 hours when kept on air. The particular chemical composition of the electrolyte used in HEC device was; ICS-PPG/AcOH/ LiI/I_2/TMS=41.4/14.9/7.2/1.4/35.2 (wt%). The specific conductivity of ICS-PPG based sol-gel electrolyte was reported to lay significantly above 0.35 $mS.cm^{-1}$ [1].

7.2.1 Electrochemical behaviour

Before implementation into HEC device the electrochemical behaviour of ISC-PPG based gels was tested in our laboratory. For the investigation of electrochemical changes during polymer network formation the Fc/Fc^+ redox couple was chosen. As a supporting electrolyte an anhydrous $LiClO_4$ in 0.5M concentration was used.

Simulating preparation of material for the electrochromic device, the cyclic voltammograms were recorded in following systems:

- TMS,
- fresh mixture of sulfolane with ICS-PPG 4000 (TMS – ICS-PPG 4000 weight ratio 8.5 : 2) and
- mixture of sulfolane with ICS-PPG 4000 (TMS – ICS-PPG 4000 weight ratio 8.5 : 2) being slowly hydrolyzed by addition of 0.72 g of AcOH.

The experiments described above were repeated with Fc/Fc^+ present in 0.025M concentration in TMS.

The electrochemical measurements were performed in a glassy cell with platinum working and auxiliary electrode and PMMA-Cd-Cd^{2+} solid-state reference electrode. The cyclic voltammograms were recorded every day for 12 days since preparation.

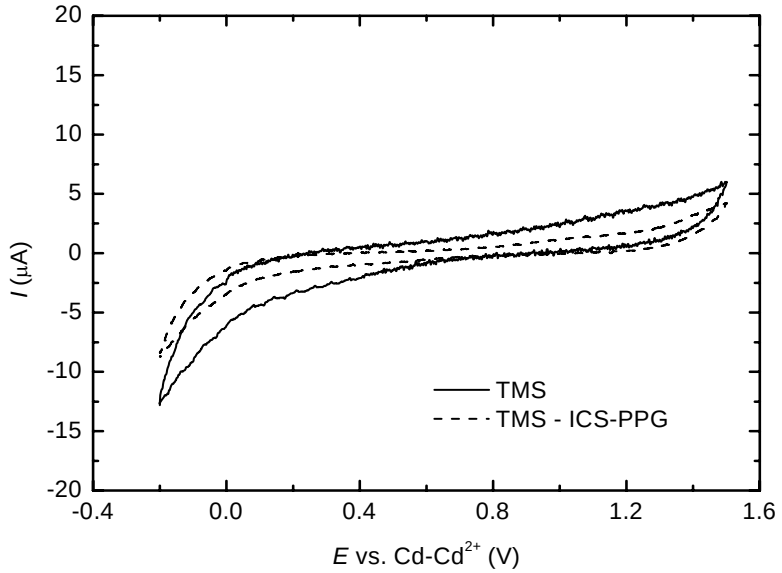

Fig. 7.2 The cyclic voltammogram of 0.5M $LiClO_4$ in fresh TMS or TMS – ICS-PPG 4000 (8.5:2 wt.); working and auxiliary electrode platinum, PMMA-Cd-Cd^{2+} reference electrode, scan rate 0.005 $V.s^{-1}$.

The measurements of system without redox pair showed wide potential window from +0.1 to +1.5 V vs. Cd-Cd^{2+} (see Fig 7.2). This window is stable and wide after hydrolysis of ICS-PPG 4000 and no residual peak appeared within 12 days since preparation.

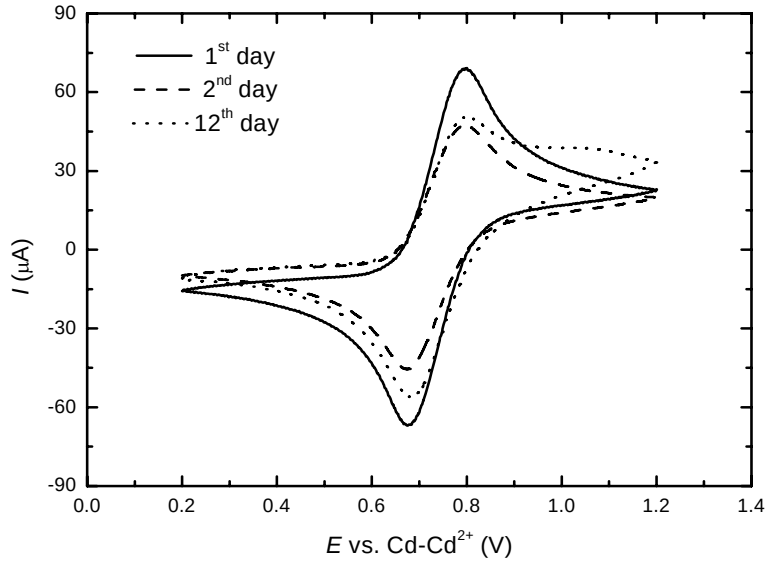

Fig. 7.3 The cyclic voltammograms of 0.025M Fc-Fc+ in TMS – ICS-PPG 4000 (8.5:2 wt.) measured 1^{st}, 2^{nd} and 12^{th} day after hydrolysis; 0.5M $LiClO_4$ supporting electrolyte, working and auxiliary electrode platinum, PMMA-Cd-Cd^{2+} reference electrode, scan rate 0.005 $V.s^{-1}$.

Figure 7.3 shows the cyclic voltammograms of Fc/Fc^{+} in TMS-ICS-PPG based sol-gel electrolyte during precursor hydrolysis. The Fc/Fc^{+} couple exhibits reversible wave with peak potentials $E_{pf} = 0.791$ V and $E_{pr} = 0.683$ V vs. Cd-Cd^{2+} (confidence

interval ± 0.003 V). The peak separation value, ΔE_p was found 0.108 V, higher than the theoretical value 0.059 V, but corresponding to the composition of the matrix (refer to chapter 6.2.2).

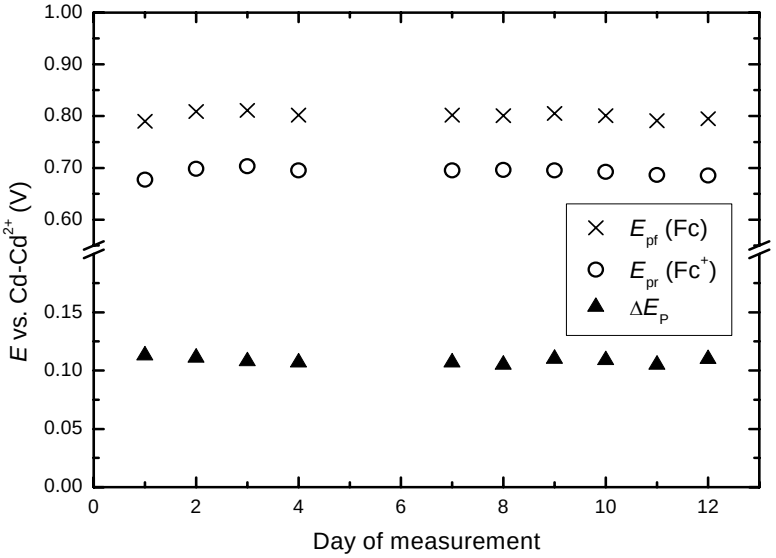

Fig. 7.4 Dependence of peak potentials (E_P) for Fc and Fc^+ and their separation value (ΔE_P) on time during the polymerization; 0.5M $LiClO_4$ supporting electrolyte.

From the qualitative point of view, the peak potentials and ΔE_p values do not change during creation of polymer network (see Fig. 7.3 and 7.4). No shift of peak potentials was observed on contrary to tetraorthomethoxysilane or tetraorthoethoxysilane based silica sol-gel glass monoliths with embedded propylene carbonate [3].

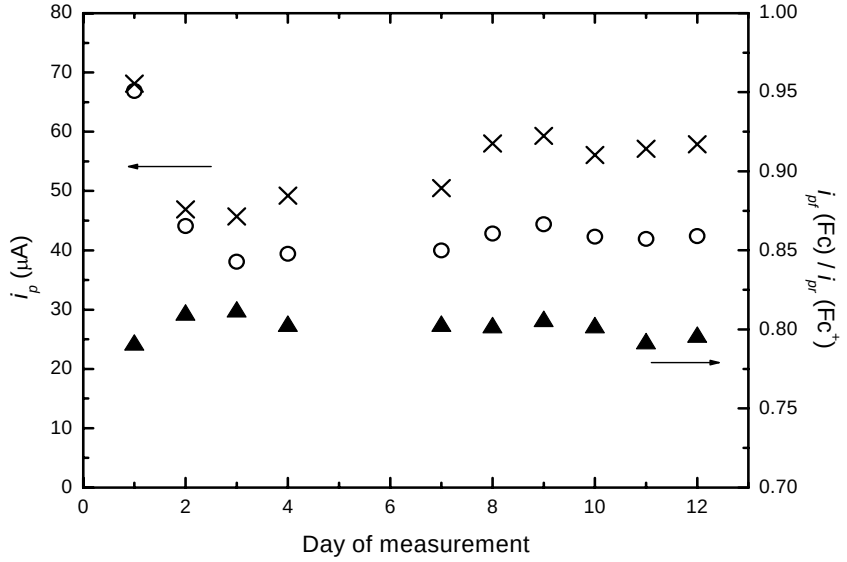

Fig. 7.5 Dependence of peak currents (i_p) for both redox reactions of Fc/Fc^+ couple and their ratio (i_{pr}/i_{pf}) on time during the polymerization; 0.5M $LiClO_4$ supporting electrolyte.

The relationship between peak current and apparent diffusion coefficients was analyzed using Randles-Ševčík equation (4.1). The results from quantitative study including changes of peak currents, (i_p) during polymerization – hydrolysis of ICS-PPG

4000 are summarized in Fig. 7.5. The voltammetrical measurement showed small, ca. 14% decrease of peak currents. The decrease was identical for both forms of ferrocene, the i_{pf} (Fc)/i_{pr} (Fc^+) value stayed identical within the error of measurement. Observed ca. 14% decrease of the anodic and cathodic peak currents was caused by 26% decrease of the apparent diffusion coefficients of both redox forms of ferrocene during polymerization (see Fig. 7.3). This means, that the TMS – ICS-PPG materials do not restrict the motion of ferrocene more than 25 – 30% after change from liquid to solid state. The decrease is much lower than in the case of MMA/SA based polymer gel electrolyte, where the decrease of diffusion coefficients for ferrocene is approximately about three orders (see chapter 7.1.2).

7.3 *HEC device fabrication*

The two types of hybrid electrochromic cells based on MMA/SA gel and ICS-PPG sol-gel polymer electrolytes were prepared. The redox I_3^-/I^- couple was represented by lithium iodide-iodine system dissolved in aprotic PC (MMA/SA) or TMS (ICS-PPG) solvents. The electrolyte blends, prepared as described in the chapters 5.2.1 (MMA/SA) and 7.2 (ICS-PPG), had following chemical composition:

- MMA/PC/LiI/I_2 = 60.3/34.1/4.7/0.9 (wt%)
- ICS-PPG/AcOH/ LiI/I_2/TMS = 41.4/14.9/7.2/1.4/35.2 (wt%).

Furthermore, to compare the electrochemical properties of active layer with different pre-treatment, one sample of HEC cell with pre-heated WO_3 is included.

7.3.1 Substrate characterization

The hybrid electrochromic devices comprised following electrode composition;

glass | FTO | WO_3 | electrolyte | Pt | FTO | glass,

where on the WO_3 side the 3 mm glass plate with sputtered SnO_2:F –FTO ($\rho < 50\Omega/\square$) was coated with nanocrystaline WO_3 film, with the grain size 30 nm, prepared using a peroxo sol-gel route [4]. The optically active layer was deposited by dip coating and heat-treated at 450 °C for 30 minutes, resulting in optically perfect film with a thickness of 200-300 nm. The other side comprised of few nm thick Pt layer vacuum sputtered on the top of another FTO coated glass (see Fig. 7.6).

7.3.2 Device assembly

The ICS-PPG based device with LiI-I_2 was prepared in a such way that a drop of the redox electrolyte was placed on the WO_3 film and immediately covered with a platinised SnO_2:F substrate serving as a counter electrode. The upper glass was manually pressed onto the lower one (see Fig. 7.6), in this way obtaining approx. 10 to 50 μm thick electrolyte layer in the cell. No sealing of HEC device was used and therefore the evaporation of AcOH from the redox electrolyte was not prevented. The gelation took place within next 24 hours. As the conductivity is strongly dependent on AcOH content a TMS with high melting point (20–26 °C) was used to reduce its evaporation. With relatively low viscosity the fresh mixture exhibits enough cohesive force to prevent sliding off the electrode and creating uniform film with no need of spacing.

A HEC device with modified WO_3 had the electrochromic layer thermally treated at 450 °C for 30 minutes and then *re-heated* at 300 °C for 10 minutes before

assembling. This device is further referred as “heated” whereas “cold” suggests it was a cell accommodating the same electrolyte but without any post-treatment on WO_3-FTO electrode.

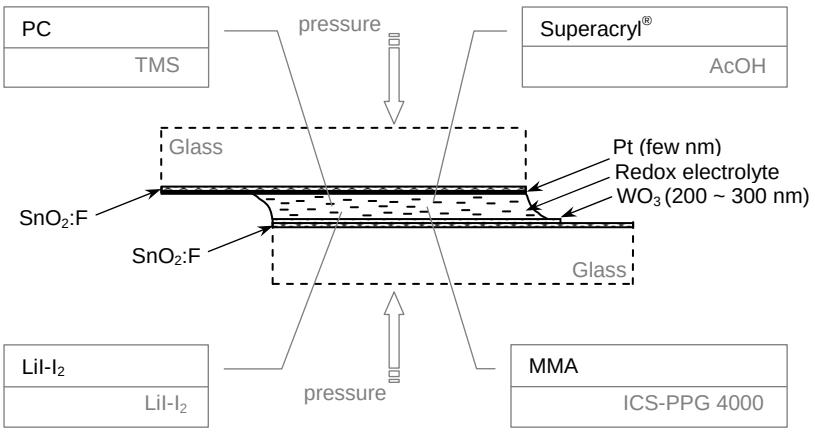

Fig. 7.6 A HEC cell electrode arrangement and assembly comprising the MMA/SA (black) and ICS-PPG (grey) based redox electrolyte.

For HEC cell with MMA/SA based GPE the new method of preparation was developed. Comparing to above mentioned preparation procedure we faced two main problems during the in-situ electrolyte formation:

» High viscosity of the blend causes that the electrodes tend to slide down when sandwiched. Moreover the loss of electrolyte was observed due to a low surface tension of propylene carbonate, supported by good substrate wettability.

» The microparticles, originating from an oligomeric resin, with a mean particle diameter of 59.88 μm, attract an air creating bubbles when sandwiched between the electrodes. The volume of captured air increases during the polymerization, the process connected with the shrinkage in the bulk of the electrolyte.

First attempts were done on the thin MMA/SA membrane prepared into a Petri dish following the procedure described in chapter 5.2.1. The minimal thickness that the gel can withstand without being damaged was experimentally found to be above 200 μm. Thinner membranes were usually pulled apart during removal from Petri dish. Originally the HEC device comprised 500 μm thick membrane sandwiched between the electrodes. Prior the assembly we etched the membrane surface by placing the drop of the solvent on its both sides. We presumed that the modified surface would provide better adhesion towards microcrystalline electrodes. Moreover the microscopic surface inhomogeneities of the membrane, similar to these from Fig 6.7, would be eliminated. The device was then stored in a desiccator for 24 hours. However, visually inspected with no indication of possible disruption, during the initial optoelectrochemical tests, the phase separation was observed and followed by the delamination of the electrode-electrolyte interface.

In order to increase the electrode-electrolyte compatibility the method of *in-situ* polymerization in a vacuum bag was employed. The preparation of HEC cell with MMA/SA based GPE comprised of following steps;

(1) The 4×4 mm square of 250 μm thick double side 3M-VHB tape was placed into each corner of the Pt coated electrode.

(2) Both electrodes were placed into the oven (with the coating facing up) and pre-heated at 40 °C for 10 min

(3) The active surface area (5×5 cm) was covered on both electrodes, using automatic pipette, with approx. 2 ml of the electrolyte solution. In this way a homogeneous film of a thickness approx. 300 μm was obtained on both electrodes.

(4) After 15 minutes of pre-curing at 40 °C the electrodes were quickly removed, sandwiched and thoroughly sealed inside the bag made of enforced vulcanized rubber.

(5) The bag was placed to the oven and connected to a standard rotary type vacuum pump.

(6) The pump was set for the air evacuation and the thermoregulator to follow the temperature ramp from Fig. 7.7.

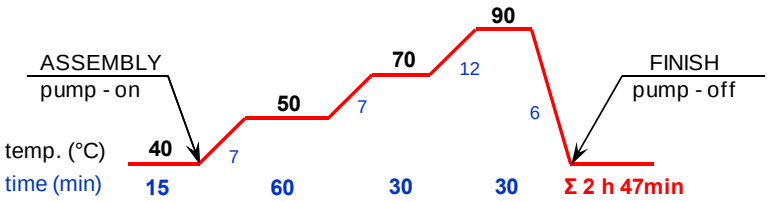

Fig. 7.7 The in-situ curing step of HEC device with MMA/SA based GPE in a vacuum bag.

After withdrawal the HEC device was stored in a desiccator over night. The pressure imposed on electrodes inside the bag was found to compensate the volume losses during the polymerization. The minimal thickness was defined by 3M-VHB tape at 250 microns. The tape also served as a short-circuit precaution. Usually polymerization of the monomer - Superacryl® blend is initiated immediately. Still, when the substances are combined at RT the initial viscosity drop can occur in a days. On the other hand when exposed to pre-heated electrodes the major viscosity drop can be observed after few minutes.

For large electrode surface a stainless steel Mayer rod (the rod with tightly wound stainless steel wire of varying diameter) can be used. With the rod, the excess of the electrolyte solution can be easily controlled while producing an even coating of defined thickness. We claim the thickness of 6 mils (125 μm) to be a threshold under which the precursor particles were observed to be trapped along the wiring resulting in a highly grooved surface.

Another coating alternative can be a Doctor blade, frequently used for a coating in lithium-ion battery technology [5].

7.4 *In-situ testing procedures*

In-situ UV-visible optoelectrochemical measurements of the HEC cells were made using the HP 8453 diode array spectrophotometer in combination with an Eco Autolab potentiogalvanostat PGSTAT 12. The coupled experiments followed the testing procedure from APPENDIX B. The cyclovoltammetric curves were obtained by the scan rate of 20 $mV.s^{-1}$. The voltage was swept between 0 V to -2 V, reversed to 2 V and then finished at 0 V. The kinetics of the coloration and bleaching was obtained by applying a chronoculometric technique by performing the intercalation of Li^+ ions at -1,5 V for 100 s and deintercalation at 2 V (100 s). Reported potentials correspond to the potential applied to the WO_3 film (working electrode) with respect to the platinised SnO_2:F glass substrate (counter electrode). Due to HEC cell arrangement it was not possible to incorporate the reference electrode hence the potentials of WO_3 and Pt electrodes are not known exactly. Nevertheless, the presence of I_3^-/I^- couple in the electrolyte can determine the platinised counter electrode as a quasy-reference electrode with a definite constant potential according to the actual activity of the redox pair close to its surface.

In order to thoroughly investigate the optoelectrochemical behaviour of prepared HEC cells the above mentioned experimental procedure was employed, comprising; (a) initial cycling at a constant scan rate; (b) observation of the UV-visible transmittance during colouring/bleaching; (c) estimation of the monochromatic transmittance modulation – applied potential dependency; (d) study of the intercalation kinetics versus time in a potentiostatic mode; (e) estimation of the monochromatic transmittance values at a various scan rates; (f) the monochromatic transmittance recovery in a time upon disconnecting the device after Li^+ intercalation (called self erasing).

The peak transmittances (λ = 634 nm) gathered during the chronocoulometric scans, as listed in the experimental procedure -cycles 11, 21, 42 and 191, were used for the evaluation of the cycling stability of PMMA based HEC device.

7.5 *Optoelectrochemical performance of HEC cells*

The device formatting took initial 8 scans and was performed between -2 and 2 V with the 20 $mV.s^{-1}$ scan rate. A desorption of the H_2O (or its fraction OH^- and O^+ species), molecularly adsorbed on an oxidized tungsten surface, was anticipated similar to one reported by Gillet et al. [6]. Furthermore an irreversible cathodic lithium intercalation postulated by Kim and Pyun [7] can be explained with Li^+ loss due to an ion-ion exchange expressed schematically, as

$$W - O - H + Li^+ \leftrightarrow W - O - Li^+ + H^+ \tag{7.1}$$

The phenomenological model of the above mentioned reaction was formulated by Yoshiike and Kondo [8] and involves the proton liberation on the pore surfaces, insertion of the liberated protons into interstitial positions in the WO_3 lattice, and adsorption of a H_2O next to a W=O bond. The change in a structure of WO_3 is usually reflected in its transmittance. The initial monochromatic transmittance (λ = 634 nm) was found to be 75.2% for MMA/SA and 72.6% respectively 77.4% for ICS-PPG based HEC devices with heated and cold WO_3.

Figure 7.8 shows the monochromatic transmittance response of the HEC cells measured at λ = 634 nm. The HEC devices with ICS-PPG electrolytes showed the

intercalation of Li at approximately -0.75 V in negative direction. The transmittance began to fade and the devices turned dark blue. The coloration of HEC cell with MMA/SA electrolyte was slower starting at around -1 V in cathodic direction. The ICS-PPG based HEC cells had only 15% monochromatic transmittance compared to MMA/SA in which the 32.8% transmittance lapse was observed. Surprisingly the HEC device with pre-heated WO_3 showed markedly higher transmittance in bleached state (72.2%) when compared to HEC cells with no WO_3 pre-treatment where the almost identical transmittance of 61.6% (ICS-PPG-cold) and 61.8% (MMA/SA) was recorded. Furthermore the initial transmittance recovery was, after several colouring/bleaching cycles, found lower comparing to above mentioned initial values suggesting stoichiometry changes in WO_3 layer.

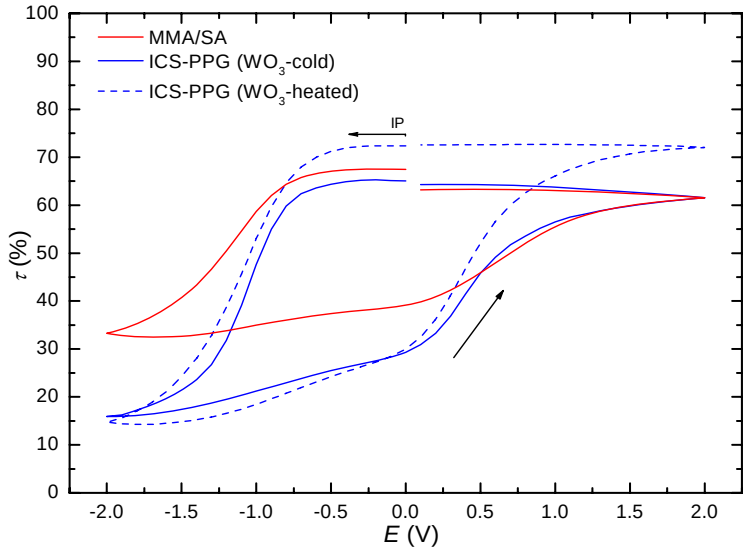

Fig. 7.8 The monochromatic transmittance response of HEC devices with MMA/SA and ICS-PPG based electrolytes; λ = 634 nm, scan rate 20 mV.s^{-1}.

In figure 7.9, cyclic voltammograms of the MMA/SA based HEC device with corresponding cathodic and anodic waves that reflected the insertion/extraction of Li^+ ions into the WO_3 film are displayed. From the in-situ UV-visible optoelectrochemical measurements, performed at various scan rates (10, 20, 40, 60 and 80 mV·s^{-1}), we can see that the intercalation of Li^+ ions into WO_3 film induced the current response, in negative direction notable at ca. -0.75 V (see Fig. 7.9A). During deintercalation, when the potential was swept towards positive values, the linear increase of transmittance was observed. This could be explained by additional electrode reaction (i.e. $I_3^- \rightarrow 3I^- + e^-$) on the WO_3|electrolyte interface, facilitating the extraction of Li+ ions from the WO_3 film as reported by Orel et al [1]. The faradaic response taking place on cathodic side suggests that the redox reaction (i.e. $3I^- \rightarrow I_3^- + 2e^-$) occurred at the same time on Pt electrode (see Fig 7.9A). From figure 7.9B we conclude that the Δτ is strongly dependent on polarization speed, the colouring/bleaching ratio was found larger for lower scan rates and vice versa. However even at a high scan rate (60 mV·s^{-1}), the device response was rapid exceeding with the transmittance ratio exceeding 23%.

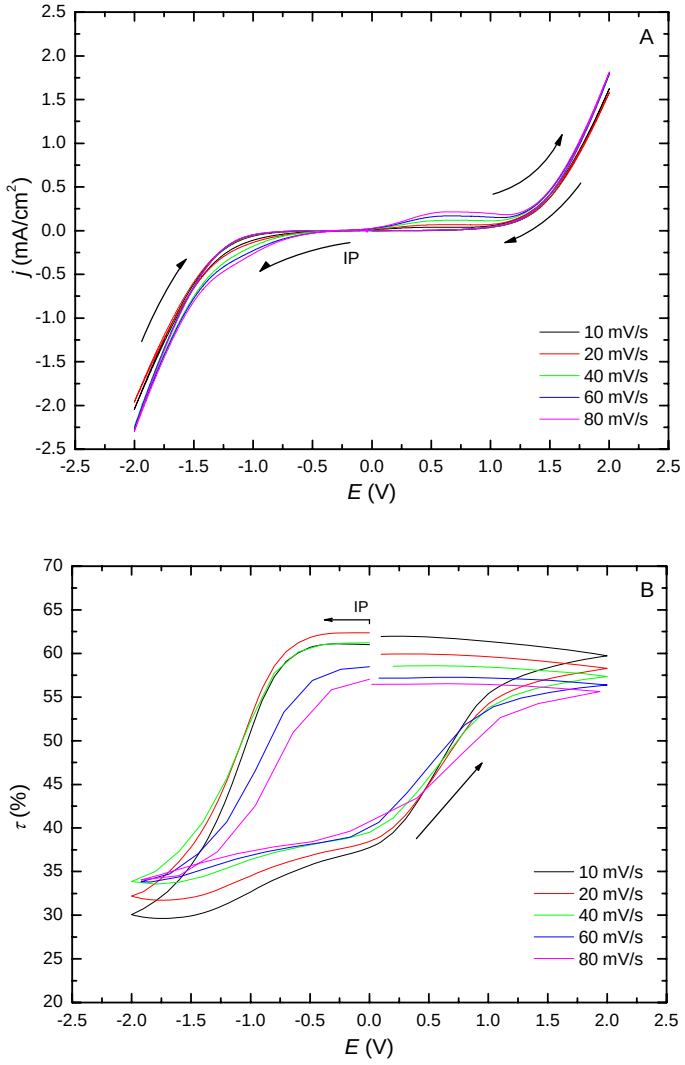

Fig. 7.9 Cyclic voltammetry curves (A) and monochromatic (λ = 634 nm) transmittance response (B) of HEC device with MMA/SA based GPE measured at different scan rates.

Figure 7.10 shows the colouring/bleaching changes of the HEC cells with MMA/SA and ICS-PPG redox electrolytes. The decrease of maximal transmittance values of as-prepared HEC devices, measured in the visible spectra, was observed when compared to single electrodes transmittance, owing to yellowish tint caused by I_2 content in the electrolytes. The transitions of MMA/SA based HEC device revealed that the optical change is lower than 10% for wavelengths below 500 nm while it can even exceed 30% at higher wavelengths. In the bleached state (Fig. 7.10A) the cells with cold WO_3 behaved almost identically, while at above 500 nm the departure towards higher transmittance values in case of HEC cell with pre-heated WO_3 was observed. Figure 7.10B shows the optical properties after Li^+ insertion; in this case the drop of transmittance observed for both ICS-PPG based HEC cells at ca. 500 nm was not followed by the MMA/SA based cell. Furthermore the transmittance onset of MMA/SA based cell, observed at 430 nm, followed by steep increase in optical permeability occurred in both ICS-PPG based cells at lower wavelengths (380 nm). When combined, the transitions from Fig 7.10A and B we conclude that higher transmittance ratio observed in case of ICS-PPG based HEC cells is mainly given by their optical properties during cathodic coloration.

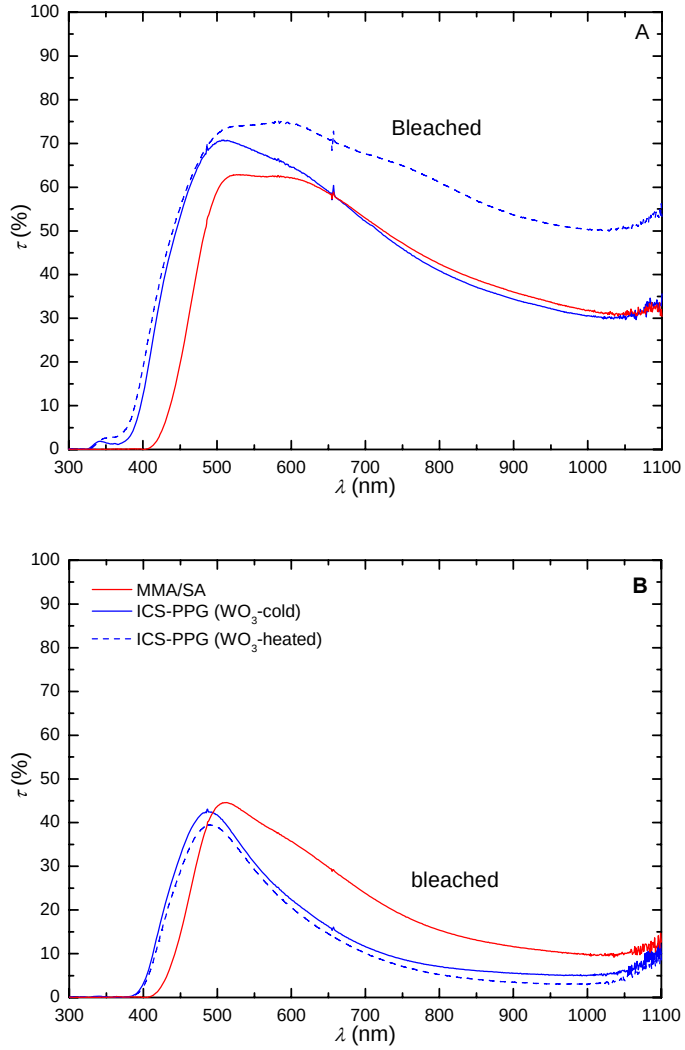

Fig. 7.10 In-situ UV-visible optoelectrochemical measurements of HEC devices with MMA/SA and ICS-PPG based electrolytes in their bleached (A) and coloured (B) state; λ = 330~1100 nm.

Figure 7.11 shows the results on kinetic behaviour of HEC cells observed during potentiostatic colouring and bleaching. The devices first coloured for 100 s at -1.5V and then bleached at +2 V for another 100 s. The monochromatic transmittance showed the major drop in first 10 s while complete coloration took place within approximately 20 to 60 s. The bleaching was even faster, the devices with cold WO_3 bleached almost instantly (in 5 s). According to Heckner and Kraft [9] faster bleaching velocity is in connection with nearly metallic state of intercalated WO_3 layer that presents an electronic conductivity much higher than that of bleached state. Slower bleaching kinetics was observed for the cell with pre-heated WO_3 layer with the initial transmittance recovered after ca. 40 s. An interesting finding was linear response of charge during intercalation/deintercalation process versus time. The characteristic feature of standard battery type ECD is the saturation plateau observed due to limited ion storage of the intercalation electrodes (compare to Fig. 8.13A) [8]. Since in HEC devices the maximal optical change is attained in about 20 to 40 s, the linear charge density versus time response is an additional proof that the $3I^- \leftrightarrow I_3^- + 2e^-$reaction may occurred at either Pt or WO_3 electrode|electrolyte interface during both intercalation and deintercalation processes.

Combining the value of effectively intercalated charge and the transmittance ratio we receive an important operating parameter of an electrochromic device, the coloration efficiency (CE) ($cm^2.C^{-1}$) defined as;

$$CE = \frac{\Delta OD}{Q} = \frac{\Delta\left[\log\left(\frac{T_0}{T}\right)\right]}{Q} \tag{7.2}$$

Where T_0 is the optical transmittance in the bleached state and T is the transmission after the flow of the electrical charge Q ($C.cm^{-2}$) through the device. The coloration efficiency and optical density (OD) depend on the wavelength and are usually higher in the near IR than in the visible region [9].

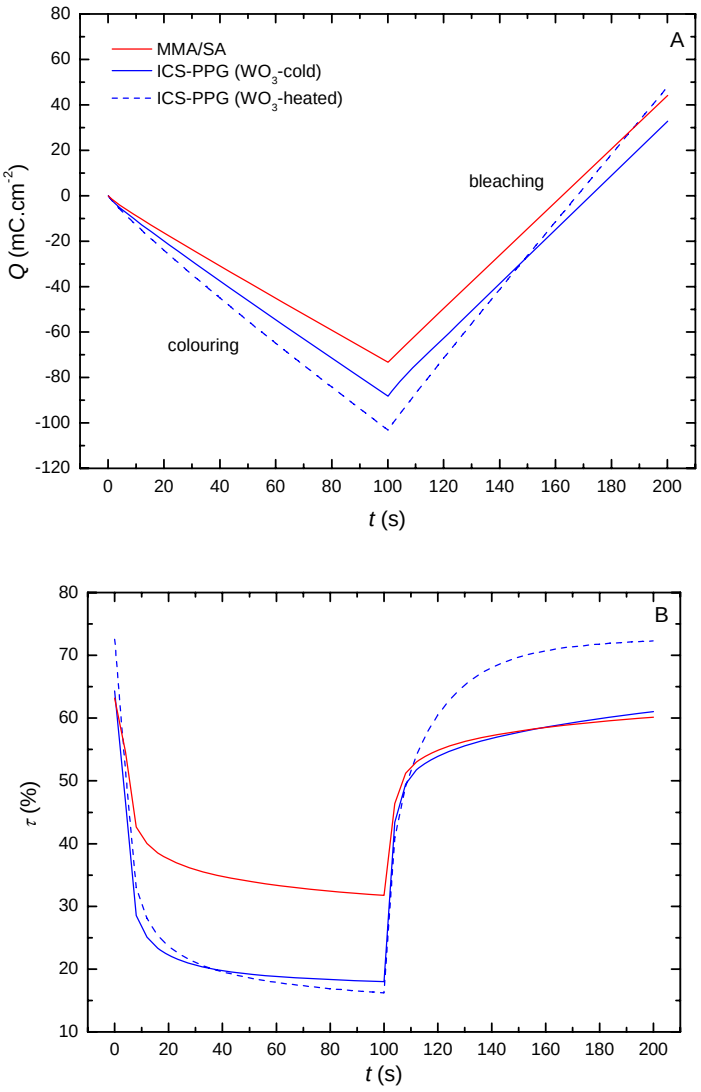

Fig. 7.11 In-situ UV-visible optoelectrochemical measurements of HEC devices with MMA/SA and ICS-PPG based electrolytes during chronocoulometric colouring/bleaching: (A) chronocoulometric curves and (B) monochromatic transmittance (λ = 634 nm).

Using the data from Fig. 7.11B we estimated a coloration efficiency of ICS-PPG and MMA/SA based HEC devices. In order to eliminate the contribution of a charge signal generated by attendant redox reaction, the transmittance at a peak values had to be excluded. Instead, substituted by the transmittance values induced mostly by Li^+ insertion (t = 30 s). The results are summarized in following table.

Table 7.2 The colouring efficiency (CE) and optical density (OD) values of HEC devices with redox MMA/SA and ICS-PPG based electrolytes.

HEC device	T_0 (t = 0 s) (%)	T (t = 30 s) (%)	ΔOD	Q ($mC.cm^{-2}$)	CE ($cm^2.C^{-1}$)
MMA/SA	63.2	35.6	0.25	23.70	10.5
ICS-PPG (WO_3-cold)	64.3	20.5	0.50	28.87	17.2
ICS-PPG (WO_3-heated)	72.6	20.7	0.54	34.78	15.7

The highest CE value from Tab. 7.2 reflects the fast bleaching kinetics of ICS-PPG based cell with cold WO_3. On the other hand CE of MMA/SA based ECD cell reached approximately 63% the values received for cells with ICS-PPG electrolyte. The colouring efficiency, however, is a parameter predominantly connected with an intercalation properties of optically active WO_3 layer, in this case, also the transport of electrically active Li^+ from the bulk of electrolyte need to be considered. We presume that the colouring/bleaching kinetics are to some extend influenced by rather moderate specific conductivity of MMA/SA gel when compared to ICS-PPG electrolytes.

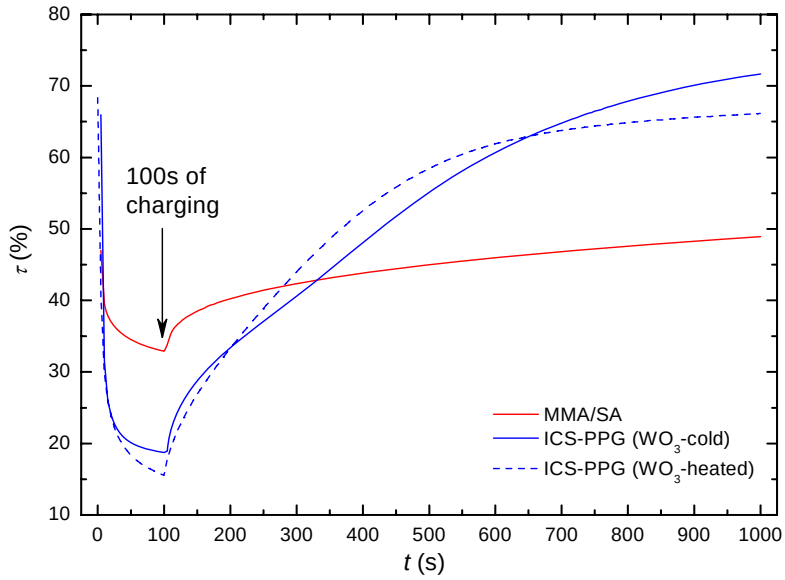

Fig. 7.12 Self erasing properties of HEC devices with MMA/SA and ICS-PPG based electrolytes; λ = 634 nm.

Figure 7.12 shows the monochromatic transmittance response during spontaneous bleaching of redox based HEC cells, called self-erasing effect. Due to the presence of I_3^-/I^- pairs and possible redox reaction at both sides of the electrode|electrolyte interface the coloured device will self-bleach when disconnected from the electrical contacts. Here the devices were charged at -2 V for 100 s and then disconnected. The UV-visible spectra were recorded every 5 s during first 1000 s. It is visible that most of the bleaching at λ = 634 nm occurred by 1000 s while the fastest recovery showed MMA/SA based HEC device.

Figure 7.13 shows the evolution of a transmittance ratio in time for MMA/SA based HEC device measured during potentiostatic cycling. There is a shift of approximately 10% between the initial transmittance in the bleached state and after 40 cycles whereas, no apparent changes during colouring were observed. Further decrease in transmittance ratio observed after 150 colouring/bleaching cycles was found less than 5%.

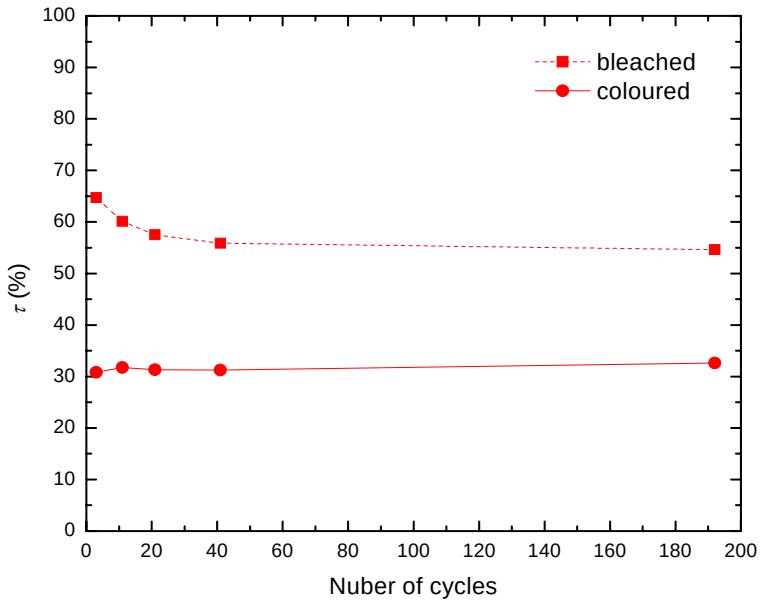

Fig. 7.13 The monochromatic transmittance modulation of MMA/SA based HEC device in bleached (dashed curve) and coloured (solid curve) state; λ = 634 nm.

The HEC device with MMA/SA based redox electrolyte prepared by *in-situ* thermal polymerization showed; (a) a broad optical modulation in visible spectra, $\Delta\tau_{(500-750)} \approx 30\%$; (b) fast switching speed, tens of seconds; (c) colouring efficiency 10.5 $cm^2.C^{-1}$ and (d) cycling stability (up to 190 cycles) [10,11].

Besides, pre-heating WO_3 at 300 °C for 10 minutes prior HECD assembly caused significant increase in UV-VIS transmittance ratio. The transmittance once after bleaching was about 15% higher for device with pre-heated WO_3. We assume that thermal modification of intercalating layer somehow influences the OH modes on the electrode surface. On the other hand slower switching kinetics than that of HEC cells with cold WO_3 were observed [12].

References

[1] OREL, Boris, et al. Development of sol-gel redox I_3^-/I^- electrolytes and their application in hybrid electrochromic devices. In *Solid State Ionics*. The Netherlands: Elsevier, 2003. 165. s. 235-246.

[2] REITER, J., VONDRÁK, J., MIČKA, Z. The Electrochemical Redox Processes in PMMA Gel Electrolytes-behaviour of Transition Metal Complexes. In *Electrochimica Acta*. The Netherlands: Elsevier, 2005. 50. s. 4469-4476.

[3] OPALLO, M., KUKULKA-WALKIEWICZ, J. The electrochemical redox reaction in silica sol-gel glass monoliths and films with embedded organic electrolyte. In *Electrochimica Acta*. The Netherlands: Elsevier, 2001. 46. s. 4235-4242.

[4] OREL, Boris, et al. IR Spectroscopic Investigations of Gasochromic and Electrochromic Sol-Gel—Derived Peroxotungstic Acid/Ormosil Composite and Crystalline WO_3 Films. In *Journal of Sol-Gel Science and Technology*. The Netherlands: Kluwer Academic Publishers, 2002. 24. s. 1113-1121.

[5] TRACTON, Arthur A. *Coatings Technology Handbook*. 3rd edition. USA: CRC Press, 2005. 936 s. ISBN 978-1574-44649-4.

[6] GILLET, M., et al. The role of surface oxygen vacancies upon WO_3 conductivity. In *Surface Science*. The Netherlands: Elsevier, 2003. 532-535. s. 519-525.

[7] KIM, Dong-Jin, PYUNG, Su-Il. Hydrogen transport through rf-magnetron sputtered amorphous WO_3 with three kinds of hydrogen injection sites. In *Solid State Ionics*. The Netherlands: Elsevier, 1997. 99. s. 185-192.

[8] GRANQVIST, C. G. *Handbook of Inorganic Electrochromic Materials*. The Netherlands: Elsevier, 1995. 2 sv. (337, 296 s.). ISBN 0-444-89930-8.

[9] HECKNER, Karl-Heinz, KRAFT, Alexander. Similarities between electrochromic windows and thin film batteries. In *Solid State Ionics*. The Netherlands: Elsevier, 2002. 152-153. s. 899-905.

[10] KREJZA, Ondřej. Hybrid Electrochromic Cells Employing Sol-Gel and Polymeric I_3^-/I^- Redox Electrolytes. In *Proceedings of the Junior Scientist Conference*. Vienna: Vienna University of Technology, 2006. s. 145. ISBN 3-902463-05-8.

[11] KREJZA, Ondřej, et al. Hybrid Electrochromic Cells Employing I_3^-/I^-; Redox Pair Immobilized in Sol-Gel, Organic-Inorganic or PMMA Polymer Electrolyte. In *6th Advanced Batteries and Accumulators – ABA-2006*. Brno: BUT-Brno, 2005. s. 124-128. ISBN 80-214-2298-0.

[12] ŠURCA VUK, A., KREJZA, O., JEŠE, R., et al. Comparison of Hybrid Electrochromic Cells Employing Sol-Gel and Polymeric I_3^-/I^- Redox Electrolytes. In *6th International Meeting on Electrochromism*. Brno: BUT-Brno, 2004. s. 150-151. ISBN 80-214-2622-5.

8 Electrochromic devices incorporating EMA and EOEMA based GPEs

Section 8.1 introduces the EOEMA and EMA based gel polymer electrolytes designed for the application in ECDs. Section 8.2 deals with characterization of intercalation electrodes and details the assembly of ECD with *in-situ* polymerized GPEs. The section is sub divided into paragraphs 8.2.1 dealing with fabrication parameters and morphology of active electrode layers, further 8.2.2 elucidating the intercalation properties by means of CV and QCM techniques, and finally 8.2.3 showing the ECD fabrication. The experimental methods for *in-situ* EC cell testing are detailed in section 8.3. Finally the results from coupled UV-VIS optoelectrochemical tests are used to demonstrate the relationship between the electrolyte composition and the parameters such as change of transmittance, response time and stability are discussed in section 8.4.

8.1 *EMA and EOEMA based gels with $LiClO_4$-PC electrolyte*

For the application in the battery-type electrochromic device, the EOEMA and EMA based GPEs were designed. A chemical composition of the membranes was proposed with respect to the results obtained during basic electrochemical characterization of aprotic systems as discussed in general in chapter 5, further also in 5.2, 5.3 and 5.4. The particular component concentration, expressed in a molar percentage together with the ionic conductivity as of prepared membranes is summarized in following table.

Table 8.1 The chemical composition and ionic conductivity of PEMA and PEOEMA based GPEs for ECDs; experimental temperature 30 °C.

Gel Polymer Electrolyte	Chemical composition (mol%)	c($LiClO_4$) ($mol.l^{-1}$)	σ ($S.cm^{-1}$)
EMA	EMA/PC/$LiClO_4$ 51.2/44.9/3.7	1	0.67×10^{-3}
EOEMA	EOEMA/PC/$LiClO_4$ 48.3/45.5/6.3	1.6	0.35×10^{-3}

As discussed earlier in chapter 5 the optimal ratio of initial components fully determines mechanical and electrochemical properties of the gel. The present polymer is responsible mainly for the mechanical properties (elasticity and good adhesion to the substrate). For improvement of the mechanical properties, a partial cross-linkage of the network was employed. Cross-linking agents EDMA and HexadiMA were already successfully copolymerized with PEMA and PEOEMA electrolytes. The suitable cross-linking agent concentration was found to be 0.3 mol% of the monomer. Another important aspect is the adhesion towards a substrate with amorphous electrochromic coating. Particularly the monomer-solvent ratio is suppressed on behalf of a solvent increasing the gel cohesiveness and the electrolyte-electrode contact. However an *in-situ* polymerization inside the electrochromic device is expected to enhance the contact at the interface, we experienced an immediate delamination of the membrane

with higher solvent content. Therefore a 180° peel test conducted according to ASTM and ISO standards was used to evaluate the optimal monomer-solvent ratio of the membranes with a stress on the high membrane adhesion towards various substrates (see chapter 9.1).

As discussed earlier in chapter 5 the ionic conductivity strongly depends on the amount of solvent in the system. For the ECD application the conductivity was provided by $LiClO_4$-PC electrolyte immobilized in the polymer matrix. However the achieved values of ionic conductivity decreases (comparing Tables 8.2 and 5.5) they are still higher above the limit value 10^{-6} S.cm^{-1} declared by MacFarlane as a minimum for electrolyte in electrochromic window applications [1].

Table 8.2 The ionic conductivity and apparent activation energy values of EMA and EOEMA based GPEs from Tab. 8.1; E_A estimated using VTF equation (4.14.1) within 70 and -70 °C.

Gel Polymer Electrolyte	σ (-20 °C) (S.cm^{-1})	σ (30 °C) (S.cm^{-1})	σ (60 °C) (S.cm^{-1})	$E_A(70 < \varsigma < -70)$ (kJ.mol^{-1})	T_g (K)	T_0 (K)
PEMA	10.87×10^{-5}	0.67×10^{-3}	1.34×10^{-3}	15.5	188.2	153
PEOEMA	1.59×10^{-5}	0.35×10^{-3}	0.78×10^{-3}	20.4	195	139

From Fig. 8.1 and Table 8.2 one may note that the samples used in the ECDs are more resistant considering the influence of temperature on ionic conductivity. Bulk conductivity remains high even at low temperatures around -20 °C (above 10^{-5} S.cm^{-1}), which is an important condition for practical application in smart windows or smart displays [2]. It is obvious that the specific conductivity decreased 3 to 5 times when compared to the results presented in Tab. 5.5. The remarks on electrochemical stability of EOEMA and EMA based gels as discussed in chapters 5.3.5 and 5.3.6 can be adopted for gels recently used for ECD assembly.

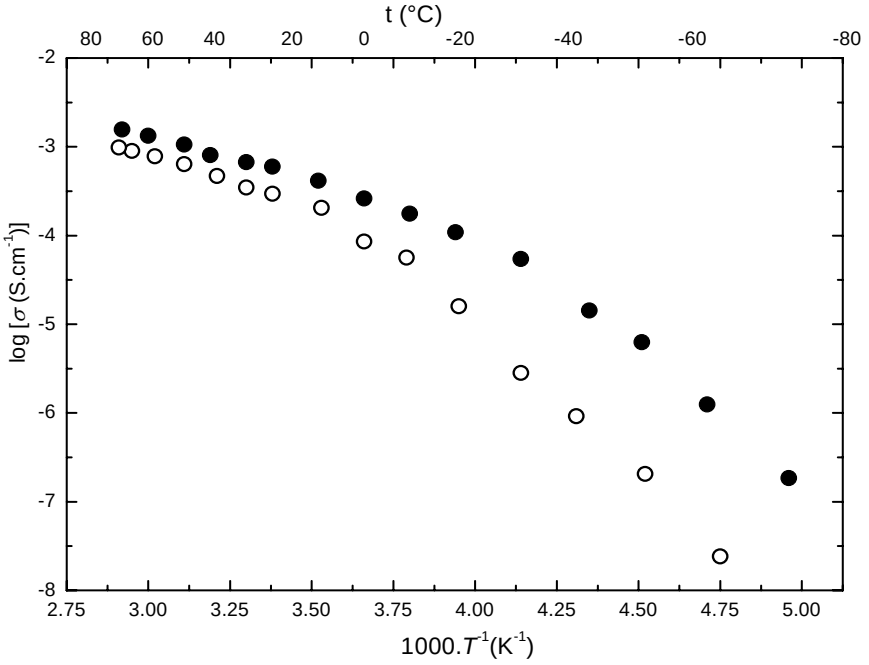

Fig. 8.1 Arrhenius plot of the specific conductivity of EOEMA (empty circles) and EMA (full dots) based GPEs used in ECDs; measurement temperature from -70 to 70 °C.

8.2 *Battery-type EC device fabrication*

The electrochromic devices with EOEMA and EMA based gel electrolytes were prepared with following layer composition;

glass | FTO | WO_3 | Li-electrolyte | V_2O_5 | FTO | glass,

where the 3 mm Pilkington K-Glass^{TM} (SnO_2:F) with $\rho < 30\Omega/\square$ on the WO_3 side was coated with amorphous WO_3 film. The other side comprises of another 3 mm K-Glass^{TM} with V_2O_5 intercalation layer on the top of it (see Fig. 8.7).

8.2.1 Deposition parameters and optical characterization of WO_3 and V_2O_5

A deposition of intercalational WO_3 and V_2O_5 layers was done in Optical Development Workshop of Academy of Science in Turnov, Czech Republic. The optically active layer was produced by sublimation of WO_3 powder from resistive boat onto unheated substrate (K-Glass^{TM}). The deposition rate was kept constant at ca. 3 nm.s^{-1}. The thickness of the resulting layer was controlled by QCM during the evaporation process and lately confirmed by Laser Microscope to be ca. 300 nm.

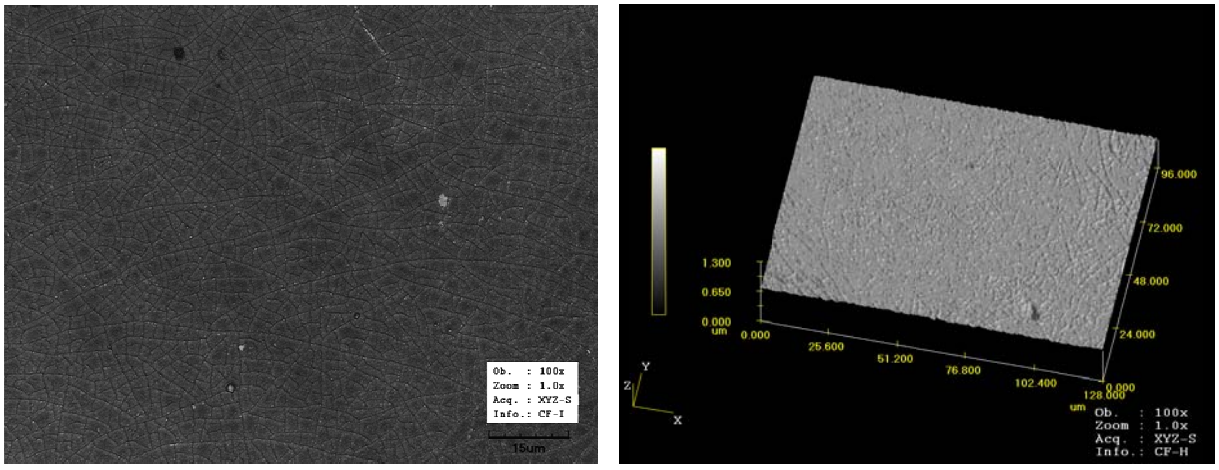

Fig. 8.2 LM micrographs of as-prepared WO_3 layer.

The morphology and the surface topography of as-prepared evaporated WO_3 and V_2O_5 layers are displayed in figures 8.2 and 8.3 respectively. An amorphousness of the WO_3 layer was checked with X-ray diffraction.

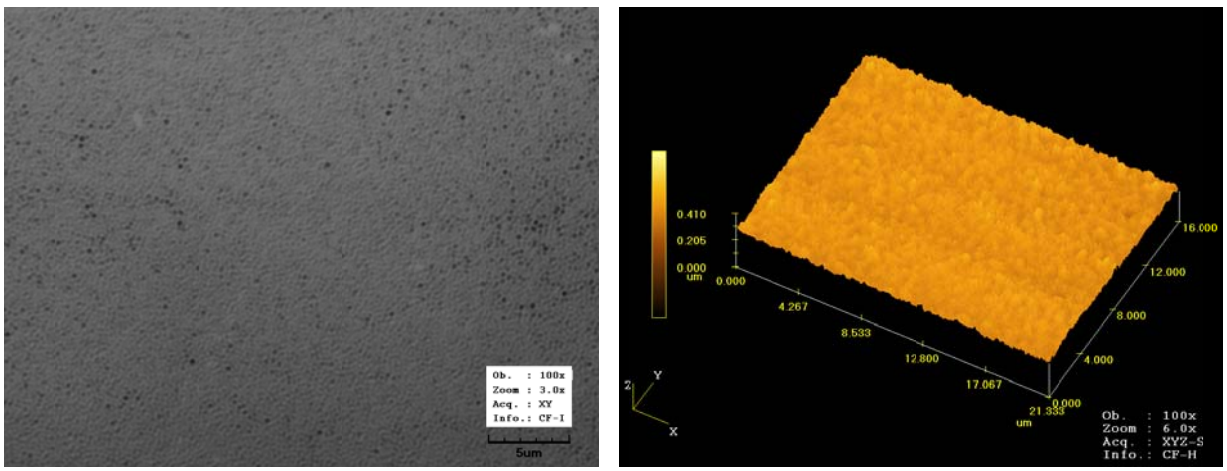

Fig. 8.3 LM micrographs of as-prepared V_2O_5 layer.

Contrary to WO_3, the V_2O_5 layer in its as prepared stage was a pale yellow film with increased absorbance near to UV region. In order to increase the layer transmittance the deposition rate was kept constant at ca. 5 nm.s^{-1} and the thickness estimated from the interface scan did not exceed 200 nm. Both the WO_3 and V_2O_5 layers were deposited in oxygen controlled atmosphere.

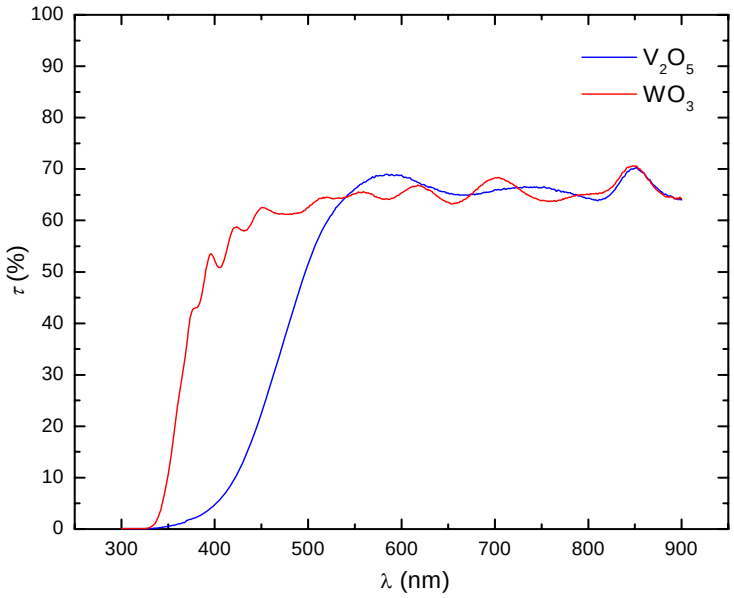

Fig. 8.4 UV-Visible transmittance of as-prepared WO_3 (red curve) and V_2O_5 (blue curve) layers; $\lambda \approx 300$ - 1100 nm.

Figure 8.4 shows the optical properties of resulting electrochromic layers in their as-prepared stage. The monochromatic ($\lambda = 634$ nm) transmittance of EOEMA and EMA based gels was found over 90% (refer to chapter 5.3.2), hence one can assume, looking at Fig. 8.4, that the maximal transmittance of as-prepared ECD will be fully determined by the optical properties of the intercalation layers.

8.2.2 Intercalation of Li into WO_3 and V_2O_5 studied by CV

The electrochemical behaviour of FTO/WO_3 and FTO/V_2O_5 electrodes was studied in order to confirm the electrochemical compatibility with the developed polymer electrolyte. The electrochemical insertion of lithium cations into WO_3 is performed in the potential range from +1.5 to -0.3 V vs. Cd/Cd^{2+} in agreement with literature [2-4] expressed as

$$WO_3 + xLi^+ + xe^- \leftrightarrow Li_xWO_3 \qquad (8.1)$$

(colourless) (blue)

A similar reaction occurs on the V_2O_5 counter electrode, where the electrochemical process can be described by reaction

$$V_2O_5 + xLi^+ + xe^- \leftrightarrow Li_xV_2O_5 \qquad (8.2)$$

and takes place at potentials from +2 to -0.5 V vs. Cd/Cd^{2+}. Ward [5], Livage [6] and Cao [7] described a similar behaviour of V_2O_5. Comparing the voltammograms from Fig. 5.13 and 5.14, where the voltammetrical curves of EOEMA and EMA based polymer electrolytes are displayed, with those from Fig. 8.5, we see that both

electrochemical processes from Fig. 8.5 take place within the electrochemical potential window of the used polymer electrolytes.

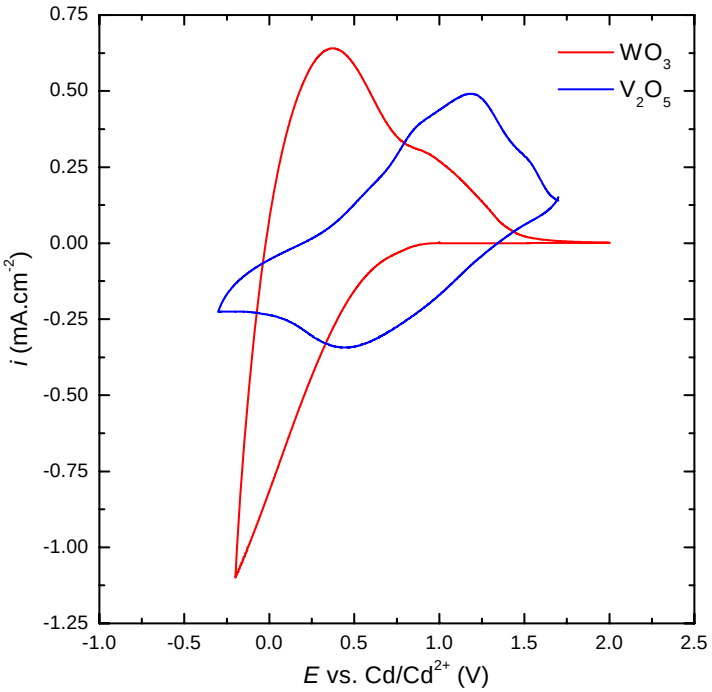

Fig. 8.5 Cyclic voltammograms of WO_3 and V_2O_5 electrochromic layers in 1M $LiClO_4$ in PC; counter electrode platinum, reference PMMA-Cd-Cd^{2+} electrode; scan rate 10 $mV.s^{-1}$.

The shape of red curve from Fig. 8.5 representing the reversible Li^+ intercalation/deintercalation into WO_3 is similar to one reported by Judeinstein and Livage [2] on amorphous WO_3 film evaporated onto unheated substrate.

8.2.3 Insertion of Li into WO_3 studied by QCM

Insertion of Li^+ ions into WO_3 layer was studied by Vondrák et al. [8] by mean of electrochemical quartz crystal microbalance (QCM), the method based on the observation of resonance frequency. As a sensor, the WO_3 was deposited by vacuum evaporation on a quartz crystal element (resonator) placed among above mentioned K-Glass^{TM} substrates (later used for ECDs assembly) in a coating chamber. The crystal probe with deposited WO_3 layer was submerged into 0.1 $mol.l^{-1}$ $LiClO_4$-PC solution and swept between -1.5 and 0.75 V (E vs PMMA-Cd-Cd^{2+}). The change in WO_3 mass upon Li^+ insertion was evaluated directly from an output of QCM and compared with theoretical value using the correction factor representing the effective molecular weight of particles that enter the WO_3 lattice (see Fig. 8.6).

According to Vondrák et al., Li^+ ions entering the space lattice were found to be accompanied by molecules of the solvent. The apparent molecular weight equal to 125 was postulated for the insertion of solvated Li^+ ions. The number corresponded to one molecule of PC for one lithium ion entering the WO_3 layer.

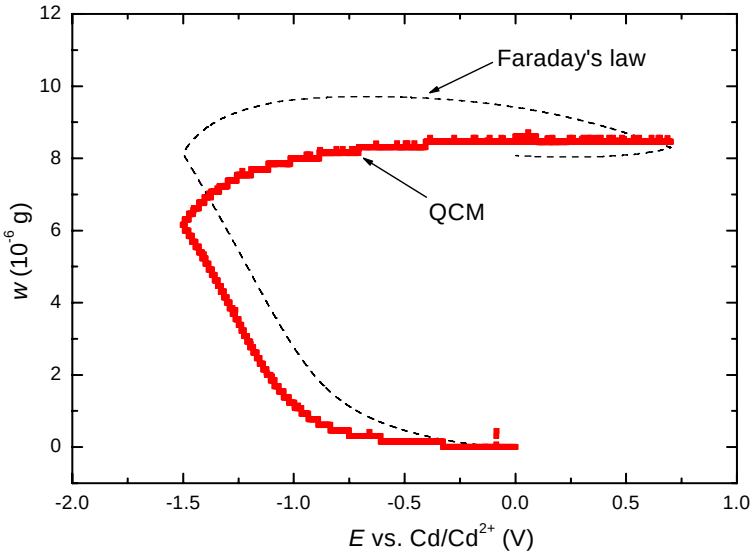

Fig. 8.6 Mass changes of a WO_3 deposited on a QCM probe in a 0.1-mol l^{-1} solution of $LiClO_4$ in PC. Solid line, mass changes were evaluated from the output of the QCM; broken line, mass estimated under the assumption of molecular weight of inserted species equal to 125. Reference electrode PMMA-Cd-Cd^{2+} in PC; scan rate 2 mV.s^{-1} [8].

Furthermore the irreversible uptake of the solvent in the 1:1 molar ratio (ion vs solvent) was observed supporting the ion-ion exchange theory proposed by Yoshiike and Kondo [2].

8.2.4 Device assembly

During the ECD assembly the electrodes consisting of FTO/WO_3 and FTO/V_2O_5 glasses (5 × 6 cm) were distanced using 1 mm thick double side VHB 3M (3M, UK) tape. In order to ensure better charge distribution and contact between the electrodes and measuring probe a copper tape was used (see Fig. 8.7 and 8.8).

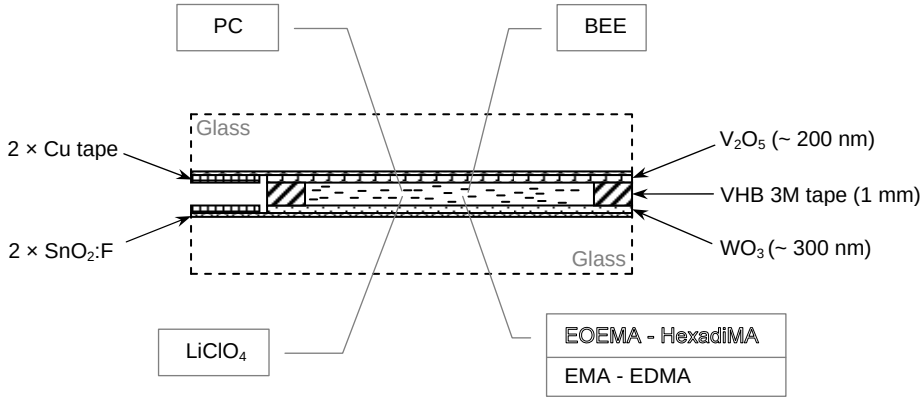

Fig. 8.7 Assembly of an ECD with the EOEMA and EMA based GPEs.

The electrode assembly was filled with argon and then the initial mixture was carefully injected using a syringe. Upon filling, the polymerization was initiated by

exposing the cell to the UV light for a period of 3-5 hours at room temperature using a pair of 15 W lamps emitting wide UV-A and UV-B light (Hagen, Czech Republic).

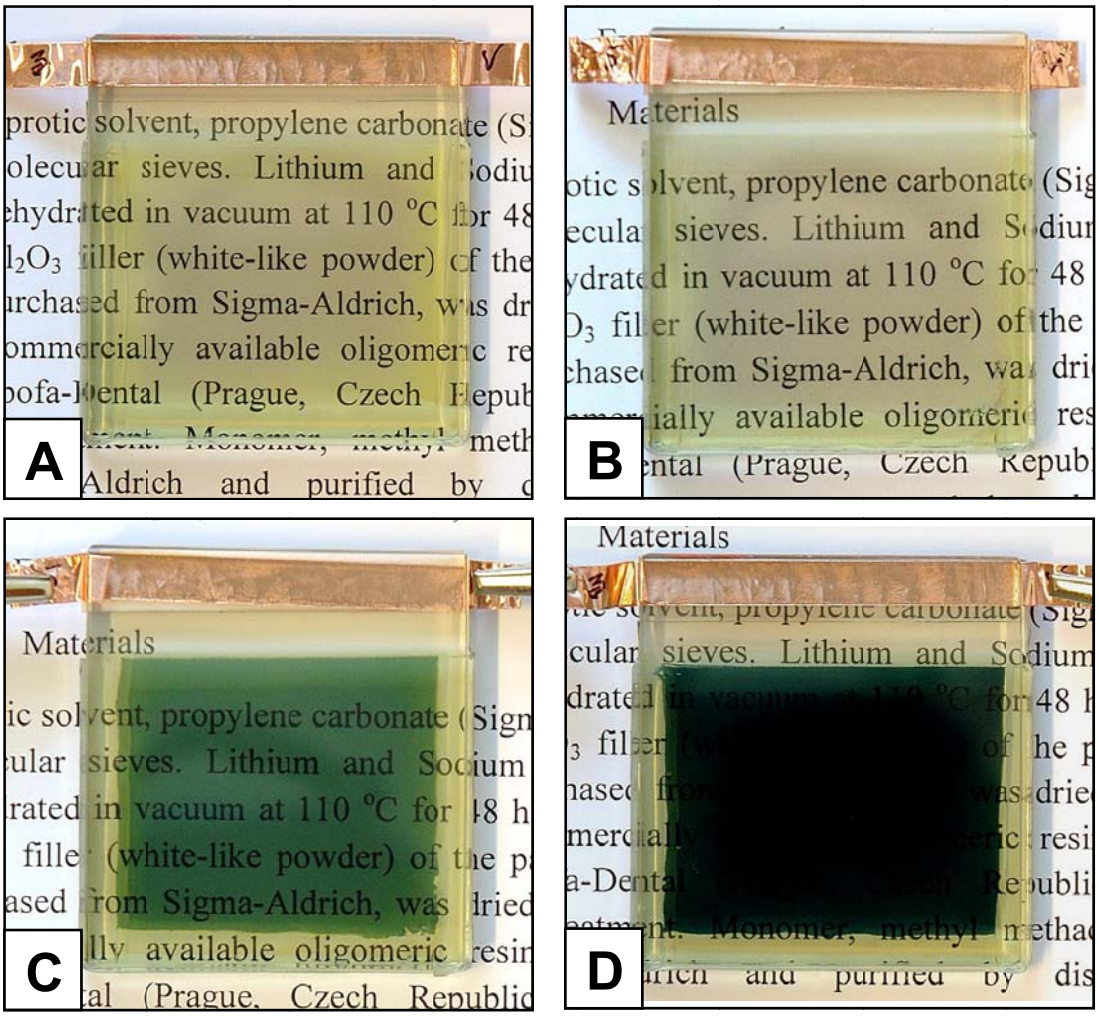

Fig. 8.8 The EOEMA based EC device in its as-prepared (A), bleached (B), partially coloured (C) and fully coloured (D) stage; displayed approx. in a full scale.

Figure 8.8 shows an illustrative picture of prepared ECDs with EOEMA based gel electrolyte at the different operating stages. The VHB 3M tape along the edges creates a frame marking off an active electrode area of approx. 14 cm^2 (clearly visible from Fig. 8.8C and D). Developed technology of the ECD assembling assured that no gas bubbles appeared during the polymerization and the whole cell volume was completely filled with the electrolyte (see Fig. 8.8).

8.3 *In-situ testing procedures*

In-situ UV-visible optoelectrochemical measurements of the EC cells were made using the Perkin Elmer UV/VIS spectrophotometer in combination with an Eco Autolab potentiogalvanostat. The coupled experiments followed the testing procedure from APPENDIX C. The cyclovoltammetric curves were obtained by the scan rate of 20 $mV.s^{-1}$. The voltage was swept between 0 V to -3 V (-2.5 V), reversed to 1.5 V and then finished at 0 V. The kinetics of the coloration and bleaching were obtained by applying a chronoculometric technique by performing the intercalation of Li^+ ions at -3 V or -2.5 V for 100 s and deintercalation at 1.5 V for another 100 s. Reported

potentials correspond to the potential applied to the WO_3 film (working electrode). Similarly to HEC cells we were not able to incorporate the reference electrode directly inside the device hence the true potentials of WO_3 and V_2O_5 electrodes were unknown.

The above mentioned testing procedure comprised; (a) initial cycling at a constant scan rate; (b) observation of the UV-visible transmission during colouring/bleaching; (c) measuring the monochromatic transmittance values at a various scan rates; (d) study of the intercalation kinetics versus time in a potentiostatic mode.

A cycling stability test was performed under potentiostatic conditions during which the WO_3 potential was altered between -2 V and +1.5 V for 230 times in total. The devices were kept in a steady state for 15 minutes at each potentiostatic step.

8.4 *Optoelectrochemical performance of EC devices employing EMA and EOEMA based electrolytes*

In the battery-type ECD the V_2O_5 layer acts as a counter electrode and at the beginning of the experiment does not contain any Li^+ cations in its structure. Hence the electrochromic devices had to be formatted by voltammetrical cycling from +1.5 V to -3 (-2.5) V with a scan rate of 20 $mV.s^{-1}$ for about 10 cycles. After this procedure, the optoelectrochemical experiments were performed. Although, this formatting can be eliminated by using V_2O_5 layers with intercalated Li^+ ions similarly to Orel and Bulhões [9,10].

Figure 8.9 shows monochromatic transmittance of ECDs with EOEMA and EMA based GPEs during coupled cyclic voltammetric measurements. The potential of WO_3 layer was swept, with 20 $mV.s^{-1}$ polarization speed, from the initial potential (IP) at 0 V down to -3 V, the device first coloured (refer to Fig. 8.8D), and then was reversed back towards positive 1.5 V, the device bleached (see to Fig. 8.8B).

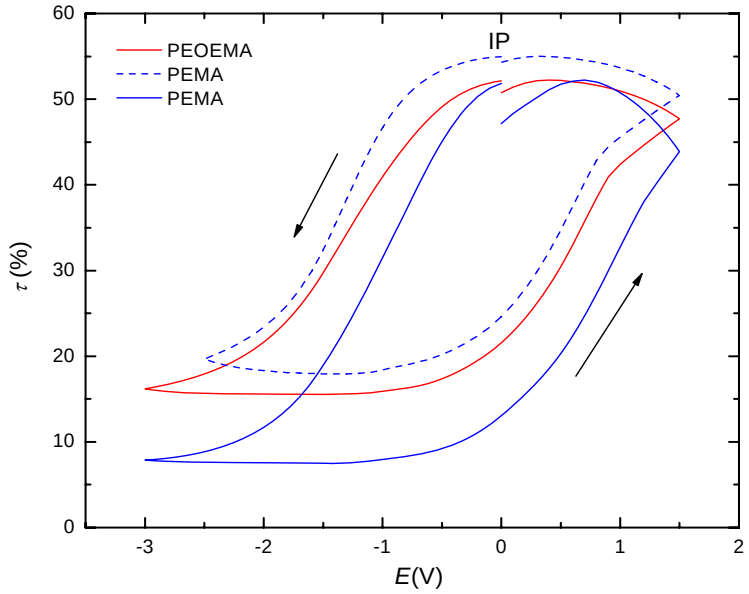

Fig. 8.9 The monochromatic transmittance response of EC devices with EOEMA (red curve) and EMA (blue curves) based polymer electrolytes; λ = 634 nm, scan rate 20 $mV.s^{-1}$.

From the comparison of monochromatic responses of EOEMA and EMA based EDCs in Fig. 8.9 one can see that the transmittance of the latter one was altered in between ca. 53% and 7% giving the total modulation of 46% at 634 nm while the modulation of EOEMA based ECD was considerably lower ca. 53% at bleached and 15% at coloured state with the total monochromatic modulation of 38%. In fact both devices performed similarly during bleaching whereas the major difference in the transmittance occurred in colouring step. Therefore we included tests with a lower cathodic potential down to -2.5 V (in Fig. 8.9 represented by the dashed line). In the case of PEOEMA based ECD only a slight difference in the ECD coloration was found. On the other hand in the case of PEMA-based ECD (see dashed curve from Fig. 8.9B) we observed major drop of transmittance during colouring step (from ca. 7% down to 20%). The liability of PEMA based ECDs reflected in the increased transmittance-bias dependency is probably connected with higher conductivity of the gel. Moreover the PEMA based device when coloured at -2.5 V showed better recovery of the initial monochromatic transmittance during subsequent bleaching than the same device coloured at -3 V (compare blue lines from Fig.8.9B).

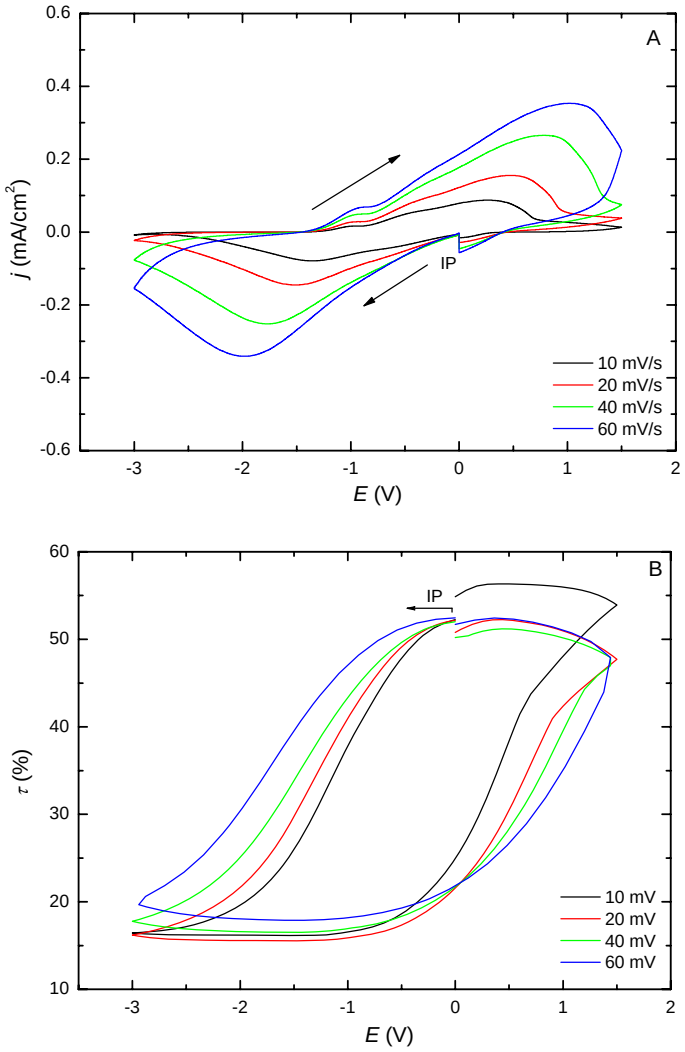

Fig. 8.10 Cyclic voltammetry curves (A) and monochromatic (λ = 634 nm) transmittance response (B) of EC device with EOEMA based GPE measured at different scan rates.

Figures 8.10A and 8.11A shows the results from the coupled optoelectrochemical measurements, performed at various scan rates (10, 20, 40 and 60 $mV \cdot s^{-1}$), figures

8.10B and 8.11B then corresponding cathodic and anodic waves of monochromatic transmittance that reflected the insertion/extraction of Li^+ ions into the WO_3 film.

When we compare the results from the in-situ UV-visible optoelectrochemical measurements performed on PEOEMA and PEMA based ECDs we note; (a) even at a high scan rates (60 $mV \cdot s^{-1}$) the devices respond rapidly, (b) increased scan rate influences the transmittance response during the cathodic polarization (intercalation), (c) higher consistency of the transmittance values during bleaching was observed together with only a slight increase of the transmittance once the potential was reversed back towards negative values (with the reference to Fig.8.10), (d) higher consistency of the current response suggests rather moderate redox activity of PEOEMA based ECD (compare Fig. 8.10A and 8.11A), (e) the oxidative peak with the onset at ca. -1.5 V that appears on both voltammograms is probably connected with the formation of Li_xO_x film, subsequently being reduced in the following scans (fully diminishes after ca. 50 CV scans).

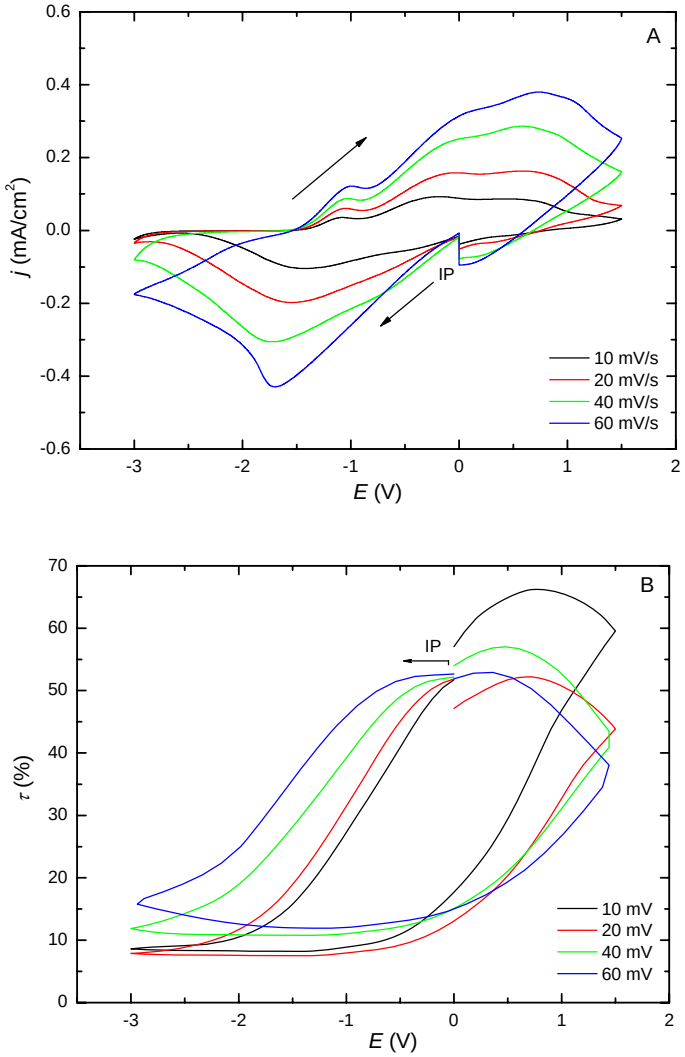

Fig. 8.11 Cyclic voltammetry curves (A) and monochromatic (λ = 634 nm) transmittance response (B) of EC device with EMA based GPE measured at different scan rates.

Figure 8.12 shows the transmission characteristics of the ECDs recorded in a bleached (+1.5 V) and a coloured state (-3 V resp. -2.5 V) within the 300-900 nm range. It is important to note that both devices featured the minimal transmittance modulation

of ca. 20% between 400 and 900 nm. As it is visible from the spectra, the device with PEMA based electrolyte offers a higher transmittance change in the whole spectrum range as compared to the one with PEOEMA electrolyte. The major difference (ca. 10 τ%) in between prepared ECDs was observed upon altering the cathodic potential between -2.5 and -3 V (see Fig. 8.12B).

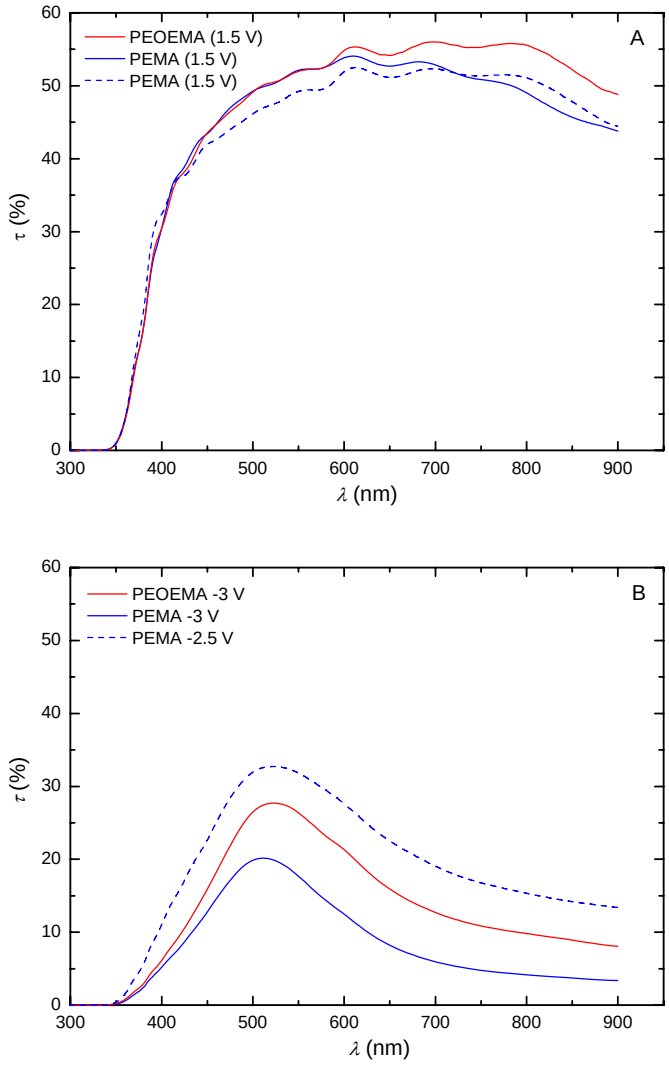

Fig. 8.12 In-situ UV-visible optoelectrochemical measurements of EC devices with EOEMA (red curves) and EMA (blue curves) based GPEs in their bleached (A) and coloured (B) state; λ = 300~900 nm.

Figure 8.13 shows the results from the potentiostatic tests performed on both types of ECDs. During chronocoulometric colouring the electrochromic device became first dark blue, upon negative pulse applied onto WO_3 (see Fig. 8.8D), and then again rapidly bleached when the potential was reversed (see Fig. 8.8B).

From Fig. 8.13B one can see that the optical modulation was fully reversible in case of the both ECDs even at higher cathodic potential. During colouring step the main transparency change occurred within the first 20 s. The PEOEMA based ECD featured the typical knee during colouring step reaching the minimal transmittance of ca. 17% in 20 to 30 s (red line). The colouring of PEMA based ECD, however was slower with the limiting monochromatic transmittance seen after approx. 80 s, was ca. 8% giving the total transmittance change (Δτ) over 50% (blue solid line). Moreover we note a faster

recovery of the PEMA based ECD after polarizing from -2.5 to +1.5 V. On the other hand, with the respect to cathodic potential, the PEOEMA based ECDs provide a deeper coloration change $\Delta\tau \sim 40$ - 45 % contrary to 35 % for the PEMA based device. The results from Fig. 8.13B suggest that the kinetics of ECDs with PEOMA-based electrolyte is less affected by the bias voltage applied to WO_3 electrode. Despite our assumptions the PEMA based devices featured slower switching kinetics. We believe it is due to intrinsic allocation of conducting centres in the bulk of polymer electrolyte.

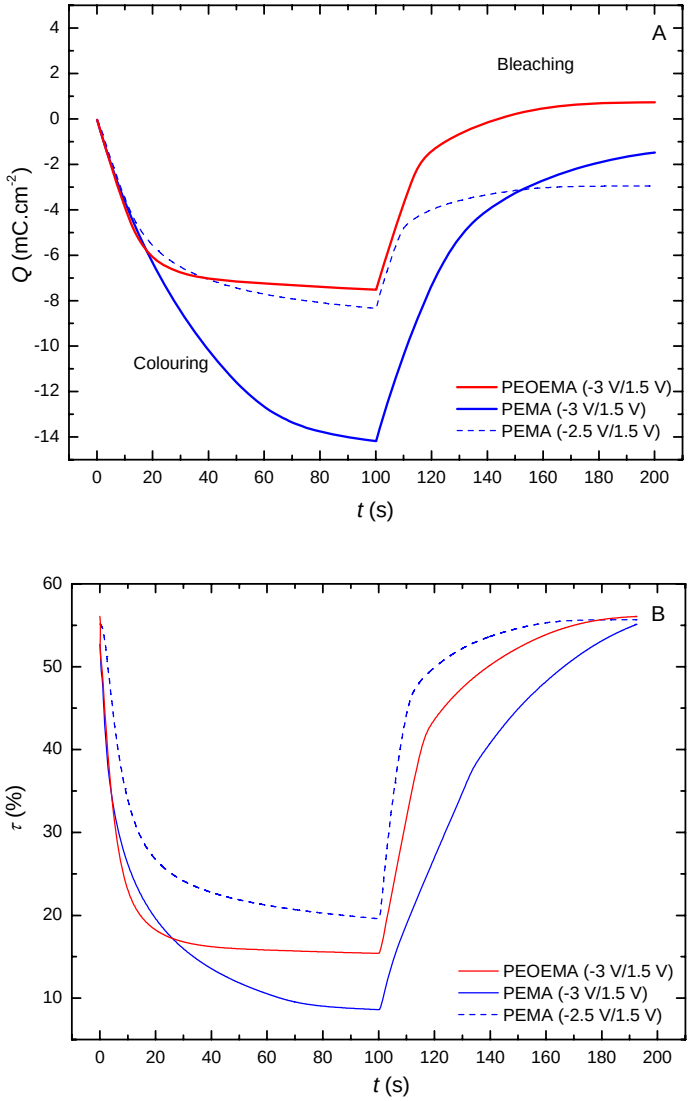

Fig. 8.13 In-situ UV-visible optoelectrochemical measurements of EC devices with EOEMA (red curves) and EMA (blue curves) based electrolytes during chronocoulometric colouring/bleaching: (A) chronocoulometric curves and (B) monochromatic transmittance; $\lambda = 634$ nm.

Figure 8.13A shows the chronocoulometric response of the ECDs with PEOEMA and PEMA based electrolytes after sudden Li^+ intercalation followed by violent recovery. Contrary to hybrid ECDs discussed earlier in chapter 7.5 a typical charge saturation was observed. The red curve in Fig. 8.13A, representing the amount of effectively intercalated charge into the electrochromically active layer of ECD, increases steeply during first 40 seconds and then level at the value of 7 $mC.cm^{-2}$. In the case of PEMA based ECD, perceptible saturation occurred after 80 s with the total charge exceeding 14 $mC.cm^{-2}$. During recovery both devices with WO_3 biased at -3 V

(solid lines) discharged into their initial states, while the one polarized at -2.5 V (blue dashed line) retained the charge equivalent to 3 $mC.cm^{-2}$.

The data from Fig. 8.13 were transformed into the optical density (OD) and coloration efficiency (CE) values using the equation (7.2). The results are summarized in following table.

Table 8.3 The colouring efficiency (CE) and optical density (OD) values of EC devices with PEOEMA and PEMA based GPEs.

EC device	T_0 (t = 0 s) (%)	T (t = 100 s) (%)	ΔOD	Q ($mC.cm^{-2}$)	CE ($cm^2.C^{-1}$)
PEMA (-2.5 V)	55.15	19.58	0.45	8.34	53.92
PEMA (-3.0 V)	52.68	8.61	0.79	14.18	55.46
PEOEMA (-3 V)	56.06	15.41	0.56	7.52	74.59

From Tab. 8.3 the highest coloration efficiency, 74.6 $cm^2.C^{-1}$, was reached for PEOEMA based ECD. Furthermore there is remarkable discrepancy between CE values of the both PEMA based ECDs. The ECD polarized at -3 V, however showed superior transmittance modulation among all tested devices, has retained a number of effectively intercalated charges uncompensated with rather moderate increase of ΔOD. The coloration efficiency values are close to the CE of similar systems earlier reported by Yanoulis et al. [11,12] as shown in Tab. 8.3.

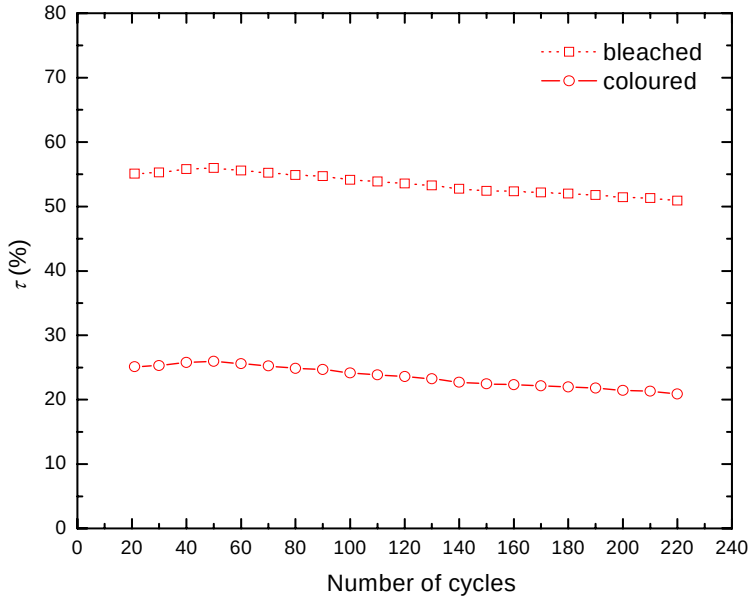

Fig. 8.14 The monochromatic transmittance modulation of EOEMA based EC device in bleached (squares) and coloured (circles) state, λ = 634 nm.

Figure 8.14 shows the evolution of a transmittance ratio in time for EOEMA based ECD recorded during potentiostatic cycling between -2 V and +1.5 V. The monochromatic transmittance ratio (Δτ) approached 30% after 230 colouring/bleaching cycles. The decrease of transmittance observed after 230 cycles was found to be within 3% of the initial values. The assembled electrochromic device was functional for more than 230 potentiostatic cycles with no observed phase separation or visible decomposition/delamination of either the electrolyte or the electrodes.

With regards to the chosen battery-type ECD, the long-term memory effect (keeping of the transmittance in the coloured state without applied voltage) was preserved and self-erasing was practically not observed during a period of hours.

The optoelectrochemical tests showed that the electrolytes are suitable media for lithium ion transportation towards the WO_3 and V_2O_5 thin layer electrodes and for subsequent reversible lithium intercalation. The transmittance change $\Delta\tau$ was found to be 37 respectively 46% at 634 nm and the potentiostatic tests showed that the main transparency change is performed within the first 20 seconds. Superior coloration efficiency values and electrochemical stability together with better switching kinetics and durability are in favour of PEOEMA based ECDs [13-15].

References

[1] MACFARLANE, D.R., et al. Polymer electrolytes for electrochromic window applications. In *Solid State Ionics*. The Netherlands: Elsevier, 1996. 86-88. s. 959-964.

[2] GRANQVIST, C. G. *Handbook of Inorganic Electrochromic Materials*. The Netherlands: Elsevier, 1995. 2 sv. (337, 296 s.). ISBN 0-444-89930-8.

[3] VARSHNEY, P., et al. Photo-polymerized films of lithium ion conducting solid polymer electrolyte for electrochromic windows (ECWs). In *Solar Energy Materials and Solar Cells*. The Netherlands: Elsevier, 2003. 79. s. 449-458.

[4] BISWAS, P.K., et al. Optical and electrochromic properties of sol–gel WO_3 films on conducting glass. In *Material Letters*. The Netherlands: Elsevier, 2003. 57. s. 4429-4432.

[5] PARK, H.K., SMYRL, W.H., WARD, M.D. V_2O_5 xerogel films as intercalation hosts for lithium 1. Insertion stoichiometry, site concentration, and specific energy. In *Journal of Electrochemical Society*. The USA: Electrochemical Society, 1995. 142. s. 1068-1073.

[6] LIVAGE, J. Sol–gel chemistry and electrochemical properties of vanadium oxide gels. In *Solid State Ionics*. The Netherlands: Elsevier, 1996. 86-88. s. 935-942.

[7] WANG, Y, CAO, G. Li^+-intercalation electrochemical/electrochromic properties of vanadium pentoxide films by sol electrophoretic deposition. In *Electrochimica Acta*. The Netherlands: Elsevier, 2006. 51. s. 4865-4872.

[8] VONDRÁK, Jiří, et al. Insertion of cations into WO_3 investigated by QCM techniques. In *Journal of Solid State Electrochemistry*. Germany: Springer, 2007. 11. s. 1459-1462.

[9] BRAZIER, A., et al. Ionic liquids in electrochromic devices. In *Electrochimica Acta*. The Netherlands: Elsevier, 2007. 52. s. 4792-4797.

[10] BUENO, P.R., et al. Electrochromic properties of undoped and lithium doped Nb_2O_5 films prepared by the sol–gel method. In *Electrochimica Acta*. The Netherlands: Elsevier, 2001. 46. s. 2113-2118.

[11] SYRRAKOU, E., et al. Eco-efficiency evaluation of a smart window prototype. In *Science of the Total Environment*. The Netherlands: Elsevier, 2006. 359. s. 267-282.

[12] PAPAEFTHIMIOU, S., et al. Development of electrochromic evacuated advanced glazing. In *Energy and Buildings*. The Netherlands: Elsevier, 2006. 38. s. 1455-1467.

[13] KREJZA, O., REITER, J., VONDRÁK, J. Methacrylate-based Polymer Electrolytes for Electrochromic Devices and Lithium-ion Batteries. In *8th Advanced Batteries and Accumulators: [A.B.A. -8]*. Brno: BUT-Brno, 2007. s. 76-78. ISBN 978-80-214-3424-0.

[14] REITER, J., KREJZA, O., VONDRÁK, J. Methacrylate-based Polymer Electrolytes for Electrochromic Devices. In *11th EuroConference on Science and Technology of Ionics: Sur Mer 2007*. Batz, 2007. s. 24-24.

[15] REITER, J., KREJZA, O., SEDLAŘÍKOVÁ, M. Electrochromic Devices Employing Methacrylate-based Polymer Electrolytes. In *Solar Energy Materials and Solar Cells*. The Netherlands: Elsevier, 2009. 93. s. 249-255.

9 Adhesion and thermal analysis of prepared Acrylic Systems

Section 9.1 deals with the mechanical properties of GPEs for ECDs. The adhesion towards either coated or uncoated glass or PET substrates was studied using the 180° peel test. Section 9.2 discusses the thermal and rheological stability of prepared acrylic systems by means of thermal analysis techniques.

9.1 *ISO and ASTM 180° peel test*

Among others, e.g. high ionic conductivity and dimensional stability, the adhesion of GPE towards the substrate is a crucial parameter that has to be considered while designing an ECD. An use of relatively thick (up to 500 microns) adhesive polymer membrane is beneficial for constructing ECDs from flexible substrates (e.g. poly(ethylene terephthalate) (PET) foil). Such lightweight solar control film can be easily mounted (retrofitted) on top of a standard window pane with no need of replacement, resulting in product price reduction, or simply shaped into virtually infinite forms (e.g. eyewear, motorcycle visors, shelf displays, etc.) [1,2].

In order to obtain valuable information on adhesion of our GPEs we employed the 180° peel test obeying to ASTM D903-98 and ISO 8510-2:2006(E) standards [3]. The first step was to test the adhesion of PEOEMA and PEMA based GPEs towards non-treated substrates. As we explained earlier, the amount of monomer in the composition of GPE impress the intrinsic mechanical properties to the sample. According to this fact we prepared two batches of PEOEMA and PEMA based GPEs, first one with low monomer and the second with high monomer content. Particular chemical composition of prepared membranes is summarized in the following table.

Table 9.1 The chemical composition and naming of PEMA and PEOEMA based GPEs used during 180° peel tests.

Polymer Matrix	Chemical composition (mol%)	Peel-test Abbreviation
PEMA	EMA/PC/$LiClO_4$ 51.2/44.9/3.7	hi-EMA
	EMA/PC/$LiClO_4$ 39.2/56.0/4.8	low-EMA
PEOEMA	EOEMA/PC/$LiClO_4$ 48.3/45.5/6.3	hi-EOEMA
	EOEMA/PC/$LiClO_4$ 35.5/59.4/5.1	low-EOEMA

For better contact between examined layers 500 μm thick GPEs membranes were prepared using the UV-initiated polymerization method described in chapter 5.3.1. A variability of the mould allowed us to substitute and alter the PP backing and upper glass plate in order to measure the adhesion towards various substrates. Each sample comprised following the sandwich structure: Substrate A|GPE|Substrate B. During the initial tests the substrate A was plain 3 mm thick glass plate and the substrate B was

100 μm thick strip of PET foil. The surface adjacent to the membrane was treated with ethanol and dried prior mould assembly. Both substrates were uncoated (without any electrochromic or TCO layers). In order to avoid time consuming measurements, all samples were peeled in the two ways (to receive the adhesion data towards both surfaces at the same time). Literally, we created a defect at the contact between the membrane and each substrate, hence the membrane could be peeled first from Substrate A and then out of Substrate B without possibly affecting previous measurement.

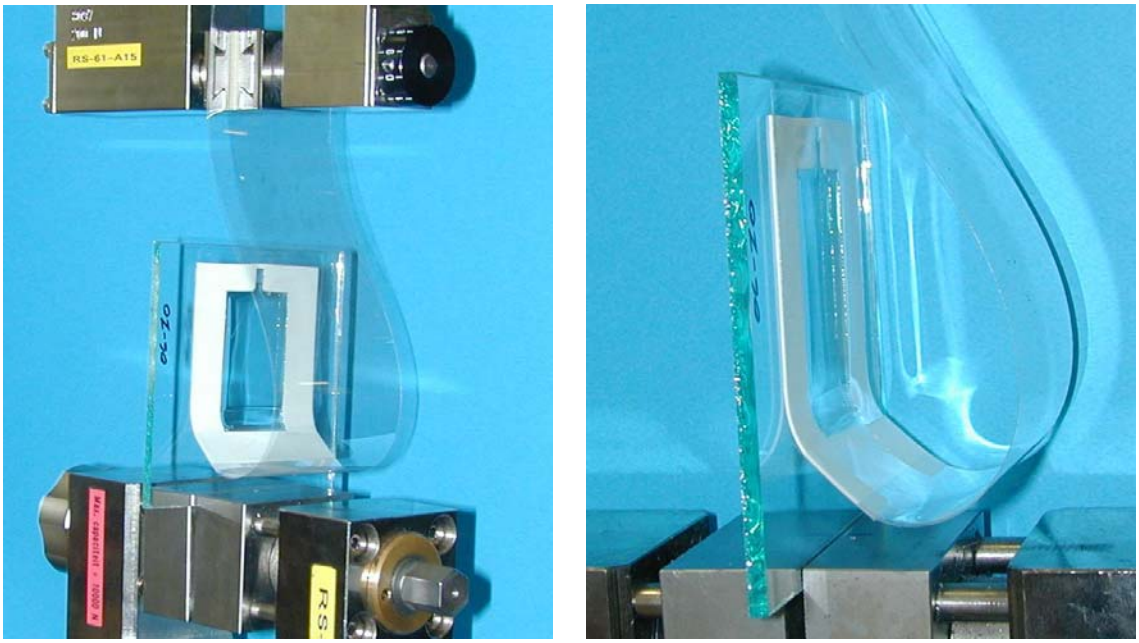

Fig. 9.1 General view on tensile tester with GPE membrane during the 180° peel test on the left, and the detail with a visible defect realized by folded PET foil on the right.

Figure 9.1 shows vertically clamped sample with the GPE membrane situated inside the white silicon frame. The measurements were carried out up to the rupture point of the substrates. Testing path varied from 20 to 50 mm (due to composition of the membrane). The results are summarized in following table.

Table 9.2 The F_{avg} values received during 180° peel tests of PEMA and PEOEMA based GPEs on untreated glass or PET substrates; experimental temperature 25 °C.

Substrate A		Tested membrane	Substrate B	
Material	F_{avg} (N)		F_{avg} (N)	Material
plain glass	0.184	hi-EMA	0.245	PET foil
	0.122	low-EMA	0.016	
plain glass	0.266	hi-EOEMA	0.706	PET foil
	-	low-EOEMA	-	

Due to the defect realized at the beginning of the test path, the results from Table 9.2 correspond to the average force (F_{avg}), the constant force necessary to peel the membrane after the initial delamination. The initial delamination occurs at a maximal force (F_{max}), the moment at which the flexible substrate starts to go off the membrane (overcome due to the defect). The F_{avg} values from Table 9.2 correspond to a load applied to the 30 mm cross-sectional area. In general, both membranes with low

monomer content showed poor adhesion. Moreover, the test path of low-EMA respectively low-EOEMA membranes suffered from premature separation and did not exceed 20 mm. When the load was applied to the low-EOEMA membrane almost instant rupture was observed (most probably due to superficial moisture on the surface caused by excess of the solvent). The overall highest F_{avg} values of 0,706 N (out of PET) and 0,266 N (out of plain glass) were observed in case of hi-EOEMA membrane.

Based on the results gathered from non-coated substrates we prepared two hi-EOEMA based samples in the following layer arrangement;

(a) WO_3 coated K-glass^{TM}|GPE|neat PET foil (red curve in Fig. 9.2) and

(b) ITO coated PET foil|GPE|ITO coated PET foil (blue curve in Fig. 9.2).

This time the GPE|Substrate cross-section remained unaffected. Hence the measurements were carried out through the delamination point to the rupture of the examined substrates. The testing path was extended to 100 mm, the thickness of neat PET and ITO coated PET foils was 50 μm and 100 μm respectively.

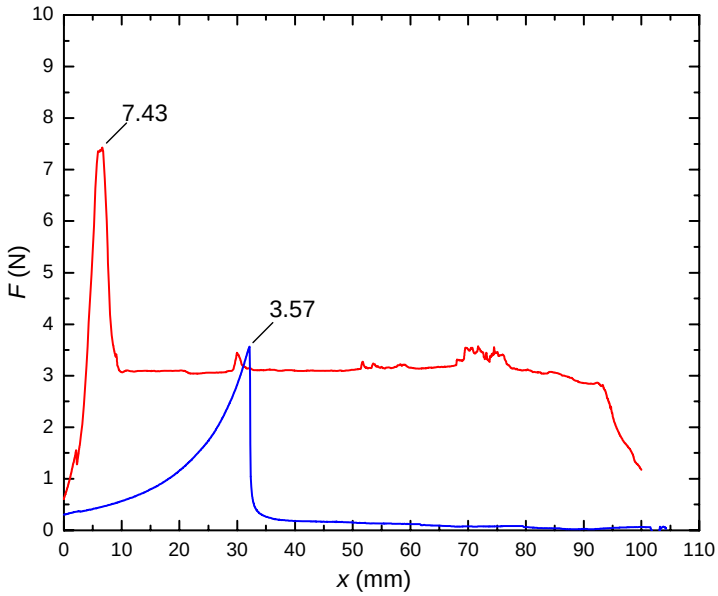

Fig. 9.2 The 180° peel test profile with maximal (F_{max}) and average (F_{avg}) force performed with WO_3-ITO (red curve) and ITO-ITO (blue curve) coated substrates, hi-EOEMA membrane, experimental temperature 25 °C.

From figure 9.2 one can clearly indicate the maximal (delamination) force, as a sharp spike, followed by levelled average (up to rupture point) force. The red curve suggests that a force equivalent to 7.43 N has to be applied at the 30 mm cross-section of WO_3 coated K-glass^{TM} laminated using hi-EOEMA based GPE to the neat PET foil to receive delamination. After delamination the membrane remained on WO_3 coated substrate and is peeled off by F_{avg} equivalent to 3.18 N. In case of ITO coated PET foils the delamination occurred at F_{max} followed by F_{avg} corresponding to 3.57 N and 0.09 N respectively. The superior adhesion, towards WO_3 coated K-glass^{TM}, can be attributed to higher surface porosity of the WO_3 layer permitting profound electrolyte penetration.

9.2 *DMA, TGA and DSC analysis*

Dynamic mechanical analysis (DMA), thermogravimetric analysis (TGA) and differential scanning calorimetry (DSC) were chosen to characterize our acrylic materials, quantitatively and qualitatively, over a considerable temperature range.

The main purpose to involve the thermal analysis (TA) might be summarized as follows; (a) the sample can be studied over a wide temperature range using various temperature programmes (estimation of Tg by DMA and DSC and exclusion of curing inefficiency by DSC), (b) almost any physical form of sample (solid, liquid or gel) can be accommodated using a variety of sample vessels or attachments (customized dual cantilever clamping by DMA), and last but nevertheless, (c) only a small amount of sample (0.1 μg-10 mg) is required (thermal stability determined by DSC and TGA).

Using TA we were able to determine; (a) *Glass Transition Temperature (Tg)*, temperature of transition of an amorphous or semi-crystalline polymer from a rubbery (or viscous) state to a glassy state, (b) *Decomposition Temperature (Ti,Tf)*, the one-stage reaction process is characterized by two temperatures, *Ti* and *Tf ,* which are called the procedural decomposition temperature and the final temperature, respectively. *Ti* merely represents the lowest temperature at which the onset of a mass change can be detected for a given set of experimental conditions. Similarly, *Tf* represents the lowest temperature by which the process responsible for the mass change has been completed, (c) *Young's Modulus (E),* unaxial force exerted on a polymer (stress) versus force applied to a material (strain) [4].

Outcomes from DMA measurements

During DMA the samples of GPEs (with a solvent in a polymer matrix) were supported by either stainless steel or wooden backing in order to increase their mechanical stability during dimensional displacement and clamped by a horizontal-dual cantilever bending. The polymer foils (with no solvent in a polymer matrix) were clamped in a vertical-single cantilever bending with no need of the backing.

The Tg is a temperature where the chains, inside the material, can move during a the predefined time scale. The time scale of the DMA measurements is equal to the frequency. This means that we are watching movement of the molecules during a period of 1 s. When the molecules can move next to each other during the time of 1 s than can be said that the Tg of the material is reached.

In a DMA's data presentation (see Fig. 9.3, 9.4 and 9.5) there can be found three different transitions; (a) the E' (storage modulus) onset defines the temperature at which the material's strength will begin to decrease, such that the material may no longer be able to bear a load without deforming, (b) the peak in the loss modulus (E'') represents the temperature at which the material is undergoing the maximum change in polymer mobility, which corresponds to the chemical definition of the Tg, and finally, (c) the loss tangent ($tan\ \delta$) peak describes the damping characteristics of a material [5].

Figures 9.3, 9.4 and 9.5 shows the results from DMA measurements on gel polymer membranes used in electrochromic and hybrid electrochromic devices. The Young's modulus of PMMA, PEOEMA and PEMA based GPEs was estimated to be 0.148 MPa, 0.181 MPa and 0.150 MPa respectively (measured at RT). The Tg of examined GPEs, obtained as an onset from the storage modulus (E') curve, was almost equal in the case of PEMA and PMMA based GPEs; -90.9 °C and -89.4 °C. On the other hand the lowest observed value was -68.7 °C for PEOEMA based GPE.

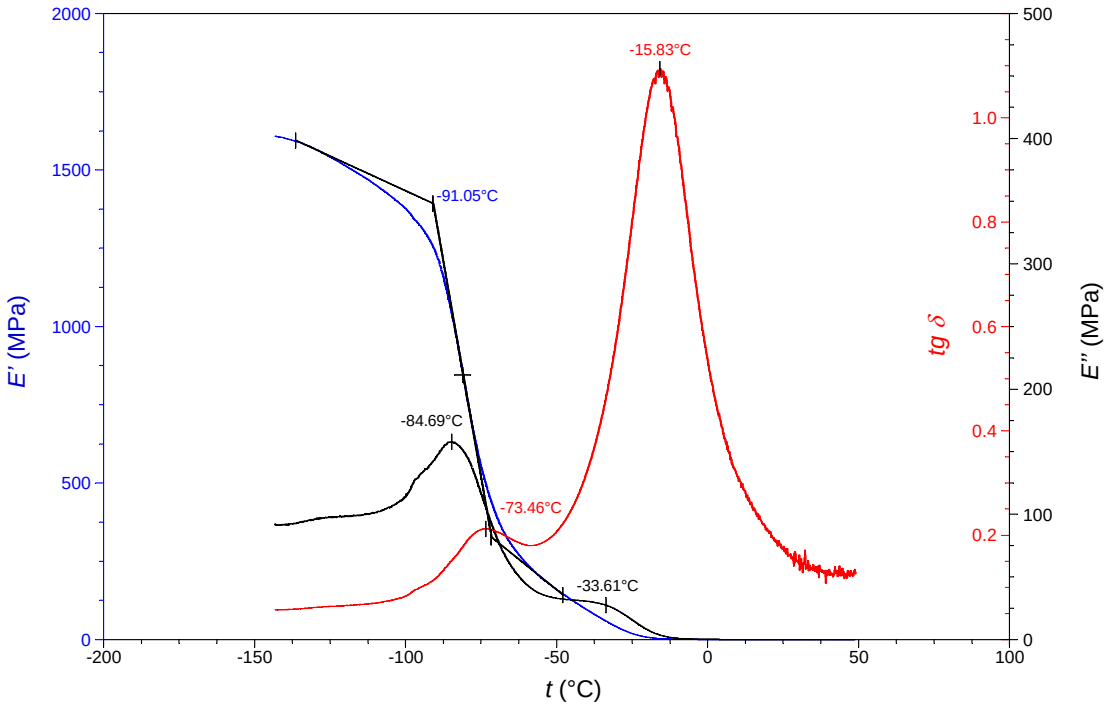

Fig. 9.3 Storage modulus (E'), loss modulus (E'') and damping behaviour (tan δ) as a function of temperature for the SA based GPE; MMA/PC/$LiClO_4$ 62.9/35.5/1.6 (wt %).

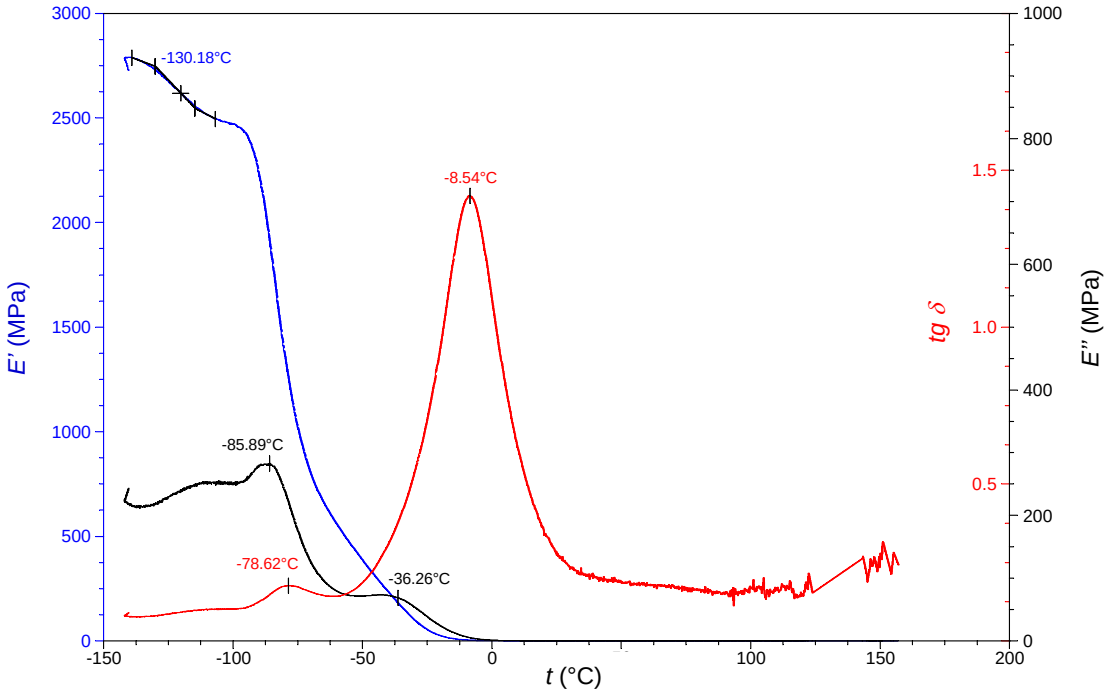

Fig. 9.4 Storage modulus (E'), loss modulus (E'') and damping behaviour (tan δ) as a function of temperature for the EMA based GPE; EMA/PC/$LiClO_4$ 51.2/44.9/3.7 (mol %).

From figure 9.5, DMA measurements of PEOEMA based GPE performed on single cantilever, the high stiffness values can be attributed to the experimental setup. In this case the sample was sandwiched between two stainless steel sheets hence there is a noise due to a displacement of the sample at lover temperatures. Nevertheless the PEOEMA based GPE showed superior transition consistency over the broad scale of temperatures. All the membranes remained flexible even at the temperatures deep below the freezing point which makes them to be good candidates for use in severe environs.

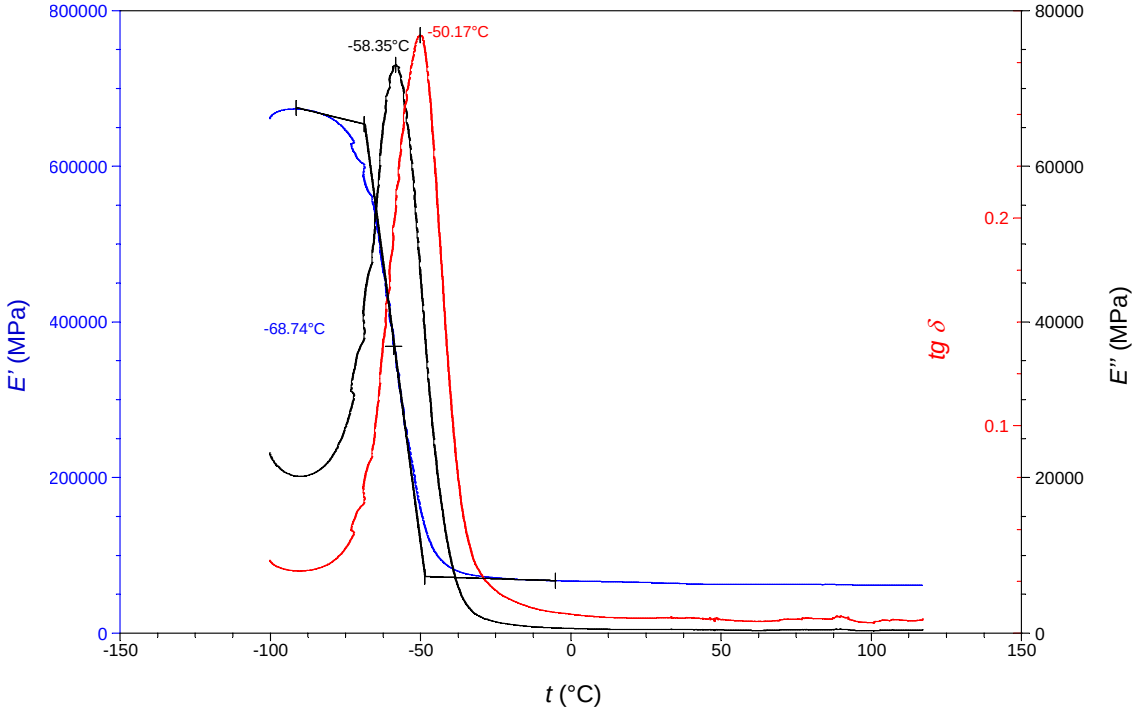

Fig. 9.5 Storage modulus (E'), loss modulus (E'') and damping behaviour (tan δ) as a function of temperature for the EOEMA based GPE; EOEMA/PC/$LiClO_4$ 48.3/45.5/6.3 (mol %).

In order to find the relationship between the rheology and chemical composition we employed the tests on; (a) GPEs containing more than one solvent (so called binary solvent systems; in our case the samples with 50:50 of PC:EC were prepared), and, (b) membranes with only a pure polymer structure (monomers, cross linking agents and initiators). Comparing two series of the samples, the binary and single solvent systems, it can be stated that additional solvent in the matrix is responsible for second E' peak at about 30 °C below the E' peak observed in a single solvent system. This peak can be attributed to the different melting point of the second solvent (in our case ethylene carbonate), which promotes an increase in the system rigidity. The drawback of binary solvent systems can be their susceptibility to faster thermal degradation. The results gathered on polymer matrixes (PMMA, PEOEMA and PEMA) without any inhibited electrolyte confirmed the high consistency and thermal stability of PEOEMA based GPE.

Outcomes from DSC and TGA measurements

Thermogravimetric analysis of PEOEMA and PEMA based GPEs showed the thermal stability up to 125 °C. The weight loss was found less than 4 wt.% up to 125 °C and 10 wt.% under 150 °C. These changes can be explained as a partial evaporation of the immobilized solvent (PC). At temperatures above 150 °C both samples start to decompose (joined processes of the polymer decomposition with evaporation of the

solvent). Moreover the incorporation of DSC tests on re-quenched (heat-cured) PMMA based GPEs served as precaution against insufficient curing times or temperature setup/ramp [6].

References

[1] AZENS, A., et al. Flexible foils with electrochromic coatings: science, technology and applications. In *Materials Science and Engineering*. The Netherlands: Elsevier, 2004. B 119. s. 214-223.

[2] WIDJAJA, E.J., et al. Process toward roll-to-roll processing of inorganic monolithic electrochromic devices on polymeric substrates. In *Solar Materials and Solar Cells*. The Netherlands: Elsevier, 2007. 92. s. 97-100.

[3] TRACTON, Arthur A. *Coatings Technology Handbook*. 3rd edition. USA: CRC Press, 2005. 936 s. ISBN 978-1574-44649-4.

[4] HATAKEYAMA, T., QUINN, F.X. *Thermal Analysis: Fundamentals and Applications to Polymer Science*. 2nd edition. England: John Wiley & Sons, 1999. 189 s. ISBN 0-471-98362-4.

[5] FOREMAN, J., SAUERBRUNN, S.R., MARCOZZI, C.L. *Exploring the sensitivity of thermal analysis techniques to the glass transition.* TA Instruments, Inc. Available from WWW: <www.tainst.com>.

[6] REITER, J., KREJZA, O., SEDLAŘÍKOVÁ, M. Electrochromic Devices Employing Methacrylate-based Polymer Electrolytes. In *Solar Energy Materials and Solar Cells*. The Netherlands: Elsevier, 2009. 93. s. 249-255.

10 Conclusion

We demonstrated that aprotic systems based on methacrylates and propylene carbonate fulfil the requirements for implementation in EC devices and other Li-ion based electrochemical cells.

The third generation GPEs with high optical transparency, good ionic conductivity, and suitable mechanical properties were prepared, modified and/or implemented into battery type or hybrid EC devices. Prepared EC cells were examined using coupled optoelectrochemical techniques. The most important findings and achievements of our research can be summarized as follows.

Following our previous results, we optimized the composition of MMA/SA based GPEs. The different polymerization initiators were employed to prepare GPEs with Li and Na ions by direct, thermally or UV initiated polymerization of MMA. The ionic conductivities of prepared systems were compared. The positive impact of the cross linking agent on ionic conductivity and mechanical stability of MMA/BEE and MMA/AIBN based GPEs was observed. Nevertheless, they featured drop in ionic conductivity when compared to MMA/SA gels. We assumed it is due to highly heterogeneous nature of MMA/SA based GPEs, lately confirmed by means of methyl violet dye assisted CLSM.

In order to enhance the mechanical and electrochemical stability of MMA/SA based GPEs, the nanosized electrically inert fillers were employed. The transport properties of redox Fc/Fc^+ couple dissolved in the liquid medium incorporating inorganic filler were studied by cyclic voltammetry. Despite the ionic conductivity decrease observed in the LEs, the nanopowder modification of Al_2O_3 was found to increase the conductivity in the gel medium by almost one half order of magnitude (in case of $LiClO_4$-PC-Al_2O_3 based GPEs, measured at RT). We suggest that the following filler-anion reaction may take place:

$$(Li^+ClO_4^-)_{associates} \xrightarrow{Al_2O_3} (Al_2O_3 \cdots ClO_4^-)_{adsorbed} + Li^+_{solvated} \rightarrow \sigma \uparrow$$

here an ion-ion associate is broken by the presence of the filler interfering with the salt's anion and liberating Li^+ cations. The experiments also included Na^+ conducting GPEs.

The MMA/SA based gel with iodide-iodine pair was introduced and implemented in a hybrid electrochromic cell (Glass|FTO|WO_3|redox GPE|Pt|FTO|Glass). Following proposed optoelectrochemical testing procedure, the HEC cell with MMA/SA redox electrolyte showed rather moderate optical modulation ($\Delta\tau_{(500–750)} \approx 30\%$), slow initial state recovery and relatively low coloration efficiency (10.5 $cm^2.C^{-1}$). On the other hand the switching speeds on the order of tens of seconds were observed. Moreover, an increase in the transmittance ratio of the HEC cell with thermally treated WO_3 was observed.

The HEC cell with MMA/SA redox electrolyte was prepared using an *in-situ* thermal polymerization in the vacuum bag. The new approach eliminating the volume loses usually accompanied by bubbles formation, observed during the thermal polymerization of MMA/SA membranes.

The undefined chemical composition of oligomeric precursor and its sensitivity to moisture uptake (resulting in relatively narrow potential window) was overcome by introduction of the new ethyl methacrylate and 2-ethoxyethyl methacrylate based gel polymer electrolytes. The membranes incorporating $LiClO_4$ and $NaClO_4$ dissolved in PC were prepared by direct radical polymerization complying with requirements of the technology of Li-ion batteries and electrochromic devices. Prepared gel polymer electrolytes exhibit a good electrochemical stability (4.5 - 4.9 V on gold) and a high ionic conductivity (between 0.3 and 1.9 $mS.cm^{-1}$ at room temperature). Their ionic conductivities at the temperatures below 0 °C were higher than those of MMA based GPEs. Moreover, optical transparency (over 90% in visible spectra), high thermal stability (up to 125 °C; PEOEMA based GPE) and good adhesion to the coated substrate.

The battery type electrochromic device with standard electrode arrangement (Glass|FTO|WO_3|GPE|V_2O_5|FTO|Glass) was prepared using the new method of direct *in-situ* preparation. The solution of either PEOEMA or PEMA based GPEs was injected into the cell and UV polymerized. Contrary to the solvent casting method of preparation, this method makes it possible to use a cross-linking agent and precise preparation of the initial mixture along with elimination of the time-consuming dissolving of the polymer and evaporation of the co-solvent. Also, the contamination of polymer with water or oxygen traces was avoided.

The electrochromic cells with PEOEMA and PEMA based GPEs featured fast transmittance changes (within tents of seconds) providing the monochromatic modulation over 46 and 53% of $\Delta\tau$ at 645 nm respectively. The optoelectrochemical tests of ECD with PEOEMA based electrolyte showed higher coloration efficiency values (74.59 $cm^2.C^{-1}$), better electrochemical stability and switching kinetics over the two polymer matrixes. The superior optical performance of PEOEMA based ECD was in accordance with the data received from the 180° peel tests on uncoated PET and glass substrates.

The method of direct *in-situ* polymerization was found suitable for possible industrial application.

The equivalent circuit of prepared GPEs was proposed. The specific circuit parameters were discussed in relation with experimental temperature.

For future work we would recommend to focus on a long term testing of battery type electrochromic device and the feasibility of flexible design implementation.

Curriculum Vitae

Name: Ondřej KREJZA

Born: April 8th 1980 in Hradec Králové

Contact: ondrej.krejza@phd.feec.vutbr.cz

Education

2003 – 2006 **Brno University of Technology / Department of Electrical and Electronic Technology**
Ph.D. study of Microelectronics and Technology
State exam passed in September 2005

1998 – 2003 **Brno University of Technology / Department of Electrical and Electronic Technology**
Pre-graduate study of Electrical Manufacturing and Management
State exam passed in June 2003
Diploma thesis: *Ionic conductivity of polymer electrolytes containing different salts* in June 2003

Experience

4/07 – 2/08 **NV Bekaert SA – Bekaert Technology Centre, Zwevegem, Belgium**
Internship/research stay
Applied electrochemical research on acrylic-based EC Devices

9/04 – 9/05 **Technical School of Engineering, University Rovira and Virgili, Tarragona, Spain**
Study stay

4/04 – 5/04 **National Institute of Chemistry – Laboratory for the Spectroscopy of Materials, Ljubljana, Slovenia**
Research stay
Electrochemical research on HEC Devices

Languages

Czech, English, Spanish

Other activities

Interest in new technologies, architecture, design, movie, rock climbing, golf, badminton, travelling, culture

APPENDIX A[1]

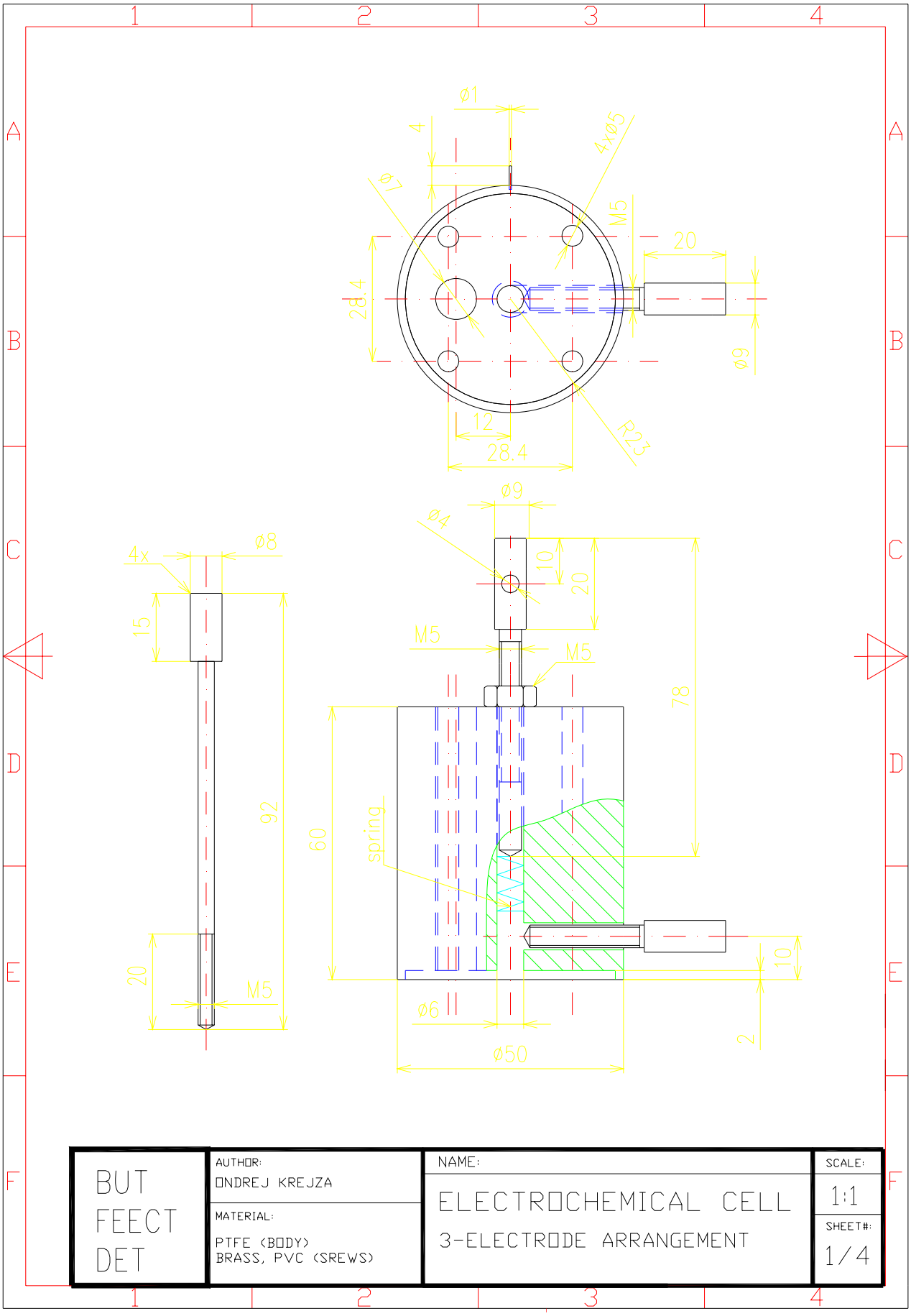
ø1
4
4xø5
ø7
M5
20
28.4
ø9
12
28.4
R23
ø9
ø4
4x
ø8
10
20
15
M5
M5
78
92
60
spring
20
M5
10
ø6
2
ø50
BUT
FEECT
DET
AUTHOR:
ONDREJ KREJZA
MATERIAL:
PTFE (BODY)
BRASS, PVC (SREWS)
NAME:
ELECTROCHEMICAL CELL
3-ELECTRODE ARRANGEMENT
SCALE:
1:1
SHEET#:
1/4

APPENDIX A[2]

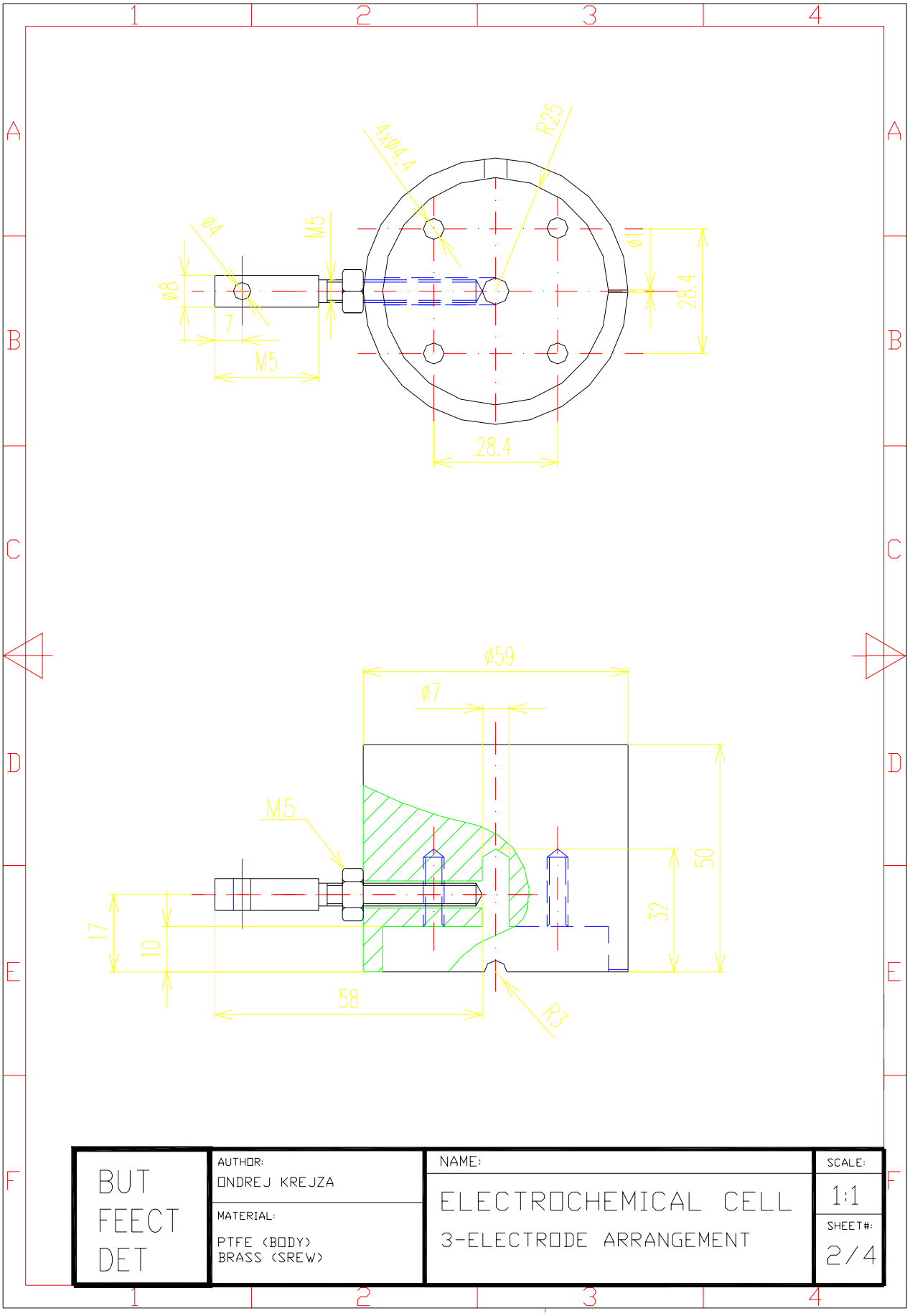

BUT FEECT DET	AUTHOR: ONDREJ KREJZA MATERIAL: PTFE (BODY) BRASS (SREW)	NAME: ELECTROCHEMICAL CELL 3-ELECTRODE ARRANGEMENT	SCALE: 1:1 SHEET#: 2/4

APPENDIX A[3]

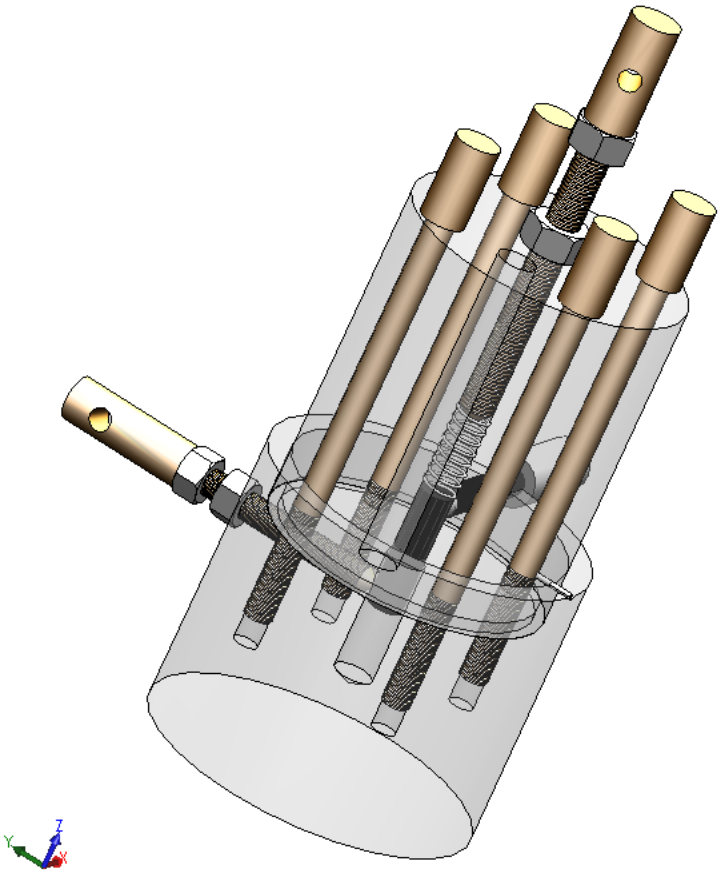

BUT FEECT DET	AUTHOR: ONDREJ KREJZA MATERIAL: PTFE (BODY) BRASS, PVC (SREWS)	NAME: ELECTROCHEMICAL CELL 3-ELECTRODE ARRANGEMENT	SCALE: SHEET#: 3/4

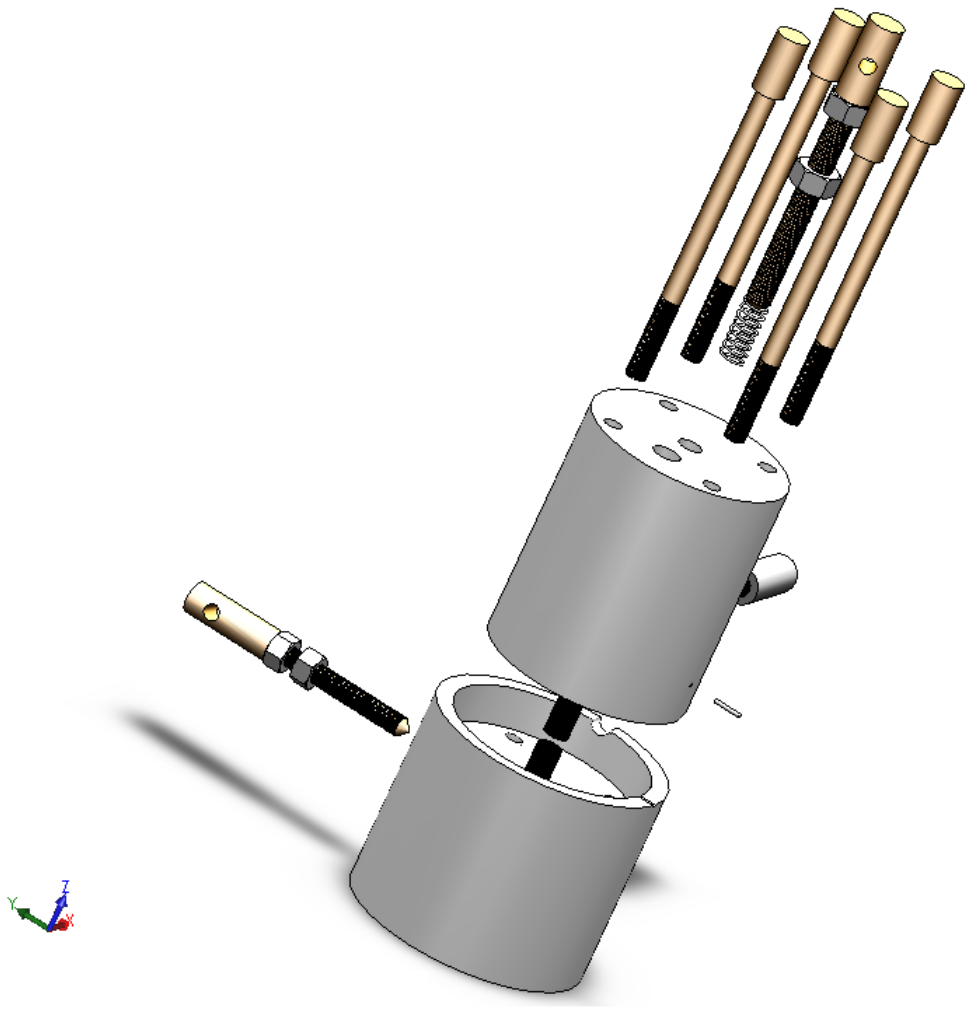

BUT FEECT DET	AUTHOR: ONDREJ KREJZA MATERIAL: PTFE (BODY) BRASS, PVC (SREWS)	NAME: ELECTROCHEMICAL CELL 3-ELECTRODE ARRANGEMENT	SCALE: SHEET#: 4/4

APPENDIX B

The experimental sequence for optoelectrochemical evaluation of the HEC cells employing redox ICS-PPG sol-gel and MMA/SA gel polymer electrolytes			
Cycle #	**Method[1]**	**Experimental details[2]**	**Remarks/Outputs**
1-8	CV	E(V) = 0 → -2 → +2 → 0; SR = 20 $mV.s^{-1}$	
	UV-VIS	CT = 400 s; CS = 5 s; λ = 634 nm	
9	CV	E(V) = 0 → -2 → +2 → 0; SR = 20 $mV.s^{-1}$	
	UV-VIS	λ = **330-1200** nm	$\tau_{bleached/coloured}$ (%) vs λ (nm)
10	CV	E(V) = **0** → **-2** → **+2** → **0**; SR = 20 $mV.s^{-1}$	
	UV-VIS	CT = 400 s; CS = 5 s; λ = **634** nm	$\Delta\tau$ (%) vs E (V)
11	CC	E(V) = **-1.5/100** s; **+2/100** s	ΔQ ($mC.cm^{-2}$) vs t (s)
	UV-VIS	CT = 200 s; CS = 4 s; λ = **634** nm	$\Delta\tau$ (%) vs t (s)
12-19	CV	E(V) = 0 → -2 → +2 → 0; SR = 20 $mV.s^{-1}$	
20	CV	E(V) = 0 → -2 → +2 → 0; SR = 20 $mV.s^{-1}$	
	UV-VIS	CT = 400 s; CS = 5 s; λ = 634 nm	
21	CC	E(V) = -1.5/100 s; +2/100 s	
	UV-VIS	CT = 200 s; CS = 4 s; λ = 634 nm	
22-23	CV	E(V) = 0 → -2 → +2 → 0; SR = 20 $mV.s^{-1}$	Recovery
24	CV	E(V) = 0 → -2 → +2 → 0; SR = **10** $mV.s^{-1}$	I (mA) vs E (V)
	UV-VIS	CT = 800 s; CS = 10 s; λ = 634 nm	$\Delta\tau$ (%) vs E (V)
25	CV	E(V) = 0 → -2 → +2 → 0; SR = **20** $mV.s^{-1}$	I (mA) vs E (V)
	UV-VIS	CT = 400 s; CS = 5 s; λ = 634 nm	$\Delta\tau$ (%) vs E (V)
26	CV	E(V) = 0 → -2 → +2 → 0; SR = **40** $mV.s^{-1}$	I (mA) vs E (V)
	UV-VIS	CT = 200 s; CS = 5 s; λ = 634 nm	$\Delta\tau$ (%) vs E (V)
27	CV	E(V) = 0 → -2 → +2 → 0; SR = **60** $mV.s^{-1}$	I (mA) vs E (V)
	UV-VIS	CT = 136 s; CS = 4 s; λ = 634 nm	$\Delta\tau$ (%) vs E (V)
28	CV	E(V) = 0 → -2 → +2 → 0; SR = **80** $mV.s^{-1}$	I (mA) vs E (V)
	UV-VIS	CT = 100 s; CS = 4 s; λ = 634 nm	$\Delta\tau$ (%) vs E (V)
29-39	CV	E(V) = 0 → -2 → +2 → 0; SR = 20 $mV.s^{-1}$	
40	CV	E(V) = 0 → -2 → +2 → 0; SR = 20 $mV.s^{-1}$	
41	UV-VIS	CT = 400 s; CS = 5 s; λ = 634 nm	
42	CC	E(V) = -1.5/100 s	Self erasing
	UV-VIS	CT = **1000** s; CS = 5 s; λ = 634 nm	$\Delta\tau$ (%) vs t (s)
43-189	CV	E(V) = 0 → -2 → +2 → 0; SR = 20 $mV.s^{-1}$	
190	CV	E(V) = 0 → -2 → +2 → 0; SR = 20 $mV.s^{-1}$	
	UV-VIS	CT = 400 s; CS = 5 s; λ = 634 nm	
191	CC	E(V) = -1.5/100 s; +2/100 s	
	UV-VIS	CT = 200 s; CS = 4 s; λ = 634 nm	

[1]CC – Chronocoulometry; CV – Cyclic Voltammetry

[2]SR – Scan rate; CT – Cycle time; CS – Cycle sampling

APPENDIX C

The experimental sequence for optoelectrochemical evaluation of the EC cells employing EOEMA and EMA based gel polymer electrolytes[1]			
Cycle #	**Method[2]**	**Experimental details[3]**	**Remarks/Outputs**
1-10	CV	E(V) = 0 → -2.5 → +1.5 → 0; SR = 20 mV.s^{-1}	
11	CV	E(V) = 0 → -2.5 → +1.5 → 0; SR = 20 mV.s^{-1}	
	UV-VIS	CT = 400 s; CS = 5 s; λ = **634** nm	$\Delta\tau$ (%) vs E (V)
12	CV	E(V) = **0** → **-2.5** → **+1.5** → **0**; SR = 10 mV.s^{-1}	
	UV-VIS	λ = **200-900** nm	$\tau_{bleached/coloured}$ (%) vs λ (nm)
13	CC	E(V) = **-2.5/100** s; **+1.5/100** s	ΔQ (mC.cm^{-2}) vs t (s)
	UV-VIS	CT = 200 s; CS = 0.1 s; λ = **634** nm	$\Delta\tau$ (%) vs t (s)
14-15	CV	E(V) = 0 → -2.5 → +1.5 → 0; SR = 20 mV.s^{-1}	Recovery
16	CV	E(V) = 0 → -2.5 → +1.5 → 0; SR = **10** mV.s^{-1}	I (mA) vs E (V)
	UV-VIS	CT = 800 s; CS = 10 s; λ = 634 nm	$\Delta\tau$ (%) vs E (V)
17	CV	E(V) = 0 → -2.5 → +1.5 → 0; SR = **20** mV.s^{-1}	I (mA) vs E (V)
	UV-VIS	CT = 400 s; CS = 5 s; λ = 634 nm	$\Delta\tau$ (%) vs E (V)
18	CV	E(V) = 0 → -2.5 → +1.5 → 0; SR = **40** mV.s^{-1}	I (mA) vs E (V)
	UV-VIS	CT = 200 s; CS = 2 s; λ = 634 nm	$\Delta\tau$ (%) vs E (V)
19	CV	E(V) = 0 → -2.5 → +1.5 → 0; SR = **60** mV.s^{-1}	I (mA) vs E (V)
	UV-VIS	CT = 136 s; CS = 2 s; λ = 634 nm	$\Delta\tau$ (%) vs E (V)
20	CV	E(V) = 0 → -2 → +1.5 → 0; SR = 20 mV.s^{-1}	
	UV-VIS	CT = 340 s; CS = 4 s; λ = 634 nm	
21	CV	E(V) = 0 → -2.5 → +1.5 → 0; SR = 20 mV.s^{-1}	

[1]Apply also for PEOEMA and PEMA based ECDs measured at E (V) = 0 → -3 → +1.5 → 0 except the CT which increases with respect to a broaden potential window

[2]CC – Chronocoulometry; CV – Cyclic Voltammetry

[3]SR – Scan rate; CT – Cycle time; CS – Cycle sampling